МОСКОВСКИЙ ГОСУДАРСТВЕННЫЙ УНИВЕРСИТЕТ

ИМЕНИ М.В.ЛОМОНОСОВА

БИОЛОГИЧЕСКИЙ ФАКУЛЬТЕТ

На правах рукописи

Лю Вэньсюэ

Исследование молекулярных свойств D-аминокислотной оксидазы

Специальность 1.5.2. Биофизика (Биологические науки)

ДИССЕРТАЦИЯ

на соискание ученой степени

кандидата биологических наук

Научный руководитель:

доктор биологических наук, профессор

Максимов Георгий Владимирович,

доктор биологических наук, профессор, академик РАН

Рубин Андрей Борисович

Москва – 2025

LOMONOSOV MOSCOW STATE UNIVERSITY

BIOLOGICAL FACULTY

As a manuscript

LIU WENXUE

Investigation of the molecular properties of D-amino acid oxidase

Specialty 1.5.2. Biophysics (Biological Sciences)

DISSERTATION (THESIS)

for the Degree Candidate of Biological Sciences

Scientific supervisor - *Georgy Vladimirovich Maksimov, Doctor of Biological Sciences, Professor*

Rubin Andrei Borisovich, Doctor of Biological Sciences, Professor, Academician of RAS

Moscow – 2025

Contents

LIST OF ABBREVIATIONS

AMO - amine oxidase gene terminator

AO - alcohol oxidase

CbDAAO - DAAO from *Candida boidinii*

CPC - Cephalosporin C

DAO - D-amino-acid oxidase

DAAO - D-amino-acid oxidase

DHAS - dihydroxyacetone synthase

FAD – flavin adenine dinucleotide

FLD - formaldehyde dehydrogenase

GL-7-ASA - glutaryl-7-aminocephalosporanic acid

hDAAO - DAAO from *Human* sapiens

NADH – Nico-tinamid-adenine dinucleotide

PAOX - Alcohol oxidase gene promoter

RgDAAO - DAAO from *Rhodotorula gracilis*.

S-GH - S-glutathione hydrolase

MOX - alcohol oxidase (methanol oxidase) in the *Hansenula polymorpha*

TvDAAO - DAO in the *Triganopsis variabilis*

PC – protein Phycocyanin

pkDAAO – D-amino-acid oxidase from porcine kidney

RS - Raman scattering

MC(K_M) – the Michaelis constant, indicates the substrate concentration when the

reaction rate is half of the maximum rate.

FAD - flavinadenine-nucleotide

FMN - flavin-mononucleotide

SERS - Surface-enhanced Raman

INTRODUCTION

D-amino acid oxidases (DAAOs) are flavoproteins containing FAD that catalyze the oxidative deamination of D-AA, strictly in a stereospecific manner, leading to the formation of the corresponding alpha keto acids as well as ammonia. Oxygen serves as the co-substrate, and it undergoes conversion into hydrogen peroxide [1]. In living organisms, DAAOs play crucial roles and have practical applications in biotechnology.

For humans, DAAOs are involved in signaling processes and participate in the synthesis of neurotransmitters. Changes in the activity of DAAOs and the concentration of D-AA have been linked to the pathogenesis of several diseases, including schizophrenia, Alzheimer's disease, and Parkinson's disease [2].

On the other hand, in lower eukaryotes, the catabolic function of DAAO holds significance. Fungal and yeast cells, with the help of DAAO, can utilize D-AA as a carbon and nitrogen source. The pH stability, temperature stability, Km, and specific activity of DAAOs vary greatly among enzymes derived from different sources. This variability in DAAO properties contributes to the diversity of practical applications associated with these enzymes. In the realm of biotechnology, DAAO-based biosensors have been designed to detect extremely low concentrations of D-AA in medicine.

Additionally, they are utilized to control bacterial contamination in food products. DAAO-based biocatalysts find application in the industrial conversion of modified D-amino acids during the synthesis of cephalosporin antibiotics. The high

stereo specificity of DAAO is exploited for the production of alpha-keto acids, both natural and non-natural L-amino acids, which is particularly significant in the preparation of certain drugs. Given the substantial biotechnological and medical importance of DAAO, the development of efficient and cost-effective systems for enzyme production is undoubtedly of great interest.

Methylotrophic yeast cells show great potential as a host organism for the production of recombinant DAAOs. By utilizing well-regulated promoters of methanol utilization genes, it becomes feasible to optimize the fermentation processes of strains that produce DAAOs through genetic engineering. The challenge of toxicity, which arises when heterologous DAAOs are introduced to *E. coli* cells, can be effectively resolved by directing the synthesized enzymes to catalase-rich peroxisomes.

Efficient production systems in *P. pastoris* cells of DAAOs from the yeasts Trigonopsis variabilis and Rodotorula gracilis have already been described [3]. However, these works do not consider the production of the host strains' own endogenous oxidases.

DAAO genes and enzymes are known from the yeast *C. boidinii* (1 gene) and *P. pastoris* (2 genes). The DAAO genes and enzymes of another important for biotechnology methylotrophic yeast strain *H. Polymorpha* DL-1 have not been previously characterized. The genome of strain Dl1 was deciphered at the Bioengineering Center of the Russian Academy of Sciences in 2013 and according to the annotation contains 4 potential DAAO genes, include HP2082, HP2165, HP2914 and HP2400, which more than any of the previously studied strains of

methylotrophic yeasts [4].

Our interest lies in elucidating the physiological role and biochemical characteristics of individual genes' products, as well as understanding their regulation. The genes HP2082, HP2165, HP2914, and HP2400 of strain DL1 encode proteins ranging in size from 332 to 359 amino-acids and belong to the superfamily of FAD-dependent oxidoreductases according to the annotation. These compounds, which have larger size and more advantageous physicochemical properties compared to reported DAAO inhibitors, have not been thoroughly investigated in terms of their structure-activity relationship. The colleagues from MSU's Department of Chemical Enzymology are currently focused on expressing individual genes in *E. coli* cells and characterizing recombinant enzymes. This provides a foundational basis for the experimental process.

The aims of this work were (1) to characterize the DAAO genes of strain DL1 in vivo using gene knockout methods and determine their expression pattern and regulation of DAAO activity depending on nitrogen and carbon sources; (2) to study the physicochemical properties and changes in molecular structures of the protein upon enzyme activation using Raman and IR spectroscopy, picosecond fluorescence (single-photon counting method) and SERS (Surface-enhanced Raman).

In order to achieve the aim, the following **objectives** were set:

1. Create constructs for DAAO knockout of HP2082, HP2165, HP2914, HP2400 genes and perform inactivation of these genes in H. polymorpha strain DL1.

2.To study the effect of knockouts on DAAO activity under different culture conditions and when strains were cultured with different nitrogen and carbon sources.

3. To investigate the dynamics of DAAO gene expression and oxidase activity.

4. Develop a method for recording SERS and IR spectroscopy for studying DAAO;

5. Study changes in the flavin structure during DAAO activation using SERS;

6. Study changes in the protein structure during DAAO activity using IR spectroscopy;

7. Study the protein structure during DAAO activation using picosecond fluorescence (single-photon counting method).

1. LITERATURE REVIEWS

1.1 D-amino acid oxidases.

D-amino acid oxidase (DAAO, KF 3.5.3.10) are flavoprotein containing FAD that catalyze the oxidative deamination of D-AA with strict stereospecificity, resulting in the production of alpha-keto acids and ammonia. Oxygen serves as the co-substrate in this reaction and is converted to hydrogen peroxide [1]. These enzymes, also known as DAAOs, perform crucial functions in living organisms and have extensive practical applications in biotechnology. (Fig. 1)

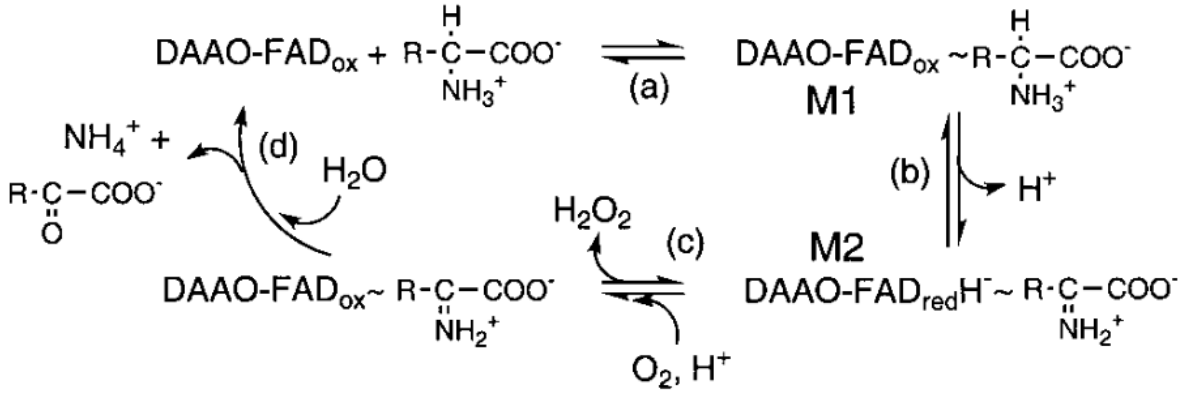

Fig. 1 Minimal reaction scheme for DAAO at pH<8. (a) Formation of the Michaelis complex (M1) through the binding of D-amino acid. (b) The enzyme undergoes reversible conversion into the reduced enzyme-product complex (M2), accompanied by the release of H+. (c) (Re)oxidation by dioxygen, and (d) subsequent release of the products α-ketoacid and NH4+.[5]

The diverse functions of DAAO span various areas, including direct

participation in catabolism (enabling lower eukaryotes to utilize D-amino acids as sources of nitrogen and carbon) and a signaling role in the mammalian nervous system [2,6]. Human DAAO fulfills an important role of neurotransmitter synthesis. In the case of a number of diseases (schizophrenia, Alzheimer's and Parkinson's diseases), significant changes in the concentration of DAAO, its activity and the level of some D-amino acids - D-Ser, D-Ala, D-Asp - are observed in brain tissue, blood serum, and cerebrospinal fluid [2]. Schizophrenia is characterized by a decrease in the level of D-Ser in both blood serum and cerebrospinal fluid. This decrease is linked to an increase in the activity and expression of hDAAO [7]. Therefore, ongoing efforts are being made to discover effective inhibitors of hDAAO. [8]. In ischemia, on the contrary, an increase in hDAAO levels can prevent damage and disease progression [9].

The variability of DAAO amino acid sequences is reflected in marked differences in the enzymatic and physicochemical properties of these enzymes. Enzymes from different sources have wide variations in pH stability (from 4 to 11), temperature stability (from 15 to 70 g), K_m, and specific activity toward different substrates [10]. In general, microbial DAAOs show greater activity towards D-ala with hydrophobic side chains. Two distinct groups of DAAOs are identified based on their substrate specificity. Enzymes from *F. oxysporum, C. parapsilosis, and C. boidinii* have a preference for substrates containing small nonpolar groups such as D-Ala. On the other hand, enzymes from *A. niger, V. luteoalbum, R. gracilis, and T. variabilis* exhibit better oxidation of substrates with larger hydrophobic side chains including D-Trp, D-Met, D-Val, and D-Phe. [1]. These are the enzymes that are most

promising in industry in biocatalytic conversion processes of modified D-amino acids such as cephalosporin C [10]. The high stereospecificity of DAAO is used to produce alpha-keto acids and natural and non-natural L-amino acids [11].

1.2 General characterization of the enzymes

DAAOs consist of a single unit of FAD that is non-covalently bound, leading to their characteristic spectral features as flavo-containing oxidases. These features include two major absorption peaks in the visible region (360-380 nm, 455 nm) and one peak in the UV region (273 nm) [12].The process of catalysis involves the transfer of two electrons from the substrate to the cofactor, resulting in the disappearance of the visible absorption peaks as the cofactor becomes reduced. Moreover, FAD bound to apoprotein exhibits fluorescence at 530 nm when excited at 450 nm. [13].

The pH and temperature stability of microbial DAAOs have been extensively studied due to their wide range of biotechnological applications. RgDAAO and TvDAAO exhibit similar stability patterns, remaining stable within the pH range of 6.0 to 8.2. Nonetheless, there is a gradual decrease in stability with increasing pH [14] [15].

On the other hand, CbDAAO demonstrates greater stability, particularly at alkaline pH levels. However, these proteins diverge considerably in terms of thermostability. While TvDAAO remains completely stable at 45°C, RgDAAO experiences thermal inactivation at temperatures exceeding 30°C, with complete loss of activity after a 30-minute incubation at 45°C [14] CbDAAO displays a similar

sensitivity to temperature changes [15]. Interestingly, the addition of external FAD to the incubation buffer offers significant protection against RgDAAO inactivation at temperatures above 40°C, whereas it does not impact the stability of TvDAAO. Additionally, hydrogen peroxide can render yeast DAAOs inactive [14]

1.3 Substrate specificity

Microbial D-amino acid oxidases (DAAO) display a wide range of substrate specificity, allowing them to oxidize amino acids with side radicals of varying sizes and polarities. Additionally, they exhibit strict stereoselectivity, with L-amino acids being neither substrates nor competitive inhibitors. Unfortunately, comparing the kinetic parameters of different microbial DAAOs is challenging due to variations in data collection methods and experimental conditions. Generally, microbial DAAOs show higher activity towards D-alanine (D-AlA) with hydrophobic side radicals. These enzymes can be categorized into two groups based on their substrate specificity. [5]

The first group includes enzymes that prefer amino acids with small nonpolar side chains, with D-alanine being the optimal substrate for these enzymes. Examples of such enzymes are DAAOs from *Fusarium oxysporum*, *Candida parapsilosis*, and *Candida boidinii*. On the other hand, enzymes from *Aspergillus niger, Vibrio luteoalbum*, *Rhodotorula gracilis*, and *Thermus variabilis* belong to the second group. The preferred substrates for this group are D-alanine and amino acids with large hydrophobic side radicals, such as D-tryptophan, D-methionine, D-valine, and D-phenylalanine. [1,7] Glycine and charged (acidic or basic) amino

acids are generally poor substrates for DAAOs, although D-arginine is a good substrate for TvDAAO, and D-glutamic acid is a good substrate for CbDAAO. Microbial DAAO are also capable of oxidizing modified D-AA, which are of considerable interest for biotechnology. For example, RgDAAO can effectively oxidize CPC [14],[16] and D-naphthyl-alanine [16].

1.4. DAAO spatial structure

In the last two decades, there has been a progressive deciphering of variants or co-crystal structures involving DAAO complexes. These structures have been derived from diverse sources such as human or porcine kidney, as well as microbial origins [2,17–22]. The three-dimensional structure of RgDAAO was successfully deciphered, making it the sole available structure of a microbial DAAO until now [5].

The protein monomers of DAAO in yeast, pig, and human exhibit a highly similar general conformation. In terms of the active site, all conserved residues play a role in the correct positioning of the substrate for the reaction. However, not all of these residues directly participate in the chemical catalysis. The substrate's side chain is situated within a hydrophobic cavity of relatively broad dimensions. The presence of a volumetric methionine residue restricts the available volume of this cavity and greatly influences the substrate specificity of RgDAAO [16].

Despite the overall structural similarity, a meticulous comparison of the 3D structure of RgDAAO and mammalian DAAO reveals the existence of distinct characteristics. These features account for some of the enzymatic variations

observed between the two enzymes [23]. One notable feature is the presence of a C-terminal loop spanning 23 residues in RgDAAO, absent in other forms of DAAO. This loop is crucial for the dimer formation and stabilization of RgDAAO. Additionally, RgDAAO lacks a loop that acts as a "cap" for the active site, as seen in mammalian enzymes. The active site of RgDAAO exhibits a more open conformation, facilitating faster substrate/product exchange [23].

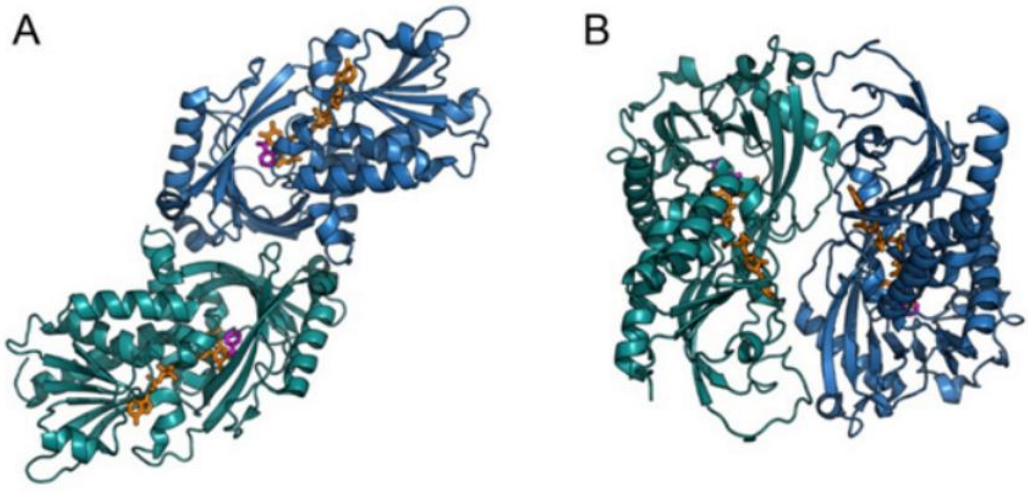

Fig. 2. Models of the two different monomer-monomer dimerization modes of DATA from different sources: hDAAO (panel A, PDB code: 2DU8) and RgDAAO (panel B, PDB code: 1C0I).

Yeast and mammalian DAAOs show about 30% sequence identity, whereas pkDAAO shares an 85% sequence identity with hDAAO. Although the catalytic mechanism of DAAO is shared among various sources, significant variations exist in numerous biochemical properties. These variances encompass factors such as catalytic efficiency, specificity towards substrates, oligomeric state, stability, kinetic mechanism, and FAD binding. All DAAOs bind the FAD cofactor in a

noncovalent mode. The binding is tighter in yeast enzymes (K_d = 2×10^{-8} M for RgDAAO) than in mammalian enzymes (K_d = 2.2×10^{-7} M for pkDAAO and 8×10^{-6} M for hDAAO)[6,24]

DAAOs also differ in oligomeric state. RgDAAO and hDAAO are stable homodimers, whereas porcine DAAO exists in solution as a mixture of monomers, dimers, or higher oligomers, depending on the concentration and the presence of ligands [6,25].

It is intriguing to note that exclusively hDAAO exists as a homodimer even in the absence of the flavin cofactor [24]. Monomeric apoenzymes can be derived from RgDAAO and pkDAAO. Although the 3D structures of pkDAAO and hDAAO display significant resemblance, the mechanism of dimerization varies between mammalian and yeast enzymes. Both pkDAAO and hDAAO show a “head-to-head” dimerization mode, whereas RgDAAO shows a “head-to-tail” mode (Fig. 2).

Each DAAO features a division of its monomer into two domains, namely the FAD-binding domain and the interface domain [265,27]. the FAD-binding domain containing the typical βαβ dinucleotide-binding motif known as the Rossmann fold and the interface domain forming the contact surface with the second monomer. The FAD binding domain includes the well-known Rossmann fold, a dinucleotide binding motif βαβ. In contrast, the interface domain serves as a contact surface for the second monomer. The FAD cofactors are buried within the protein in an elongated conformation. The particular dimerization pattern seen in RgDAAO is due to a long positively charged loop (not conserved in other DAAOs) that interacts with the negatively charged residues belonging to two α-helices from the

other monomer [528].

1.5. Molecular properties of DAAO active center

DAAO, which is an enzyme responsible for the dehydrogenation of nonpolar and hydrophobic D-amino acids (EC 1.4.3.3), has been extensively studied in yeast and mammalian systems. Previous research utilizing structural analysis has provided valuable insights into the reaction mechanism [29–37]. The arrangement of specific residues in the active site of DAAO brings the substrate close to the enzyme's cofactor, flavin adenine dinucleotide (FAD), which forms a noncovalent bond with the enzyme. FAD, acting as a cofactor, accepts a hydrogen atom from the substrate, leading to the creation of an intermediate imino acid and hydrogen peroxide. Spontaneously, the imino acid undergoes deamination, resulting in the formation of its corresponding α-ketoacid, while simultaneously releasing ammonia. The presence of oxygen channels facilitates the entry of molecular oxygen into the active site, allowing for the reoxidation of FAD at the end of the reaction cycle [38,39]. Even though there are water molecules present in the active site, serving to aid in the production of hydrogen peroxide, the hydrophobic environment surrounding FAD is crucial for the oxidation of the substrate [29,33,34,36,38,40,41].

In a 2000 investigation led by Stephan Umhau, Loredano Pollegioni, and colleagues, the x-ray structure of D-amino acid oxidase was thoroughly analyzed to achieve a high level of resolution. This crucial study served as the foundation for

comprehending the structural modifications that occur in D-amino acids when they interact with DAAO. The step of hydride transfer can proceed without involvement of amino acid functional groups. These structures, together with results from site-directed mutagenesis, point to orbital orientation/steering as the major factor in catalysis [42].

Previously in research of Flavia TodoneMaria and Antonietta Vanoni et al., they have carried out the X-ray analysis of reduced DAAO in complex with the reaction product imino tryptophan (iTrp) and of the covalent adduct generated by the photoinduced reaction of the flavin with 3-methyl-2-oxobutyric acid (kVal). This research revealed that, iTrp binds to the reduced enzyme with the N, C-R, and C atoms positioned 3.8 Å from the re side of the flavin. The indole side chain points away from the cofactor and is bound in the active site through a rotation of Tyr224. This residue plays a crucial role in that it adapts its conformation to the size of the active site ligand, providing the enzyme with the plasticity required for binding a broad range of substrates. The iTrp binding mode is fully consistent with the proposal, inferred from the analysis of the native DAAO structure, that substrate oxidation occurs via direct hydride transfer from the C-R to the flavin N5 atom [41].

Flavoproteins catalyze redox reactions in cells as part of oxidoreductases. Flavoproteins contain derivatives of vitamin B2-flavin-mononononucleotide (FMN) and flavinadenine-nucleotide (FAD) (Fig. 3). Some flavoproteins contain metal ions. Typical representatives of flavoproteins that also contain non-heme iron are xanthine oxidase, aldehyde oxidase, dihydroorotate dehydrogenase, acyl-CoA

dehydrogenase, and electron transporting flavoprotein. The last two comprise up to 80% of mitochondrial flavoproteins, which play a significant role in cellular bioenergetics.

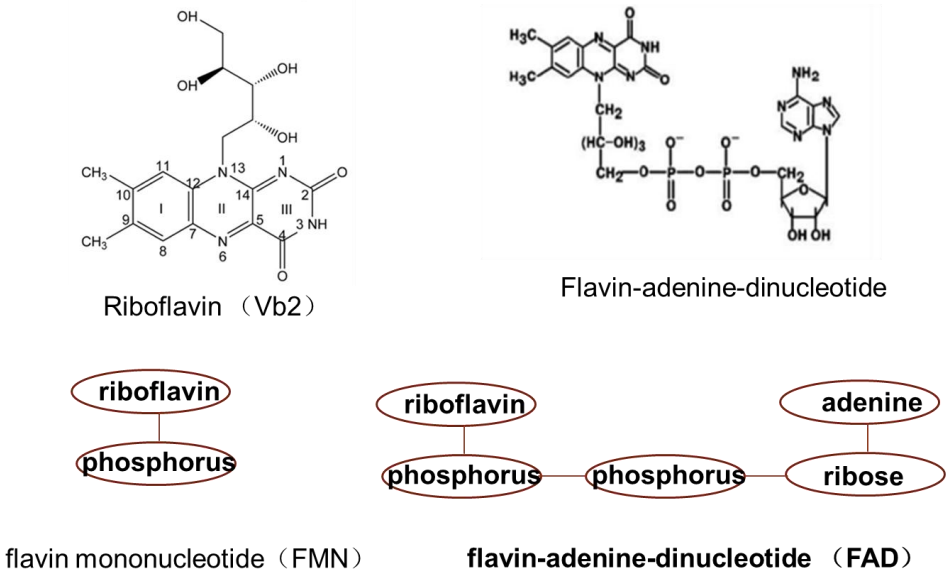

Fig. 3 Chemical structure flavones of DAAO

In past investigations, changes in riboflavin's bonding under Raman spectroscopy were shown. As seen from the chemical structure of riboflavin (Fig. 4), the molecule contains a tricyclic ring system which is composed of a benzene ring (I), a pyrazine ring (II) and a uracil ring (III). Riboflavin additionally features a carbon chain attached to the nitrogen atom of the pyrazine ring, wherein four hydrogen cations are substituted with hydroxyl groups. The most intense band at 1344cm^{-1} in the Normal Raman spectrum is attributed to the C–N stretching and the C–C stretching vibration, which represents the characteristic frequency of the

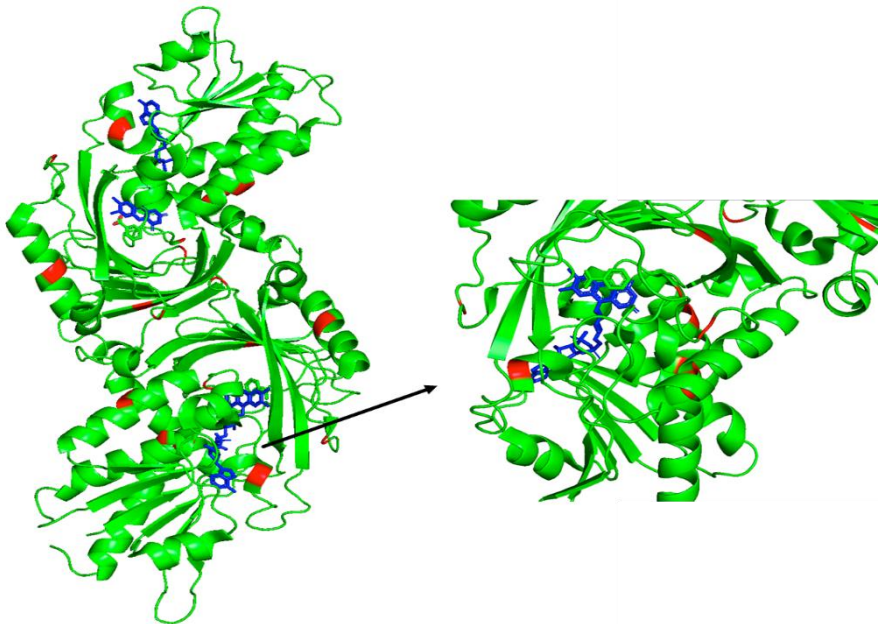

Fig. 4. 3D- structure of DAAO. Blue indicates the position of flavin-adenine-dinucleotide. The location of tryptophan is marked in red. [PDB:1VE9]

pyrazine ring of the molecule. The modes have prevailing contributions from the C–C stretching vibrations of the benzene ring of the riboflavin molecule appear as strong bands at 1461 and 1620cm^{-1}, respectively. The 1534 and 1576cm^{-1} bands have significant contributions from the C–N stretching, while the 1398cm^{-1} band has prevailing contributions from the C–C stretching. These observations indicate the relationship of vibrational modes between adjacent rings. In the solid state, the molecule's typical Raman spectrum reveals the presence of distinct and strong peaks at approximately 1178 and 1222cm^{-1}. These bands are ascribed to the C–N stretching mode of the uracil ring and the C–CH_3 stretching mode of the benzene ring. The band at 1287cm^{-1} has a dominate contribution from the CO bending vibration while the 519cm^{-1} band has salient contribution from the C–CO bending mode, both emanate from the uracil ring. The ring breathing mode appears at

740cm^{-1} while the pyrazine ring bending mode locates at 672cm^{-1} [43].

1.6 DAAO expression in homo- and heterologous systems

In recent times, numerous investigations have been conducted on the synthesis of DAAO by cultivating the initial microorganism or as a recombinant protein in different unrelated systems. DAAO serves as a peroxisomal protein: following the induction of D-Ala in R. *gracilis* cells, the size of peroxisomes enlarges by 30% and the quantity of peroxisomes more than doubles [44]. Additionally, stimulation of DAAO in *C. boidinii* cells during cell development on glucose and D-Ala leads to peroxisome expansion [45]. Despite its localization in peroxisomes, DAAO efficiently forms a functional holoenzyme in the cytosol of *C. boidinii* cells [46].

DAAO synthesis can be induced de novo in peroxisomes during growth on medium supplemented with either D-type or D-type L-AA [47]. This synthesis is induced by D-Ala, and the presence of the L-isomer in the culture medium prevents induction by inhibition of D-AA transport by a specific permease: DAAO activity was not apparent until the L-isomer was depleted from the medium [48]. R. gracilis uses D-Ala as both a carbon and a nitrogen source; maximum DAAO accumulation (~1% of total proteins in crude extracts) has been observed when D-Ala is the sole source of glucose to both nitrogen and carbon [47]. For example, expression of DAAO in *R. gracilis* cells was as high as 770 U/L and 46 units/g using 28 or 80 mM D-Ala as the inducer. The presence of ammonium sulfate had a

negative effect on translation of RgDAAO mRNA and expression of enzymatic activity.

DAAO can plays a crucial role in the growth of D-Ala as a carbon source in the methylotrophic yeast *C. boidinii*. However, a different enzyme system is responsible for metabolizing D-Ala as a nitrogen source. [45, 46] However, no sensitive elements were found in the promoter part of the DAAO gene of *C. boidinii* [46]

D-AA can induce DAAO in various fungi, but the optimal inducers vary among different species and do not necessarily align with the top in vitro substrates found for the corresponding purified enzymes. For instance, in *N. crassa* cells, where DAAO activity is linked to sulfur metabolism, the presence of D-Met as the sole sulfur source in the medium can serve as an inducer for the enzyme [49]. *T. variabilis* yeast is a good producer of DAAO, and DAAO activity is as high as 225 units/g cells using strains of D- Ala as the inducer [50]. TvDAAO was induced by all D, L-AA tested: D, L-Met, D, L-Ala, D, L-Leu, and D, L-Val proved to be the most efficient inducers. Furthermore, even D-AA analogues that cannot be metabolized induce expression of TvDAAO [51].

The effects of D-Ala as an inducer of DAAO activity were studied in more detail for R. gracilis at the level of DAO1 gene transcription and DAAO protein synthesis and active enzyme content. The following interesting patterns were revealed during yeast growth on medium with D-Ala as a source of nitrogen and carbon [47]:

1. The maximum level of DAO1 mRNA was detected after 12 hours of growth followed by a marked decline.

2. The maximum level of specific DAAO activity was detected after 18 hours of growth, (i.e. 6 hours later), followed by a decline.

3. The ratio of active enzyme to total enzyme content measured by Western blotting was maximum after 18-21 hours of growth, followed by an increase in inactive enzyme content.

4. DAO1 mRNA levels and the specific activity of DAAO increased when stationary growth phase was achieved.

In order to further investigate the effects of different sources of nitrogen and carbon, such as glucose, succinate, L-ala, D-ala, D/L-ala, the authors carried out further studies.

DAAO activity was low when grown on D-ala (L-alanine, ammonium sulfate, glucose) -free media, at a lower basal level (0.005 U/mg protein).

When growing on medium with 28 mM D-al and 100 mM glucose, the maximum specific activity of DAAO reached 0.9 U/mg protein, thus increasing almost 200-fold. Growth under these conditions yielded the highest biomass and DAAO activity per cell. The presence of additional carbon sources (glucose, succinate) did not affect the final specific activity of DAAO, but delayed the time to reach the maximum value of this value.

Culturing on mixed substrate (D/L-alanine) and glucose suppressed DAO1 mRNA induction until L-ala depletion, after which DAAO activity increased until the onset of stationary phase but was still less than 50% of the specific activity characteristic of growth on D-ala. It was concluded, therefore, that the induction of DAAO activity in *R. gracilis* is strictly dependent upon the nature of the

stereoisomeric material, in which the L-isomer is completely inactive and apparently competes with the D-isomer for delivery into cells.

The addition of ammonium sulfate also had a marked inhibitory effect on the level of DAAO activity. On medium with 28 mM D-ala and 15 mM ammonium sulfate, DAAO activity was only 14% of the value obtained when grown on pure D-ala. DAO1 mRNA levels in this study appeared comparable when grown on the two substrate variants (D-ala and D-ala + ammonium sulfate). This observation allowed the authors to conclude that ammonium sulfate somehow acts on the translation of DAO1 mRNA [47].

Note that these data were corrected in a later article by other authors on the development of an inducible expression system based on the DAO1 gene promoter [52].

The authors first characterized by RB-PCR the transcription of DAO1 when grown for 6 h on different media. DAO1 mRNA levels were 18-fold higher on D-ala medium than on L-ala medium, and when glucose and ammonium sulfate were excluded from the medium, the degree of transcription induction increased almost 100-fold. Different forms of abiotic stress and growth on glycerol medium had some depression.

In order to identify cis-elements regulating the DAO1 promoter, the authors developed a luciferase gene-based reporter system. This resulted in a collection of DAO1 promoter deletion derivatives and, combined with bioinformatics analysis, we were able to identify important conserved motifs, one of which was shown to be within the first intron of the DAO1 gene. An optimized variant of the DAO1

promoter that provided more than 200-fold induction was obtained and promoter activity was examined under the control of different D-amino acids. The authors also obtained a strain with a deletion of the DAO1 gene. In this strain, induction of the DAO1 promoter was much more effective, probably due to better maintenance of a stable concentration of the inducer, D-al, and was also less sensitive to impurities of glucose and ammonium sulfate [52].

1.7 Recombinant DAAO production systems

Due to the high biotechnological and medical importance of DAAOs, the development of efficient and cost-effective production systems for these enzymes is of undoubted interest. To date, mammalian (human, pig), and yeast (TvDAAO and RgDAAO) DAAO expression systems have been developed in *E. coli*, S. cerevisiae, and *Pichia pastoris* cells. They were able to achieve a record level of DAAO expression for recombinant porcine kidney DAAO in *E. coli* cells. As much as 40% of the total soluble crude extract protein was accounted for by the recombinant enzyme [53]. Since the specific activity of mammalian DAAO is low, the overall production of functional enzyme merely matched 200-300 units/L of the culture medium. To obtain recombinant RgDAAO, a chimeric enzyme with six extra amino acid residues at the N-terminus, an *E. coli* cell line was employed alongside the T7 expression system[54]. When using this system, a production of 2300U/L and 930U/g cells was achievable. Additionally, the target protein content in the crude extract accounted for 8% of the total soluble protein. These findings were consistent with the expression of *F. solani* DAAO cDNA in *E. coli*. [55].

In addition, TvDAAO was expressed in *E. coli* by using lactose as the inducer [56]. As much as 15% of the total soluble protein in the cell was expressed as his-tagged TvDAAO. A chimeric TvDAAO fused to an N-terminal twelve amino acid peptide was able to be expressed at levels as high as 35% of the total soluble *E. coli* protein. To suppress the toxic activity of the enzyme, included D-Met in the nutrient medium during the cultivation procedure. This resulted in a 14.5-fold increase in the total production level and a 3-fold increase in the specific activity of the enzyme [57].

Affinity tag attachment did not interfere with DAAO activity. The expression of TvDAAO fused with a synthetic oligohistidine "tail" reached levels of up to 40% in crude extracts, representing a significant proportion of the total soluble protein [56]. Moreover, the RgDAAO protein, which carried a histidine tag, demonstrated successful expression in *E. coli*, achieving a remarkable enzyme activity of 3000 units/L while maintaining complete solubility. The purification process involved a single-step metal-chelate affinity chromatography, resulting in a high-yield (82%) isolation of the enzyme with exceptional specific activity. The purified protein was obtained in a stable conformation, which further enhanced its utility in various applications. [58].

Although it was possible to express microbial TvDAAO and RgDAAO in *E. coli* cells in high yield, the creation of such strains required a complex procedure for optimization of cultivation under microaerophilic conditions. The fact is that the production of functionally active DAAO is toxic for common *E. coli* strains because it involves the release of hydrogen peroxide and suppression of cell wall

synthesis due to depletion of the intracellular pool of D-amino acids [59]. In view of the above, there have been repeated attempts to express DAAO in saccharomycetes yeast and *P. pastoris*. One of the most successful examples of -expression of TvDAAO in *P. pastoris* involved the use of a synthetic gene with optimized codon composition and an introduced C-terminal targeting site in peroxisomes[60]. A similar strategy was used to overexpress RgDAAO in *P. pastoris*[61]. An order of magnitude higher than all previous endeavors, the production level of recombinant DAAO reached a remarkable 350 ME/mL in the culture medium [62].

To simplify the procedures for further purification of TvDAAO expressed in yeast from impurities of catalases and esterases, we have developed a system for the production in *P. pastoris* of DAOcbd, a functionally active hybrid of TvDAAO with the chitin-binding domain of chitinase A1 of *B. circulans* [63]. Such a protein can be purified in one step on a chitin sorbent. The yield of DAAOcbd when cultured in flasks was 4000 IU (or 500 mg) per liter of culture, with a production level of the target enzyme on the order of 10% of the soluble protein of the recombinant strain [63].

We were able to achieve extremely high levels of DAAO production from *C. boidinii* under the control of the promoter of the alcohol oxidase gene in the original host [15]. By employing a mutant strain lacking alcohol oxidase and harboring 8 copies of the expression cassette, observed a production level of approximately 32 units/mg protein for CbDAAO. This accounted for roughly 30% of the cell's total soluble protein.

1.8 Application of enzyme in biotechnology.

DAAOs, as noted above, are of considerable interest to biotechnology. D-AA and DAAO are implicated in regulating a number of vital cellular processes. Significant changes in the concentration and activity of human DAAO and, as a result, in the levels of a number of D-amino acids (D-Ser, D-Ala, D-Asp) have been observed in the brain tissue, serum, and cerebrospinal fluid of patients with schizophrenia, as well as in the diseases of Alzheimer's disease and Parkinson's disease. Bacterial contamination may be indicated by the existence of D-AA in human food, since D-AA is a component of the peptidoglycan found in bacterial cell walls [64]. This peptidoglycan serves as a diagnostic foundation for various diseases, highlighting the significance of developing DAAO-based biosensors in the fields of medicine and the food industry. In 2013, the creation of biosensors enabled the detection of exceptionally small amounts of D-AA in physiological fluids of humans [65]. An amperometry biosensor was designed to measure D-AA content in fruit juices [66].

DAAO is used to produce α-keto acids and non-natural L-amino acids [2], which are used to synthesize precursors of various drugs[67] . Together with catalase and ω-transaminase, DAAO is used to produce optically pure L-Ala, a key intermediate for the manufacture of drugs such as brivaracetam and levetiracetam (antiepileptic drugs) [68]. TvDAAO was used to produce optically pure L-Met from D-amino acid in 100% yield [69]. The use of recombinant TvDAAO and RgDAAO enzymes has led to the development of phenylpyruvate production systems [70]. In

addition, the enzymatic oxidation of D-methionine by the enzyme DAAO results in the production of 4-methylthio-2-oxobutyric acid (MTOMA), a methional precursor (apoptosis inducer), which serves as an anti-cancer agent. This method of producing MTOMC is the most efficient of the existing methods [71].

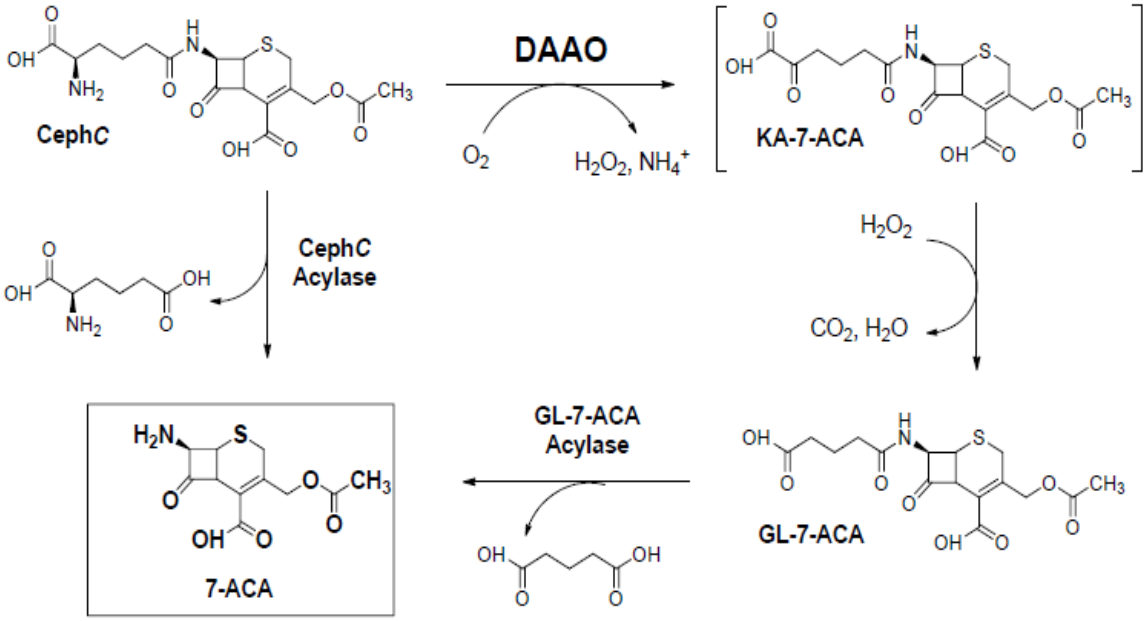

Fig. 5 Biocatalytic cephalosporin C processing.

One of the most important industrial applications of microbial DAAOs is the creation of biocatalysts based on them for the production of cephalosporin antibiotics. Cephalosporin C is a natural beta-lactam antibiotic that forms the backbone of antimicrobial therapy to date [72]. The common core of all cephalosporin antibiotics is 7 aminocephalosporanic acid (7-ACC), consisting of beta-lactam and dihydrothiosin rings. 7-ACC is the starting compound for the production of semi-synthetic cephalosporin antibiotics[73]. Natural cephalosporins have low antimicrobial activity, but the addition of different radicals at position 7 and 3 increase their biological activity and resistance to beta lactamases. There are

over 50 semisynthetic cephalosporins derived from 7-ACC, the market for this precursor compound is estimated to be in the region of ~200 million US dollars. 7-ACC is derived from cephalosporin C by two methods: chemical (treatment of a similar compound (cephalosporin C) with phosphorus chloride at reduced temperature to produce iminochloride) and enzymatic. The chemical method has a number of disadvantages: multistage, low yield of the target product and use of organic solvents. In order to prepare 7-ACC, instead of using a chemical method, a biocatalytic approach involving two enzymes, namely D-amino acid oxidase and glutaryl hydrolase, was proposed. The initial step of this process involves DAAO facilitating the oxidative deamination of cephalosporin C to produce α-ketoadipyl-7-amino cephalosporanic acid (ketoadipyl-7-ACC). Subsequently, in the presence of hydrogen peroxide generated during the initial stage, ketoadipyl-7-ACC undergoes nonenzymatic decarboxylation, leading to the formation of 7-β-(4-carboxy-butanamido) cephalosporanic acid (glutaryl-7-ACC). Finally, glutaryl-7-ACC acylase catalyzes the hydrolysis of glutaryl-7-ACC, resulting in the generation of 7-aminocephalosporinic acid (7-ACC). (Fig. 5)

It has been shown that for all biotransformation processes that utilize DAAO, the enzyme can be efficiently stabilized by immobilization [11]. Showed that immobilization of DAAO using a highly activated glyoxylagarose substrate improved the stability of RgDAAO by a factor of 15000, whereas the stability of TvDAAO was minimally affected[74]. Due to the catalytic efficiency of an immobilised flavoenzyme such as DAAO that requires molecular oxygen as an electron acceptor, is significantly limited because of external and internal

constraints on the mass transfer of oxygen into the gel matrix. One approach to eliminating this limitation is to increase the partial pressure of oxygen and/or stir the reaction mixture; however, this reduces the operational stability of the immobilized enzyme. As an alternative approach, a chimeric enzyme can be obtained by fusing the bacterial hemoglobin domain of *Vitreoscilla* (used as an oxygen donor) with RgDAAO, resulting in a significant increase in the efficiency and stability of the biocatalyst [75]. The process of DAAO-mediated bioconversion can also be achieved using intact cells: permeabilization has been employed to overcome the diffusion limitations resulting from the presence of the cell wall [11]. Therefore, through the utilization of polyethylenimine and glutaraldehyde crosslinking, *T. variabilis* cells have been successfully modified to obtain an enhanced DAAO catalyst

1.9 Methylotrophic yeast: scientific discovery and systematization.

Methane and its derivative methyl alcohol serve as a source of carbon and energy for many organisms living in nature, both prokaryotes and eukaryotes, thus the methane cycle occupies an important place in the biosphere carbon cycle. Metabolism of C1 compounds is carried out by various specific pathways of anabolism (assimilation) and catabolism (dissimilation) [76]. Living organisms include aerobic methanotrophic and methylotrophic bacteria as well as yeast that are able to use methane and methanol (respectively) as their sole carbon source. In the first case, methane is oxidized to methyl alcohol, which is then oxidized to CO_2 by the second [77]. The distinctive metabolic pathways exhibited by prokaryotes and

eukaryotes can effectively be employed for the synthesis of feed protein, vital amino acids, and other significant primary and secondary organic compounds..

The first of the methanol-assimilating yeasts was described was the *Candida boidinii* strain. *Hansenula polymorpha* and other similar strains were later discovered. The 50 species of methylotrophic yeasts known today belong to the genera *Pichia, Candida, Hansenula*, *Komagataella*, and *Ogataea* [78] and inhabit almost any natural environment, including soils of forests, gardens, and wetlands, as well as plant surfaces (flowers, leaves, tree bark and sap, seaweed) and plant debris (rotting fruits and vegetables) [79]. Methylotrophic yeasts are predominantly mesophilic, but thermotolerant strains such as *H. Polymorpha*, O. methanolika, P. methylivora, P. minuta, C. succiphila and C. cariosilignicola are also found [80].

Methylotrophic yeasts break down glucose hexose, disaccharides like trehalose and cellobiose, and pentoses such as xylose, ribose, and arabinose. However, they cannot break down polysaccharides, including galactose, lactose, melibiose, and rhamnose. During the growth of these yeasts on methanol, peroxisomes (PS) are created and take up to 80% of the cytoplasmic space. In these peroxisomes, enzymes involved in the initial stage of methanol metabolism, such as alcohol oxidase, catalase, and dioxyacetone synthase, are synthesized [78].

1.10 Hansenula polymorpha species

Ascospore-forming yeast species of the genus Hansenula form spherical, spheroidal, ellipsoid, cylindrical, and elongated cells. Diploid ascogenous cells arise from the conjugation of haploid cells. Species of the genus are mostly

heterothallic (different sexes and self-incompatible), but *H. Polymorpha* is homothallic, lacking sexual separation of spores and exhibiting interconversion of haploids and diploids [79]. The evolutionary closeness of methylotrophic species of the genus Hansenula is confirmed by the similarity of the G+C composition of their DNA and the electrophoretic mobility of methanol oxidases [79].

The genus *Hansenula* belongs to the family *Saccaromyceracea*, order *Hemiascomycetes*, type *Ascomycota*, kingdom *Mycota*. In 1998, Kurtzman and Robnett studied the phylogeny of all known ascomycetes based on sequence data of the large subunit (26S) of ribosomal DNA. The genus Hansenula was represented by *H. Polymorpha* (*Pichia angusta*) strain CBS 7073 isolated from Drosophila sp.

The *H. Polymorpha* species is named for its different colony type and is a model species for the study of methanol metabolism and peroxisome function, as well as important for industrial protein production. In terms of colony characteristics, diploid *H. Polymorpha* exhibits distinctions compared to haploids. These variations include disparities in color, size, and shape. Furthermore, diploids showcase an elevated sporulation rate, resulting in the formation of pink colonies as early as the sixth day when undergoing incubation on agarized medium [79].

The species complex of *H. Polymorpha*, in fact, encompasses multiple phylogenetically separate strains [81]. Presently, these strains are undergoing reclassification as *Ogataea polymorpha* and *Ogataea parapolymorpha* [82].

Three major strains of *H. Polymorpha* of independent origin are used in basic research and practical applications. Strain CBS4732 (also ATCC34438, NRRL-Y-

5445) was originally isolated from irrigated soil near a distillery in Brazil; strain DL-1 (also ATCC26012) was also isolated from soil; and strain NCYC495 was isolated in Florida from spoiled orange juice in Florida. Strains CBS4732 and NCYY495 can interbreed with each other, while strain DL-1 is incapable of interbreeding with others and is heterothallic.

These three strains differ not only in origin but also in physiology and genetic properties, including the number of chromosomes.

Many derivatives have been derived from these three strains for basic and applied research [81]. These strains have been very useful for investigating some unique features of *H. Polymorpha* metabolism and physiology. Nitrate assimilation genes' regulation in yeast was initially examined using *H. Polymorpha*, which has the capability to assimilate nitrate as the sole source of nitrogen [83]. Furthermore, extensive research has been conducted to investigate the molecular mechanisms that govern nitrate transportation in *H. Polymorpha* [84].

The strain NCYC 495 leu1.1 is capable of digesting xylose, cellobiose and glucose into ethanol at elevated temperatures (45℃ to 50℃) [85]. This is the maximum temperature known to date for yeast growth and alcoholic fermentation in eukaryotes. While ethanol yields from bioengineered *H. Polymorpha* strains are still fairly low, these strains are promising candidates for the development of saccharification and fermentation processes in parallel [86] .

1.11 Methanol biosynthesis pathway

Methylotrophic yeasts all share the same pathway of methanol utilization

consisting of enzymes abundantly present in the cell and efficiently induced during growth on methanol, localised to peroxisomes which rapidly proliferate during growth in methanol [87]. The methanol metabolism pathway is well studied. (Fig. 6). [76] Alcohol oxidase (AOX), located in peroxisomes (92), is the first enzyme of methanol metabolism in yeast and is found in membrane-bound organelles [88]. The addition of methanol to the medium results in peroxisomes occupying up to 80% of the cell volume. AOX oxidizes methanol to formaldehyde and hydrogen peroxide, and as a key enzyme in the utilization of methanol is found in all methylotrophic yeast [89]. The mature active form of AOX is an octamer with a mol. mass of 600kDa built of identical subunits of 74kDa in size, each of which contains FAD as a prosthetic group. AOX is synthesized in very large amounts during growth on methanol, and the AOX promoter is very attractive for the expression of heterologous proteins because it is tightly regulated and very easily induced by methanol [90]. The AOX promoter is one of the most potent and most tightly regulated promoters [91] . *H. Polymorpha* and *C. boidinii* contain only one AOX gene, whereas *P. pastoris* has two AOX genes (AOX 1 and AOX 2) [88]. AOX oxidizes not only methanol but also other low molecular weight alcohols and formaldehyde. For this reason, it is used in the development of alcohol detection sensors in combination with oxygen and hydrogen peroxide sensors. In addition, AOX is highly attractive for a variety of biotechnological applications including formaldehyde analysis in food production, wastewater, and pharmaceuticals. The two oxidation products of methanol, formaldehyde and hydrogen peroxide, are toxic to the cell. In peroxisomes, Hydrogen peroxide is decomposed by catalase

into two molecules of water and oxygen.

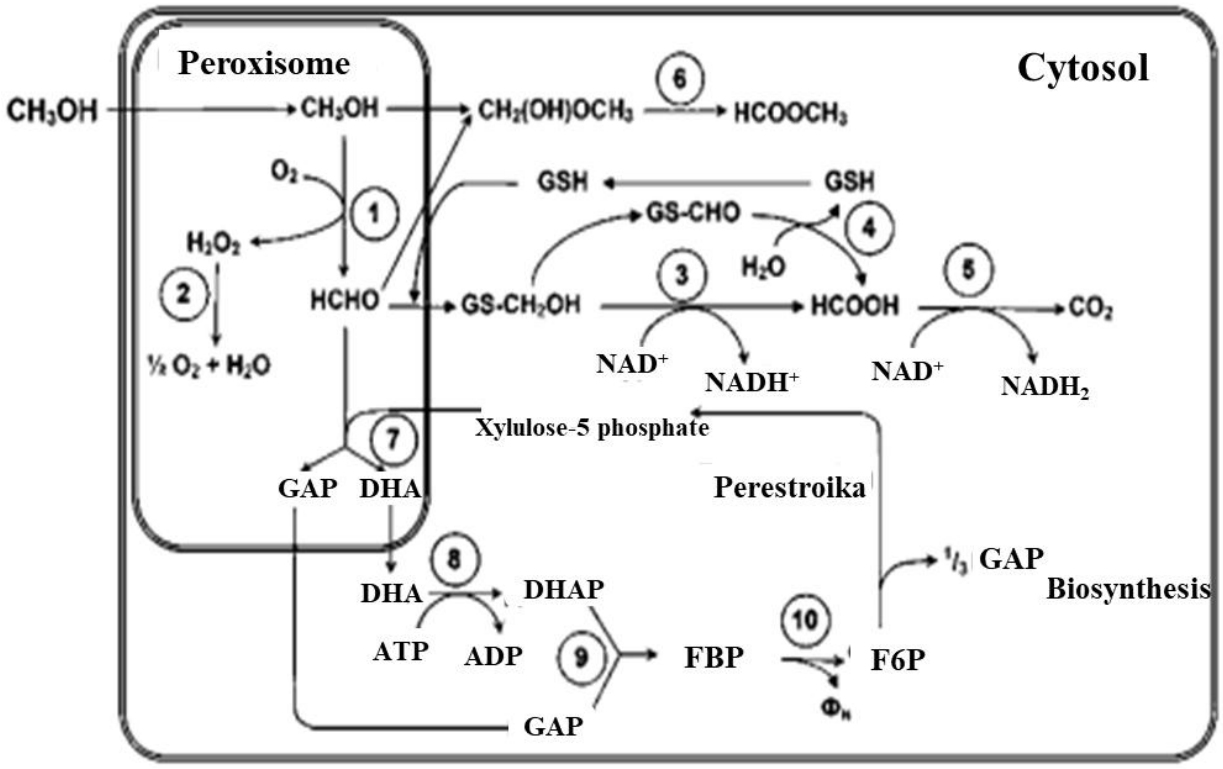

Fig. 6. Methanol biosynthesis pathway in the cell. Where DHA: dihydroxyacetone; F6P: fructose 6-phosphate; FBP: fructose 1,6-bisphosphate; GAP: glyceraldehyde 3-phosphate; GS-CH2OH: S-hydroxymethyl glutathione; GS-CHO: S-formylglutathione; GSH: reduced form of glutathione; Enzyme in process- 1. AR (MOX); 2. catalase; 3. FLD -glutathione-dependent formaldehyde dehydrogenase; 4. S-GH-S -glutathione hydrolase; 5. FDG -flavindehyde dehydrogenase; 6. methyl format synthase; 7. dioxidaceton synthase; 8. dioxidaceton kinase; 9. aldolase; 10. fructose- 1,6- bisphosphatase. [76].

Formaldehyde is the central intermediate of methanol metabolism, from which the cytoplasmic pathways of dissimilation and assimilation of oxidized

methanol begin. Intracellular levels of formaldehyde are tightly regulated [45]. AOX oxidizes methanol to formaldehyde, which is subsequently subjected to the action of transketolase (peroxisomal dihydroxyacetone synthase) or direct oxidation in the cytosol. Dihydroxyacetone synthase is a 155kDa homodimer that catalyzes the transfer of glycolaldehyde from xylulose-5-phosphate as a donor to a formaldehyde molecule as an acceptor by a "ping-pong" mechanism. If sufficient xylulose-5-phosphate is present in peroxisomes, DHAS immediately fixes formaldehyde, otherwise, formaldehyde diffuses into the cytosol where it is oxidized to CO2 by S-formylglutathione hydrolase and format dehydrogenase (FDH) [92]. FDH is essential for optimal growth on methanol because it plays an important role in formaldehyde detoxification, energy production, and regulation of glutathione levels in cells [93]. Formaldehyde can be oxidized to format by a glutathione-dependent or glutathione-independent mechanism [94].

The use of well-regulated and effective promoters in gene expression and the production of recombinant proteins is common in scientific research. These promoters are often employed in the development of robust protein production systems for various methylotrophic yeast species, including *Pichia pastoris*, *Hansenula polymorpha*, and *Candida boindii*. [78, 95–97]. In addition, methylotrophic yeasts are widely used in studies of peroxisomal biogenesis, protein targeting, and function [98,99]. Due to their widespread use as cellular factories and in fundamental research, methylotrophic yeast is currently the focus of intense systems biology and genomic studies [99–101].

1.12 Methylotrophic yeast genomics.

For *Komagatella pastoris*, previously known as *Pichia pastoris*, the genomes of several strains have been fully sequenced [102–104] These advancements have greatly facilitated subsequent progress in transcriptomic, proteomic, and systems biology research (see, for example, [99,105–107].

The sequencing project of *H. Polymorpha* strain CBS4732 [108] has proven to be immensely valuable for comparative genomics and proteomics studies [105]. It allows for studying the mechanisms by which the strain adapts to methanol-based growth [109].

Another widely utilized and well-liked *H. Polymorpha* strain with multiple host advantages is DL-1, which is currently classified as *Ogataea parapolymorpha* DL-1 [82]. Traits such as tolerance to heavy metals, resistance to oxidative stress, and thermotolerance make DL-1 strain an appealing host for various metabolic engineering purposes, including the development of novel ethanol producers [107]. Strain DL1 is characterized by a relatively high frequency of homologous recombination, which allows several techniques of molecular genetic manipulation worked out for S. cerevisiae to be applied to it. The DL-1 strain also has a higher growth rate and adapts more rapidly to changing cultivation conditions [95]. Several host strains suitable for expression of the heterologous protein, including auxotrophic mutants, strains defective in proteases, and in methanol utilization have been engineered in strain DL-1, mainly using "gene knockout" techniques (see below).

The genome of strain DL-1 was deciphered in 2013 at the Bioengineering Center of the Russian Academy of Sciences [103]. Analysis of the DL-1 genome [110] determined its size (9,056,077 bp) and GC composition (47.8%). The nuclear and mitochondrial genomes are represented in GenBank under the numbers AEOI02000000 and HQ616673, respectively. The DL-1 genome consists of 7 chromosomes (0.99 to 1.52 million bp) containing a cDNA locus (7.7 tbp) of 25 repeats [110]. A total of 5,325 protein-coding genes and 80 tRNA genes were detected.

Analysis of the transcriptome of DL1 cells grown on either glucose or methanol revealed a complex and dynamic character of the changes in gene expression patterns under the two conditions studied. Subtelomeric gene families, LTR 'element clusters, and putative centromere sites were identified. In this study, we established the evolutionary position of *H. Polymorpha* DL1 within a distinct clade of yeasts together with the methylotrophic yeast *Pichia pastoris* and the non-methylotrophic yeast *Dekkera bruxellensis*. Phylogenetic analyses revealed patterns of methylotrophy evolution in both yeast and filamentous fungi [110].

1.13 Expression vectors on the *H. Polymorpha* platform

Currently, there are numerous options of expression vectors accessible for *H. Polymorpha*. The plasmids pHIPX4 and pHIPM4 originate from the vector pOK12 [111] , which has a low copy number, and comprise a gene responsible for kanamycin resistance to facilitate selection in *Escherichia coli*. Conversely, all the remaining plasmids are derived from the high copy number vector pBLUESCRIPT (Stratagene) and possess a marker for ampicillin resistance, which aids in selecting

the desired traits in *E. coli*.

The most widely used vectors are those containing a strongly regulated promoter of the alcohol oxidase gene (PAOX) and an amine oxidase gene terminator (AMO). Glucose represses this promoter, downregulates it during growth on glycerol, and strongly induces it when cells are cultured in media containing methanol as the sole carbon and energy source. The replacement of PAOX with alternative promoter fragments has resulted in a number of vectors that provide alternative patterns of expression. For example, pHIPZ15 carries a strong and methanol inducible alternative promoter from the *H. Polymorpha* DHAS gene [112]. Like PAOX, this promoter is transcriptionally repressed by glucose. The pHIPX5, pHIPZ5 [113,114] , and pHIPN5 vectors, all of which contain the *H. Polymorpha* AMO (PAMO) promoter, are also examples of such vectors. It is somewhat weaker than either the PAOX promoter or the PDHAS promoter. The PAMO promoter is induced by culturing *H. Polymorpha* cells on media containing primary amines as a sole source of nitrogen (methylamine, p, ethylamine) and completely suppressed by ammonium sulfate. pHIPX7 / pHIPZ7 both contain the TEF1 promoter constitutive of *H. Polymorpha* and the expression of this promoter is not known [115, 116]. Because stable additional chromosomally replicated plasmids are not available for *H. Polymorpha*, the expression vectors are usually integrated into the genome of the host. This is accomplished for vectors containing PAOX, PAMO, or PTEF1 by linearization of the expression plasmid in the promoter region to allow for directed integration at the AOX, AMO, or TEF1 locus, respectively.

There are vectors with a broad range of selectable markers for *H. Polymorpha*. As well as auxotrophic and dominant markers of resistance. One of the earliest expression vectors that is still in widespread use is pHIPX4 [117]. As a marker of selection in *H. Polymorpha*, this vector harbors the heterologous LEU2 gene from S. cerevisiae under the control of its endogenous promoter. A single copy of this gene, however, is not enough to completely functionally complement the leucine auxotrophy of the leu1.1 strain of *H. Polymorpha*. As a result, fully complemented transformants usually contain multiple copies of the expression plasmid (up to about seven [115] while transformants with only one copy of integration form small colonies. This property makes it much easier to select one or more copies. Contrary to expectations, increasing copy number does not always result in improved expression. Protein production from single-copy integrants has been shown in some cases to be superior to that of transformants that carry a greater number of copies of the expression cassette [79].

One of the main advantages of *H. Polymorpha* is that despite the presence of (large) direct repeats in the genome because of the intentional integration of multiple expression cassettes, the strains are stable and can be maintained on nonselective media with little difficulty. The apparent loss of the integrated plasmid due to replication slippage during genome replication is not very effective in *H. Polymorpha*.

In the case of expression plasmids with a homologous marker of auxotrophy (e.g., *H. Polymorpha* MET6 or ADE11), a single copy of the homologous gene is usually sufficient for the complementation of the auxotrophy to be complete.

Where transformants with integration of multiple copies of the expression cassette must be achieved by these vectors, these clones need to be selected using labor intensive methods such as single colony PCR or Southern blotting [118]. Five dominant *H. Polymorpha* markers are currently available, as shown in Table 1. Indicating that the genes encoding these marker enzymes are constitutively expressed under the control of the TEF1 promoter of S. cerevisiae. Application of standard concentrations of antibiotics typically results in single copies of integrands.

On the other hand, increasing the concentration of antibiotics may lead to selection of cells with improved copies of the expression cassette. This has been shown to be the case for the marker ble pHIPZ4 [110]. It is therefore possible to select transformants with different copy numbers of these expression cassettes in order to meet specific requirements.

The ability to utilize various expression vectors has enabled the incorporation of diverse genes into a singular host strain. For instance, a recent advancement allowed for the successful integration of the entire penicillin (PEN) biosynthesis pathway (consisting of five genes) from the filamentous fungus *Penicillium chrysogenum* into *H. Polymorpha* utilizing modified vectors [119]. It has been demonstrated that all biosynthetic enzymes responsible for PEN were synthesized at a satisfactory rate, ultimately resulting in the efficient secretion of the antibiotic penicillin G into the surrounding culture medium. Due to the availability of various promoters and markers, the quantities of different proteins can be precisely adjusted by choosing appropriate promoters and employing expression cassettes

with specific copy numbers.

1.14 Using the Gateway recombination scheme in *H. Polymorpha*

In the past ten years, there have been advancements in genetic engineering technologies that involve reduced dependence on conventional cloning methods. A noteworthy alternative is the Gateway M system, which has been pioneered by Invitrogen and incorporates recombination cloning along with specific genetic components such as promoters, terminators, tags, markers, and others. Recently, novel modular Gateway-compatible vectors have been created exclusively for *H. Polymorpha* genetic engineering purposes. These vectors have already demonstrated remarkable efficacy. The range of available modules and vectors now encompasses gene expression elements (promoters, terminators), gene deletion tools, and the ability to generate hybrid genes that encode fusion proteins containing green fluorescent protein (GFP) [120].

There are now five different promoter modules for expression of heterologous genes in *H. Polymorpha,* either for high-level inducible expression (PAOX, Pamo), relatively high-level constitutive expression (Ptefi), or relatively low-level constitutive expression (PPEXI4 or Ppexii) [120]. Fusion proteins based on GFP are widely used to investigate protein localization using fluorescence microscopy in molecular and cell biology studies.

Previous work has shown that gene deletion studies in wild-type *H. Polymorpha* were cumbersome and time consuming because verification of correct gene knock-out required screening of multiple colonies (due to random integration

into the *H. Polymorpha* genome).

A research paper proposes the method of choosing "knockouts" by opting for uracil-prototrophic transformants of a host strain containing the ura3 mutation. This approach proved to be advantageous because *H. Polymorpha* uracil auxotrophic strains exhibit considerably longer doubling times on glucose medium, likely attributed to restricted uracil absorption from the culture medium. Subsequently, a total of eight Gateway modules were generated, each featuring distinctive auxotrophic and dominant markers. These modules facilitated the swift assembly of deletion cassettes, enabling modifications to the *H. Polymorpha* genome and the creation of strains with multiple deletions with relative ease [121].

1.15 Cre-loxP system for obtaining knockouts in *Hansenula polymorpha* cells using self-cutting plasmid vectors.

The Laboratory of Molecular Genetics of FIC Biotechnology RAS has developed an original system that greatly simplifies the procedure of multiple rounds of insertional gene inactivation in *H. Polymorpha* cells [122]. It is based on site-specific cre-lox recombination. The plasmid pAM773 harbors a cre recombinase gene under the control of the MOX1 gene promoter, a selective LEU2 marker for selection of *H. Polymorpha* transformants, a bacterial part with an ori site, and an ampicillin resistance gene for genetic manipulation in *E. coli* cells. An intron was inserted into the cre gene to block the production of functionally active cre recombinase in *E. coli* cells. These elements are flanked by two loxP sites, followed by two polylinkers with unique restriction sites and a bacterial kanamycin

resistance gene.

To obtain constructs for genetic inactivation of target genes based on pAM773, derivatives of this plasmid are constructed, carrying sites of 500-2000 bp in size flanking the target chromosomal locus, restricted by a restriction site that is absent in the vector.

The search for such sites relies on knowledge of the locus's nucleotide sequence. Once the desired sites have been selected, a template is obtained for PCR amplification using the "reverse PCR" method. Genomic DNA is hydrolyzed with an appropriate restrictionase, the resulting fragments are circularized with a ligase, and PCR-amplification of the desired fragment is carried out using primers flanked by restriction sites appropriate for cloning into the vector pAM773 along the sites of the polylinker.

When the leu2 recipient strain of *H. Polymorpha* is transformed with a linearized plasmid by the restriction site used to obtain the matrices, leucine prototrophic clones are selected for selection. After checking the correctness of integration by PCR analysis, transformants containing the pAM773 vector insert instead of the target gene are selected. The transformants were transferred to medium with methanol. Methanol-induced cre-recombinase production results in excision of the plasmid insert and, among others, the LEU2 marker with the formation of a deletion with one loxP site in place of the target gene. The required leu2 clones are selected from the progeny of LEU2+ cells grown on methanol and the correctness of excision is checked by PCR. (Fig. 7)

Thus allowing repeated use of the same LEU2 reporter to carry out multiple

consecutive knockouts. This system was used in the present work to create knockout constructs and the subsequent genetic knockout of the HP_2082, HP_2165 and HP_2400 genes [123].

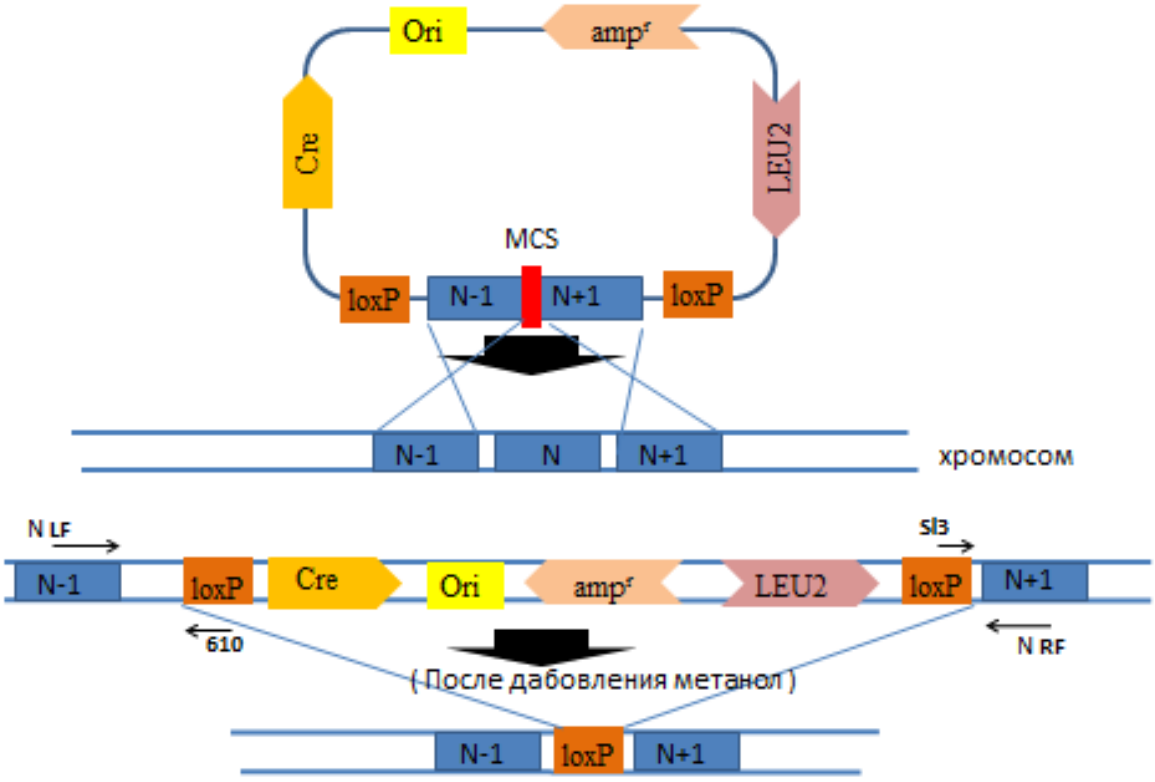

Fig. 7. Principle of cre-lox system for obtaining knockouts in *H. Polymorpha*. (Where N- target gene; N+1 - previous from target genes; N-1 - last from target gene)

1.16 Phycocyanin: molecular structure and function

Given the need for work, we are currently developing technologies to use physical methods to investigate the conformations of DAAO. Phycocyanin was a potential target. Along with allophycocyanin and phycoerythrin, phycocyanin (PC)

is a pigment-protein complex that belongs to the light harvesting phycobiliprotein family [124]. It is a pigment accessory to chlorophylls. Since all phycobiliproteins are water soluble, they cannot exist inside the membrane as carotenoids can. In contrast, phycobiliproteins aggregate to form clusters that adhere to the membrane known as phycobilisomes. The PC molecule includes α- and β-subunits forming a heterodimer, each subunit containing three linear tetrapyrrole chromophores (phycocyanobilin). Under physiological conditions, the heterodimers are organized into hexameric complexes. Phycobilisomes consist of a crucial element in the photosynthesis process, facilitating energy transfer from phycoerythrin to phycocyanin and allophycocyanin, ultimately leading to FSII. Phycocyanin, recognized by its distinct light blue hue, effectively absorbs orange and red light, especially in the vicinity of 620 nm, while releasing fluorescence at approximately 650 nm.

Phycocyanobilin serves as a chromophore in both FC and allophycocyanin molecules, but there are significant differences in the spectral characteristics of these proteins. These differences arise from the conformation of the protein, which creates a specific environment around the chromophore. This environment leads to changes in the absorption spectrum's parameters. The optical properties of the protein-bound chromophore change due to various factors, including alterations in the effective coupling length of the linear tetrapyrrole's π-electron system, local effects of charge distribution within the surrounding protein matrix, and energy coupling among neighboring chromophores. It is important to note that not all chromophores are completely immersed in the protein matrix; some remain

accessible for interaction with the surrounding solvent. All these effects contribute to specific changes in the absorption spectrum of the chromophore, which is necessary for efficient absorption of light and energy transfer within the phycobilisome antenna. The dynamics of pigment-protein complexes play a crucial role in this process, allowing for the migration of energy from blue pigments to red ones and eventually to the chlorophylls of reaction centers. Under normal physiological conditions, chromophores of phycobiliproteins (and other fluorescent proteins) exhibit isomerization, resulting in variations in the spectral properties of pigment-protein complexes.

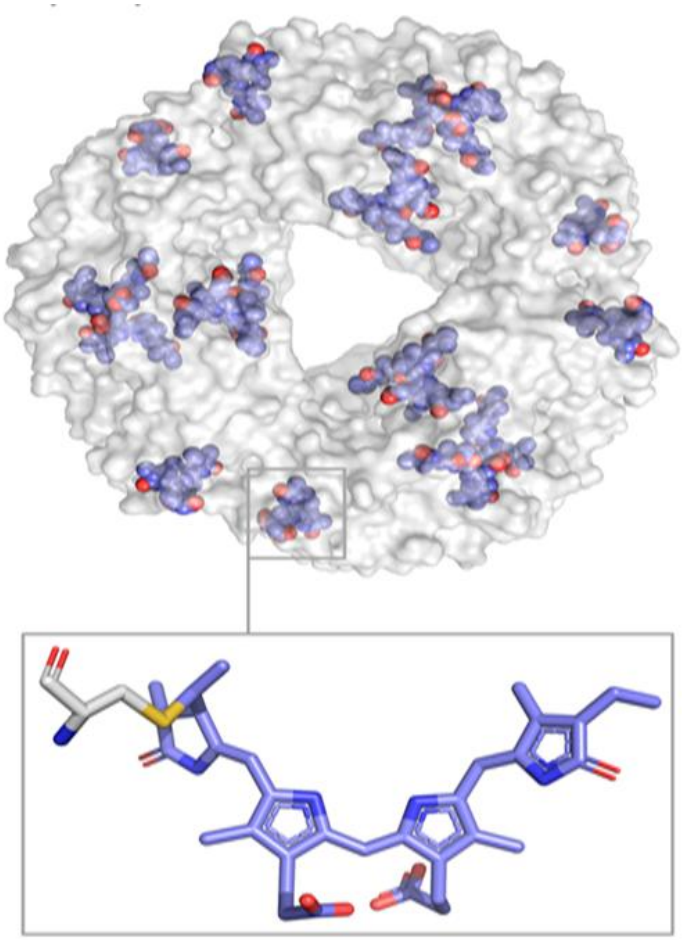

Fig. 8 Structure of phycocyanin (αβ)6 hexamer and phycocyanobilin chromophore

(inset). The amino acid cysteine, through which the phycocyanobilin chromophore is covalently bound to phycocyanin, is marked in gray and yellow. [125]

The dependence of algal photosynthetic activity on medium acidity is well known, and the activity of proteins decreases in extracellular environments at high pH, which also decreases CO_2 production, as well as chlorophyll and carotenoid synthesis, which ultimately affects the algal survival environment, and an increase in pH may contribute to antioxidant synthesis to some degree [126].

1.17 Raman scattering theory

One of the goals of the work was to study changes in protein conformation, which is most optimally studied using Raman spectroscopy. The Raman scattering effect was first discovered in 1982 by the Indian Physicist C. V. Raman, who was awarded the 1930 Nobel Prize in Physics. After that, Raman Spectroscopy has been widely used, because it can detect the fingerprint signatures properties such as frequency, intensity, and polarization of substances.

Molecular vibrations may cause changes in the polarizability of the molecule, and the corresponding Raman effect. The Raman effect is a type of inelastic scattering of light. Prior to emitting the photon, if the molecule briefly exists in a virtual energy state, upon sample excitation, the photon interacts with the molecule, acquiring energy, and subsequently transitions to the excited virtual state before returning to either the E0 or E1 state. The alteration in the molecule's rotational or

oscillatory state mirrors this transformation in the process. (Fig. 9).

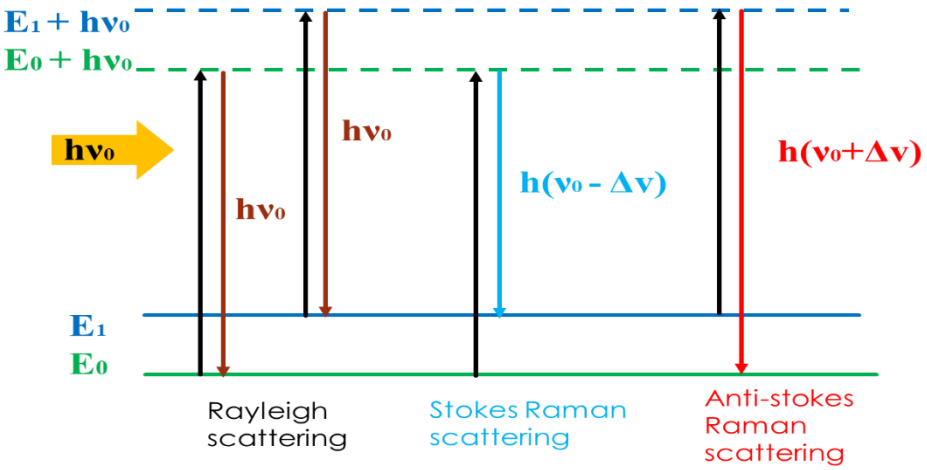

Fig. 9 Energy level diagram of molecular state in Raman spectroscopy. E_0 - ground state; E_1 - excited state; h (ν_0 - Δv), h (ν_0 + Δv) - excited virtual state.

Unlike other vibrational spectroscopy techniques, Raman spectroscopy examines the outcomes of the Raman effect within the scattered light from the sample instead of the sample's absorption spectrum. Therefore, Raman spectroscopy does not require special sample preparation and is not sensitive to absorption bands.

1.18 Surface-enhanced Raman (SERS)

One of the goals of the work was to study changes in protein conformation using high-resolution Raman spectroscopy (SERS). Surface-enhanced Raman can utilize rough surfaces to resonate surface molecules, thereby greatly increasing the Raman scattering intensity of the sample as well as the surface detection sensitivity. In our study, silver nanoparticles were utilized to increase the detection sensitivity

by 10^5-10^9 orders of magnitude.

In Raman spectroscopy, apart from the explanation provided in the previous sections regarding spontaneous and resonant Raman, there are additional distinctions made for forced, hyper-Raman, and giant Raman scattering mechanisms. The selection of these various types depends on the specific objectives of the research. Specifically, the giant Raman spectroscopy method (commonly referred to as "Surface-enhanced Raman scattering" or SERS) is employed for the detection of signals from samples with low concentrations or weakly Raman-active compounds. Through the implementation of the SERS technique, it becomes feasible to detect feeble signals originating from numerous molecules that are adsorbed on the uneven surface of specific metals. This is accomplished by significantly enhancing the intensity of the effective scattering cross-section matter, reaching levels of 10^5–10^6 [127].

The SERS effect was first registered by M. Fleishman in 1974 with observing the scattering of molecules deposited on uneven silver surface [128]. Explanations of the nature of amplification during signal registration were put forward in 1977 by D. Jeanmaire & R.P. Van Duyne), who associated the Raman amplification mechanism with the electric field [129]. Regardless of them, M. Albrecht, and J. Creighton (M. Albrecht & J.A. Creighton) explained the nature of the amplification of the Raman signal by the interaction of the molecules of the studied substances with a silver surface [130]. To date, it has been established that the enhancement of the Raman signal is associated with effect of plasmon resonance - resonant oscillation of electrons on interface dielectric constant of the material, stimulated incident

light [128]. Thus, an increase in the intensity of the Raman signal depends both on the increase in the electromagnetic field during excitation surface plasmons of noble and alkali metals, and from changes electronic structures of molecules during chemical interaction with a metal.

The method of SERS has found wide application in the analysis nanostructured complexes in semiconductors. In biology, the method is also found wide application, but due to the peculiarities of working with biological samples (Stability, oxidation, damage and deformability of cell structure and fabrics) is constantly searching for the creation of the most stable and versatile substrates for signal detection [131,132]. Also, research is underway associated with the preparation of colloidal solutions of nanoparticles with the necessary shapes and sizes. For example, it is known that hedgehog-shaped nanoparticles (with protruding spikes) give the greatest amplification of the RS signal, but at the same time, they can damage the cell structure [133].

Raman is the inelastic scattering of optical radiation from molecules substances in various states of aggregation (solid, liquid, gas, plasma), which is accompanied by a change in the radiation frequency relative to excitation light, coinciding in wavelength of excitation with the region absorption of the sample, its molecules are polarized and scatter light. Unlike Rayleigh (elastic) scattering, RR - RS i is a less likely process which is determined by the presence of spectral lines which are different from the frequency of exciting (initial) light at the frequency of the normal vibrations of the molecule under consideration.

Table. 1 Instrument parameters of Renishaw In Via-Reflex micro-confocal Raman spectrometer [134].

Parameter	Value	
Wavelength range	200 nm~2,200 nm	
Supported Lasers	229 nm to 1,064 nm	
Spectral resolution	0.3cm^{-1} (FWHM)	Usually requires a maximum of：1cm^{-1}
Stability	< ±0.01cm^{-1}	Repeated measurements of the 520cm-1 peaks of silicon using a spectral resolution of 1cm-1 or higher, and the change in the position of the center of this peak after curve fitting
low wavenumber cutoff	5cm^{-1}	Usually minimum required: 100cm^{-1}
High wavenumber cut-off	30,000cm^{-1}	Standard:：4,000cm^{-1}
Spatial resolution (horizontal)	0.25μm	Standard: 1μm
Spatial resolution (portrait)	< 1μm	Standard:：< 2μm。Depends on the objective lens and laser wavelength
Detector size (standard)	1,024 × 256 pixel	Other options available
Detector operating temperature	-70°C	
Supported Rayleigh filters	Unlimited	Up to 4 filters can be mounted on the auto turntable. Unlimited number of filters can be mounted with user-switchable, precision-positioned rotary tables.
Number of lasers supported	Unlimited	Comes standard with 1 laser. More than 4 lasers need to be mounted on an optical platform
Equipped with a Windows computer	Latest configuration of Windows® computers	Includes PC workstation, monitor, keyboard, and trackball
Supply Voltage	110V A to 240V AC，+10% -15%	
Power frequency	50Hz or 60Hz	
Typical power consumption (spectrometer)	150W	
Width (dual laser system)	930mm	Dual laser base plate
Width (three-laser system)	1116mm	Triple laser base plate
Width (compact)	610mm	Up to three lasers (depending on laser model)
Typical weight (without laser)	90kg	

Note that the shift in frequency with respect to the exciting light frequency is always the same for the chemical bonds of each substance, independent of the waves of length of the exciting light source. Raman spectroscopy is widely used in metallurgy, geology, research of semiconductor alloys and, recently, widely used in medical and biological research to assess conformational changes of the studied molecules and determination of authenticity samples [131,135]. For recording Raman spectra, it is important that molecules contain double, triple unsaturated bonds or aromatic rings containing unpaired π electrons.

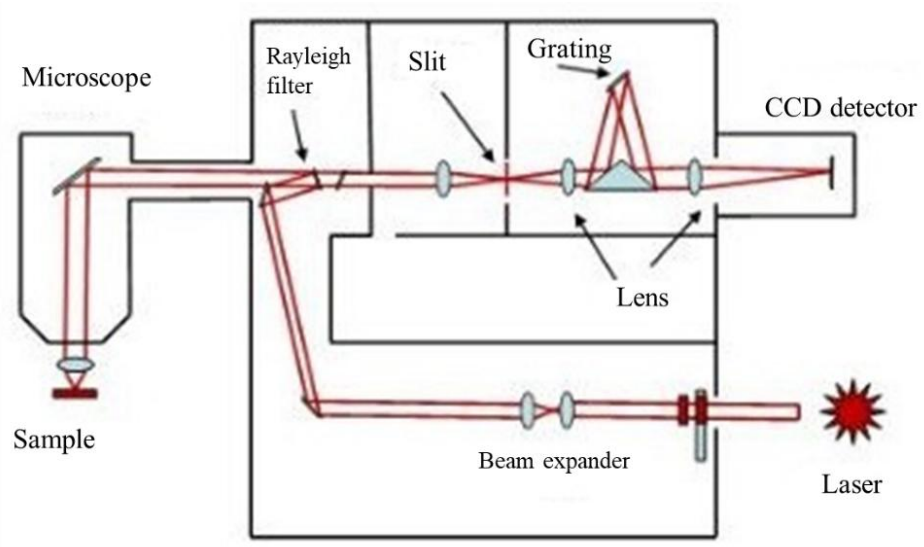

Fig. 10. Optical set-up Of In Via-Reflex micro-confocal Raman spectrometer [136].

In Via-Reflex micro confocal Raman spectrometer is mainly composed of a laser generator, sample optical path, spectral path, photo detector, data reading system and computer control system. Fig. 10 for the optical path of the device [136]. The laser emits laser light into the spectrometer, which enters the microscope objective through the reflector, and then incident on the sample micro-area to be

measured through the objective. The incident laser light interacts with the sample and scatters (including Rayleigh scattering and Raman scattering), then the scattered light is collected by the microscope objective lens, and the Raman-scattered light is obtained, after Rayleigh scattering is filtered out by the filter. After the spectral path for spectroscopy, focusing to the charge-coupled device (CCD) inlet for signal collection, the CCD converts the collected optical signals into digital signals, which are ultimately come out in the form of a spectral curve in the computer. Specific equipment parameters are shown in Table. 1.**Ошибка! Источник ссылки не найден.**

1.19 Infrared spectroscopy (IR)

Raman spectroscopy and infrared spectroscopy (vibrational spectroscopy, IR spectroscopy) complement each other. First works on IR spectroscopy were carried out by W. Koblenz in 1905 and already 30 years later, the method has become widespread as a method for quantitative analysis. Subsequently, with the creation in 1939 of the double-beam spectrometer E. Lehrer, the possibilities of IR spectroscopy for rapid qualitative analysis of substances and the determination of substances of structure by vibrations of chemical bonds in molecules. Central to the work of the IC The Fourier spectrometer is the invention in 1887 by A. Michelson of a dual beam interferometer, which is named in his honor as the Michelson interferometer. The first commercial IR Fourier spectrometer had already been established in 1968 [137].

At present, IR spectroscopy is fast and sensitive method for carrying out

quantitative and qualitative analysis, allowing take direct measurements. However, the method requires additional sample preparation for measurements (the most common method is to use a sample to KBr tablet in the room).

The method's fundamental concept is that the sample selectively absorbs a fraction of the infrared radiation that penetrates it. When investigating organic compounds, the IR absorption range utilized is 2–50 μm, which corresponds to wave number fluctuations within 5000–200cm^{-1}. Within the average IR spectrum (2–10 μm or 4000–400cm^{-1}), a series of bands with differing intensities are present, reflecting the substance's distinctive "molecular imprint" attributable to multiple molecular vibrational-rotational transitions. [138].

IR spectroscopy of organic compounds can be divided into three areas:

1. The range of 4000–2500cm^{-1} corresponds to the stretching vibrations of simple X–H bonds.

2. Within the range of 2500–1500cm^{-1}, we observe the stretching vibrations of multiple X=Y bonds.

3. Lastly, the stretching vibrations of simple X–H bonds occur within the range of 1500–500cm^{-1}

In this particular instance, the occurrence of active oscillations is accompanied by a modification in the electric dipole moment of the bond. As a result, the vibrations of polar bonds (such as C–O, C=O, C–N, N=O, S=O, C=C, O–H, C–H, carbonyl, carboxyl, amide, amine groups) are typically registered in the IR spectra. Additionally, the normal vibrations in the IR spectrum band can be categorized into

stretching (ν) and deformation (δ) motions. Symmetric and antisymmetric vibrations of stretching signify alterations in the bond length along the axis [139140]. In the characteristic spectrum Gb subtraction of the baseline, we identified bands, characterizing fluctuations in protein bonds.

1.20 Try-fluorescence (Single photon counting with time)

Single photon counting with time correlation (Time Correlated Single Photon Counting - TCSPC) tryptophan Fluorescence spectroscopy is a sensitive technique that allows you to detect trace amounts of substances and even single molecules. The method has found wide application in medical, biological, biochemical, and chemical studies of organic compounds, in in particular proteins. Basically, in the study of biological objects use the samples' own fluorescence, or fluorescent dyes and probes. As sources of fluorescence excitation lasers are used [141].

In 1966 and 1974, lasers were created that generated picosecond and femtosecond ultrashort light pulses. Their creation allowed to study the dynamics of ultrafast processes, previously considered experimentally unobservable [136]. Over the past decades, with the help ultrafast fluorescence, crystalline structures of photosynthetic pigment-protein complexes [142].

To diagnose the conformational state of a protein, register fluorescence from a mixture of internal cell fluorophores – individual aromatic amino acid residues of tryptophan, tyrosine, and phenylalanine. So, to excite tryptophan fluorescence, a laser with a wavelength excitation at 260–280nm and register the fluorescence

signal in spectral range 300–350nm [141]. It is known that most proteins intrinsic fluorescence is due to the fluorescence of amino acids tryptophan and tyrosine residues due to low quantum yield phenylalanine fluorescence [143]. Likewise, the fluorescence of tyrosine residues is quenched near amino groups, carboxyl groups, or tryptophan residues [144].

Tryptophan fluorescence is known to be affected by the proximity of other amino acid residues as well (for example, aspartic and glutamine acids cause quenching of tryptophan fluorescence). As a result, tryptophan fluorescence is highly sensitive to conformational changes in the environment of proteins and amino acids [141].

Tryptophan, both in solution and in proteins, has the most pronounced fluorescence in the ultraviolet region of the spectrum. The other two aromatic amino acids capable of fluorescence (but to a much lesser degree) are tyrosine and phenylalanine.

It absorbs electromagnetic radiation with a wavelength of 280 nm (maximum) and emits solvatochromic radiation in the range of 300 to 350 nm, depending on the molecular environment of the tryptophan. In aqueous solution, the fluorescence spectrum of tryptophan peaks at 350nm. The position of the luminescence maximum in the protein composition ranges from 328 nm to 350nm, depending on the properties of the microenvironment of the chromophore. This effect is important for the study of protein conformation.

According to the most recent clarified data, the quantum yield of tryptophan fluorescence in solution is 0.17. The value of this parameter is highly variable in

protein composition - ranging from 0.02 to 0.4 [145].

Tryptophan residues located in the hydrophobic environment in the center of the protein give a shift of its fluorescence spectrum by 10-20nm in the short-wavelength direction (values close to 300nm). If the tryptophan residues are localized to the protein surface in a hydrophilic environment, the protein emission shifts to longer wavelengths (close to 350nm). The pH of the solution also affects the fluorescence of tryptophan. Thus, at low pH values, the addition of a hydrogen atom to the carboxyl groups of amino acids adjacent to tryptophan can reduce the intensity of its fluorescence (quenching effect). The fluorescence intensity of tryptophan can be significantly increased by placing it in an organic solvent such as DMSO [146]. The indole nucleus interacts with the nitrogenous bases of the nucleic acids, resulting in a decrease in fluorescence intensity, thus establishing a role for this amino acid in protein-nucleic acid interactions.

2. MATERIALS AND METHODS

2.1 Reagents

Agarose for electrophoresis- Helicon (Russia), sodium dodecyl sulfate (SSN) - "Fluka", Germany; Tris-base, sodium hydroxide, sodium tetraborate, sodium carbonate, manganese (II) chloride, potassium chloride, calcium chloride, 2-(4-hydroxyethyl) piperazine-1-ethanesulfonic acid (HEPES), sodium phosphate, sodium chloride, sodium hydrogen carbonate, glycerol-"Serva", Germany; isopropanol (Os. ч., "Ekos-1", Russia), nutrient media - Difco, USA.

2.2 Enzymes and commercial kits

Restriction endonucleases, Taq-polymerase, Phuzion -DNA polymerase (MBI Fermentas as a subdivision of ThermoFischer Scientific, Lithuania; Sibenzyme, Novosibirsk, Russia), T4DNA ligase (Roche Diagnostics, East Sussex, England). Plasmid DNA isolation kit Plasmid Miniprep Kit (Eurogen, Russia). CleanUp Mini kit (Eurogen, Russia) for isolation of DNA fragments from agarose gel. Plasmid DNA was isolated using Plasmid miniprep kit (Evrogen, Russia).

2.3 Strains used in the work

The XL1-Blue strain of *Escherichia coli* was utilized in the preparative generation and design of plasmids. This strain possesses the following genotype: recA1, endA1, gyrA96, thi-1, hsdR17, supE44, relA1, lac [F'proAB lacIqZΔM15 Tn10 (Tetr)] (Stratagene, СШA).

The object of the study is *Hansenula polymorpha* DL1 (leu1-) strain (provided by M.O. Agafonov, FI Biotechnology Center, Russian Academy of Sciences) and knockouts of HP2165 and HP2914 genes with zeocin resistance gene insertion DL1 HP2165::.ZeoR and DL1 HP2914::.ZeoR obtained earlier by Ekaterina Lobanova.

2.4 Recombinant plasmid

For the construction of vectors for genetic knockout of the DAO genes of *H. Polymorpha*, we relied on the shuttle vector yeast pAM773 [122] . To prepare

matrices for inverted PCR, hydrolysis of *H. Polymorpha* genomic DNA was performed with a suitable restrictionase, controlling hydrolysis by agarose gel electrophoresis restrictionase was inactivated by heating (65℃, 20min) added to a mixture of 1/10 volume of 10 mM ATP/100mM DTT and 1-unit T4 DNA ligase and incubated overnight at 14 C and then ligase was inactivated by heating (65℃, 20min).

Ten times the mixture was diluted with water, and 1μl was used as template in "reverse PCR" using primers specifically chosen to carry flanking restriction sites for cloning into the pAM773 vector.

2.5 Synthetic oligonucleotides

Synthetic oligonucleotides, the structure and nomenclature of which are given in Table 1, were used for vector construction and to check the correctness of the knockouts obtained. (Table. 2)

2.6 Microbiological media and conditions for strain cultivation

The cultivation of *E. coli* was carried out using either SOB or LB media. The composition of SOB medium per one liter included 20 grams of bacto-tryptone (Difko, Detroit, USA), 5g of yeast extract (Difco, Detroit, USA), 0.5 grams of NaCl (pH 7.5), 2.4 grams of $MgSO_4$, and 186 milligrams of KCl. On the other hand, the composition of LB medium per one liter comprised 5g of yeast extract (Difco, Detroit, USA), 10 grams of bacto-tryptone (Difko, Detroit, USA), and 10

grams of NaCl (pH7.5).

Table. 2 Synthetic oligonucleotides.

Name of primer	5’-3’ - nucleotide sequence	Name
2914RTF	GAG GCC AGG TTG TGG TCA TC	Determination of HP2914 gene expression level by RT-PCR method
2914RTR	CTG CAA GTA GCC ACC CAA CA	
2165RTF	GTT CCC GAT TAA GGG CCA GG	Determination of HP2165 gene expression level by RT-PCR method
2165RTR	ATG ATC GTG CCG CCT TCT TT	
2082RTF	GCA CTA AGA TAT GCG CCG GA	Determination of HP2082 gene expression level by RT-PCR method
2082RTR	TCT CGC GAA ACG TTG ACT CC	
2400RTF	CGG AGC TTT TGA TCG ACG GA	Determination of HP2400 gene expression level by RT-PCR method
2400RTR	CAT CTC ATA GCC AGA GCC GC	
2165KOH3	CTC AAG CTT ATA GCC AGC CAC TCA TGA CAC G	
2165KOB1	CGT GGA TCC TGC TGT ACA CAC CGC AGA AA	Construction of a plasmid to perform knockout of the HPDL 2165 gene
2400KOB1	GGT GGA TCC GGC TAT GAG ATG AGC TGG GG	
2400KOEAG	GGT CGG CCG GCA CCA ACA ACC ACT AT	Construction of a plasmid to perform knockout of the HPDL 2400 gene
2082L_Bgl	TCG AGA TCT ACT CCA ATC ACA ACA ATC CGT TCT	
2082R_Spe	TCC ACT AGT GGG CAC TGA AAA GCA GGT TGT AA	Construction of a plasmid to perform knockout of the HPDL 2082 gene
2165LSc	TTC CAT GTC TTG GCT CGA TGT	Screening of HP2165 gene knockout clones
2165RSc	GGC GAG TTG CCC AGT CTT TC	
2082RSc	CCA GAA CTG TTG GCG TCC AT	Screening of HP2082 gene knockout clones
2082LSc	TGA AGG CCT GAA AAT TGC TT	
2400 LSc	GCA TCT GGG GTT GAC AAG AA	Screening of HP2400 gene knockout clones
2400 RSc	ATC GAT GAG CGT CCT CTG GT	
ActDL1F	ACG CCA TTT TGA GAA TCG AC	Determination of Act1 gene expression level by RT-PCR
ActDL1R	CTC ATT ACC GAT GGT GAT CA	
MOX_RT_F	GTC TGG GTA CCT GCT CGA TG	Determination of MOX gene expression level by RT-PCR method
MOX_RT_R	ACG TTG TCG GGA CAA ACA GAA A	
SL3N	GAT GCT GTC GCC GAA GAA GTT AAG A	Vector-specific AM773 primers for knockout testing

In order to selectively culture bacterial transformants, ampicillin at the rate of 50μg/mL and tetracycline at the rate of 25μg/mL were added to LB medium or to SOB medium. When preparing the Petri dishes, 1.5% bacto-agar was added to the appropriate liquid medium in order to obtain solid media.

Hansenula polymorpha was grown using YP media, YNB media, and YP media supplemented with 0.5% methanol and 1.5% glycerol.

To prepare one liter of YP medium, combine 10 grams of yeast extract and 20 grams of peptone.

For one liter of YPD medium, mix 1 liter of YP with 20 grams of glucose. To solidify the YPD medium, add 20 grams of agar per liter.

To create 100 ml of 10x YNB, dissolve 6.7 grams of YNB (yeast nitrogen base) in 100ml of distilled water. For selective solid medium, sterile 2.5% agar was added to water and autoclaved. Once the liquid agar cooled to approximately 50°C, combine 20ml of 10x YNB and 20ml of 20% glucose with 160ml of agar. To prepare one liter of YP c 0.5% methanol and 1.5% glycerol: for 956ml of YP, 6.25 ml of 80% methanol and 37.6ml of 40% glycerol were used

The minimal amount of liquid and dense media required to culture the knockout strains with different nitrogen sources contained 1xYNB (no amino acids or ammonium sulfate, 0.17% w/v), 30mg/L of leucine, and depending on the task, 0.5% of ammonium sulfate, 30mM D, L -Ala, or 30mM D-Ala, 2% of glucose, or a mixture of 1% glycerol and 1% of methanol. The serial dilution method was used for rapid assessment of growth parameters and degree of stress tolerance of strains.

Individual cultures of strains grown on minimal medium were diluted in sterile water to OD_{600}=1, and 100 ml of culture was transferred to the wells of a 96 well plate. Then, using a multichannel pipette, 10-fold dilutions of the obtained suspension were prepared by sequentially transferring 10 µl of the suspension into wells with 90µl of water. Next, a multichannel pipette was used to apply 3µl of dilutions (10^{-4},10^{-3},10^{-2},10^{-1}) onto dishes containing dense YNB medium. The dishes contained various nitrogen sources (such as ammonium sulfate, D-alanine, D, L-alanine), as well as carbon, supplemented with 0.5M sodium chloride to enhance resistance against osmotic stress, and 2mM hydrogen peroxide to enhance resistance against oxidative stress. The dishes were incubated for 2 days at 37 degrees and photographed.

2.7 Preparation and transformation with DNA fragments

Obtaining competent cells: An overnight culture was grown. Then, 250µl of overnight culture was added to 50ml. Cultured on a rocker at 30℃ to an optical density of OD_{600}= 0.5-0.7. The suspension was centrifuged at 40℃, 3500rpm, 7min. After centrifugation, the tube with cells was lowered into ice and the supernatant was removed. The precipitate was suspended with a sterile pipette in TFB1 buffer (30mM KAc pH5.8, 50mM $MgCl_2$, 100mM KCl, 10mM $CaCl_2$, glycerol). It was left in ice for 15min. Then centrifuged under the same conditions. The supernatant was drained, and 2ml of TFB2 buffer (10mM MOPS-Na pH7.0, 75mM $CaCl_2$, 10mM KCl, 15% glycerol) was added to each tube. Incubated for 30min. Poured 200µl each into 1.5ml microcentrifuge tubes. Stored at -70℃.

Transformation of *E. coli* cells: Inactivated the ligase mixture at 60℃, 15min. Thawed competent cells on ice. Added 40µl of cells and 5µl of plasmid DNA to each microcentrifuge tube. The mixture was incubated on ice for 30min, followed by temperature shock - incubation for 2min at 42℃, then placing the tubes in ice for 2min. 4 volumes of LB or SOB medium were added and incubated without shaking for 60min at 37℃. The cell suspension was seeded onto selective Petri dishes with LB or SOB agar. Incubated at 37℃ for 15-20 hours and colony growth was counted.

DNA fragments were isolated from agarose gel and reaction mixtures using Cleanup Mini kit (Eurogen) according to the manufacturer's recommendations. Plasmid DNA extraction from small volumes of culture was performed using the Plasmid Miniprep kit (Eurogen).

2.8 DNA sequencing and computer programs

Plasmid DNA isolation, plasmid construction and analysis were performed using known genetic engineering methods [16]. Nucleotide sequences of the PCR fragments and plasmids were determined by automated sequencing using the ABIPrizm 3100 DNA Sequencer kit with the Applera "Big dye Cycle fluorescent dye sequencing kit" software package. Nucleotide sequences were analyzed using the Ugene software package [123].

2.9 Transformation of *Hansenula polymorpha*.

The procedure was carried out according to the protocol of Bogdanova et al

[147]. Preparation of competent cells: Overnight culture of *Hansenula polymorpha* grown on YPD medium at 37°C (1-2ml) in a volume of 100µl was transferred to 5ml of fresh YPD medium and grown at 37°C on rocker to OD_{660} 1.2-1.5. Cells were transferred into 1.5ml tubes and precipitated by centrifugation at 5000rpm, 1 min, washed with water and resuspended in 20µl of 100mM Lithium Acetate pH7.5 , added 5µl of DNA carrier (denatured voiced salmon sperm DNA, 10 mg/ml), 5µl of linearized plasmid DNA, 40µl of 70% PEG4000 and incubated for 15-30min at 30°C. Cells were then temperature shocked - 20min, 43°C, cooled in ice, washed twice with water, suspended in 100µl of water and seeded onto dishes with leucine-free minimal medium (1xYNB, 2% glucose, 2% agar).

2.10 Selection of knockout clones by PCR analysis.

Primary transformants selected on SD medium cups were crossed in broad strokes onto minimal dishes and grown overnight at 37°C. The next day, a small amount of grown cell biomass was selected using a sterile glass rod and transferred into 100µl of buffer containing 0.2M lithium acetate and 1% DCN.

The mixture was thermostated for 10min at 70°C, after which 3 volumes of 96% chilled ethanol were added and centrifuged for 5min at 13,400rpm. DNA and cell wall debris precipitated at the bottom of the microtube. The supernatant was drained, followed by washing the precipitate using 70% ethanol and centrifuging it at 13,400rpm for 1min. Subsequently, the carefully extracted supernatant was discarded, and the precipitate was dried. To the dry precipitate 50µl of TE buffer (10mM Tris-HCl, 1mM EDTA) was added, mixed on a Vortex and 2µl of the

suspension was used for PCR.

2.11 Selection of knockouts with deleted insertion of pAM773 vector.

To induce "self-cutting" of the vector part of the knockout construct including the bacterial part, LEU2 gene and Cre gene under the control of the MOX1 promoter, PCR-selected transformants were transferred by a depleting stroke from a dish with SD medium to a dish with YP medium, 1% methanol and 2% glycerol. After two days of incubation at 37 degrees, individual colonies (4- 8 pieces) were transferred with a broad stroke in parallel to two minimal dishes - with SD medium and with SD medium supplemented with leucine (50mg/L). After incubation for 1-2 days at 37°C, colonies that grew well on the minimal medium with leucine and were unable to grow on the medium without leucine were selected.

PCR with flanking primers was performed to verify correct excision of the LEU2 gene insert.

2.12 RNA isolation from yeast

To the cell sediment obtained from 2-4ml of culture, glass beads (0.4mm diameter) with a volume equal to the sediment itself, 200µl of AE buffer (50mM sodium acetate, 1% DCN, 10mM EDTA pH5.0) and 200µl of phenol saturated with 50mM sodium acetate, pH5.0 were added and incubated at 65°C. The mixture was shaken vigorously on a vortex for 3-5 min and then another 400µl of acidic phenol and 400µl of AE were added, incubated for 1 h at 65°C (stirred for 5-10 min each during the hour). The test tubes were cooled on ice for 10 min. To initiate the

experiment, the suspension underwent the addition of 200µl of chloroform. A vortex was employed to shake the resulting mixture vigorously for a duration of 3-5 minutes. Next, centrifugation at 4000rpm for a period of 7 minutes occurred. Keeping the temperature at 6°C, the upper phase was carefully transferred to a test tube that contained a combination of phenol and chloroform in a 1:1 ratio. Vigorous shaking and subsequent centrifugation at 4000rpm for 7 minutes were conducted once again. Subsequently, the upper phase was transferred to another tube comprising 300µl of chloroform. The upper phase was transferred to a tube that held 300µl of chloroform. To this, 50µl of 3M sodium acetate pH5.0 was introduced. The mixture underwent vigorous stirring and subsequent centrifugation at 8000rpm. The resulting clarified upper phase was then moved to a clean tube. An equivalent volume of 100% isopropanol was added, and the mixture was allowed to incubate overnight at 0°C.

To obtain RNA samples for reverse transcription, additional purification of the obtained preparations from genomic DNA impurities was performed. For this purpose, 100µl of the suspension obtained as described above was precipitated by centrifugation (10min, 10000rpm), the precipitate was washed with 70% ethanol and suspended in 20µl of sterile water. The resulting preparations were treated with RNase free DNAase 1 (ThermoFischer Scientific) according to the manufacturer's instructions and then purified using the RNeasy minikit (Qiagen) according to the manufacturer's protocol. The preparations were stored at -70°C.

2.13 Synthesis of cDNA by reverse transcription.

The cDNA synthesis was performed using the Thermo Scientific First Strand cDNA Synthesis kit (Fermentas, Lithuania). We prepared a mixture comprising of RNA and primers. Specifically, we utilized 8µl of RNA along with 2µl of primers. Subsequently, we subjected the mixture to a temperature of 70°C for a duration of 2 minutes to facilitate the melting of RNA secondary structures. Following this, we promptly transferred the resultant samples onto a bed of ice. Finally, we supplemented the experiment with 11µl of reaction mixture: 4µl 5x Reaction Buffer, 2µl 10mM dNTP, 2µl DDT, 1µl RNAse Inhibitor, 1µl H_2O from RNase, 1 µl Reverse transcriptase (RT). The tubes were placed in the amplifier, incubated for 30-60 min at 37-42°C and then 10min at 70°C to stop the reaction.

2.14 Determination of DAO activity

The determination of DAO activity in permeabilized cells was investigated using a test based on the determination of ketoacid concentration as previously described.

For this purpose, 100µl of permeabilized cells were centrifuged for 5 min at 13000rpm. The precipitate was suspended in 250µl of 40mM Na-phosphate buffer pH 7.6, mixed and kept on ice for 3-5 min. Then 50µl of 10mM D-amino acid dissolved in 50mM phosphate buffer pH8.0 was added. The mixture was incubated for 30 min at 40°C with constant stirring (900rpm). To these samples, 100µl of a saturated solution of 2, 4-dinitrophenylhydrosine in 2M HCl was added, and the

samples were incubated for 5min followed by incubation for 5min at room temperature. Followed by the addition of 300µl 3M NaOH.

The solution was incubated for 5 to 10min at room temperature, after which absorbance at 590nm was measured and compared to the standard curve constructed using standard concentrations of pyruvic acid. Specificity was expressed as activity units per mg dry biomass.

2.15 Real-time PCR method

PCR-RV reactions were performed using SYBR Green I reaction mixture (Syntol, Russia) according to the manufacturer's recommendations. Each sample volume of 25µl contained 12µl of 0.8mM primers and 12.5µl of a 2x multiples reaction mixture containing 2µl of cDNA diluted 10-fold.

Amplification was performed on a CFX96 instrument (Bio-Rad, USA). The cycles were performed sequentially: 1) 95°C 3min, 2) 95°C 10s, 3) 60°C 50s, 4) 40 cycles, 5) melting curve from 65.0 to 95.0°C, 0.5°C 5s step. The results were processed in Bio-Rad CFX Manager program (Bio-Rad, USA).

2.16 Preparation of permeabilized Cells

Methylotrophic yeast cells grown on minimal media with different sources of nitrogen and carbon (2-5 ml) were centrifuged for 5min at 4000rpm. The cell precipitate was washed 2 times with 1ml of deionized water and suspended in 100µl of water. After lyophilic drying, 10% isopropanol was added to the dry cells at the rate of 1ml per 50mg dry weight and incubated for 4-20 hours at 4°C for

permeabilization.

2.17 Determination of DAO activity

The determination of DAO activity in permeabilized cells and protein extracts was investigated using a test based on the determination of ketoacid concentration as previously described [53]. For this purpose, 100μl of permeabilized cells or protein suspension in 70% ammonium sulfate were centrifuged for 1 min and 10 min, respectively, at 10000rpm. The precipitate was suspended in 100μl of 20mM Na-phosphate buffer pH7.6. Then 150μl of 10mM D-amino acid dissolved in 50mM phosphate buffer pH8.0 was added. The mixture was incubated for 30min at 34℃ with constant stirring (500rpm). To these samples, 100μl of a saturated 2, 4-dinitrophenylhydrosine solution in 2M HCl was added and the samples were incubated for 5min. 450μl 2M NaOH and 2ml water were then added to the mixture. The solution was incubated for 10min at RT, after which the absorbance at 440nm was measured and compared to the standard curve constructed using the standard pyruvic acid concentrations. The specific activity was expressed in units of activity per OD of dry biomass.

2.18 Selection and purification of pure DAAO colonies

The required experimental materials are backed up at the FRC Biotechnology RAS, Institute of Bioengineering named K.G. Skryabin (Kostantin Georgievic Skryabin; Federal Research Center). There were 9 samples that may be available to use need screened, according to the frozen sample record list. The list is shown in

Table.3.

All spore samples are frozen and stored in the refrigerator at -84℃. Samples, taken from the refrigerator need to be placed in ice water and thawed slowly. Take 20μl of the thawed solution and put it under a microscope to observe the state, at the same time do the morphological comparison with *H. Polymorpha*. Microscope eyepiece x10, objective lens x50.

All spore samples are frozen and stored in the refrigerator at -84℃. Samples, taken from the refrigerator need to be placed in ice water and thawed slowly. Take 20μl of the thawed solution and put it under a microscope to observe the state, at the same time do the morphological comparison with *H. Polymorpha*. Microscope eyepiece x10, objective lens x50.

Table. 3 List of cryopreserved samples.

Serial number	Name	Culture medium	T ℃
1175	PL 1 H.polymorpha	YPD	25
1174	PL 1 H.polymorpha	YPD	37
1173	PL 1 H.polymorpha	YPD	37
1232	H.polymorpha 2-2165 KO	YPD	37
1231	H.polymorpha 2-2165 KO	YPD	37
1230	H.polymorpha E4-2914 KO	YPD	37
1229	H.polymorpha E3-2914 KO	YPD	37
1228	H.polymorpha E2-2914 KO	YPD	37
1227	H.polymorpha E1-2914 KO	YPD	37

2.18.1 Culture and proliferation of strains

Individual strains need to be incubated in a YPD environment for 2 days at

37°C. Take 20µl of thawed sample and apply it evenly and flatly in a petri dish with a sterile glass rod, cover tightly and invert until the sample is absorbed in the YPD and place it in a 37°C thermostat.

In order to obtain pure strains, the cultured strains need to be screened. Petri dishes with samples were removed after 2 days. Select 3 separate strains, which edges are not in contact with any of the surrounding strains. Remove the individual strains with spiral and culture it as a "star", Fig. 11. After 2 days, selected 7 individual strains again, and transplanted into test tubes with elongated slant medium and incubated for two days.

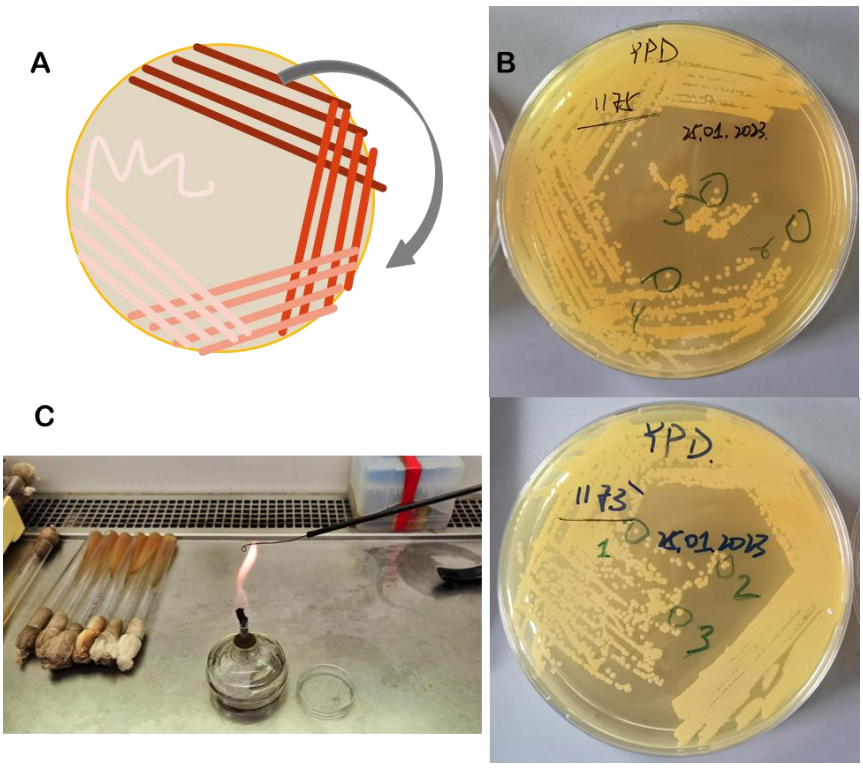

Fig. 11 The method of cell replanting individual strains. A – Form of star-shaped culture in Petri dish. B – star-shaped culture of 1173 and 1175 strain. C- artifact of star-shaped culture.

2.18.2 Freeze-dried sample *Hansenula polymorpha*

In order to accumulate the density of cells and the concentration of the solution, the live strains of *Hansenula polymorpha* were preserved by drying.

Add 1ml MQ to the test tube of the sample selected by the last generation of proliferation （1173*7+1175*7）, shake gently to peel off the proliferating colonies. Aggregate Homologous samples in a test tube, put in a centrifuge at 3500-4000 rpm/min for 5 minutes. Drain off the supernatant, add 5ml MQ, and centrifuge again to clean the colonies. If the bottom of the colony is not strongly attached after centrifugation, the centrifugation time can be increased and it is not recommended to increase for the centrifugation speed. After 3 times of cleaning, remove the supernatant, put precipitated colonies into the machine for lyophilization.

2.19 Preparation of highly purified of OpaDAAO

The opadaao1 gene was expressed in *E. coli* BL21(DE3) cells transformed with the plasmid pOpaDAAO1. The plasmid was obtained by cloning the opadaao1 gene into the pET24a (+) plasmid using NdeI and XhoI restriction sites. Culturing and purification conditions were identical to those described for TvDAAO. Analytical electrophoresis in a polyacrylamide gel in the presence of sodium dodecyl sodium dodecyl sulfate indicated that the purity of the preparations obtained was a minimum of 98%. [148].

2.20 The isolation of hexamer of PC.

[The joint authors of this investigation: Parshina E.Yu., Li V., Yusipovich A.I., Gvozdev D., He Yang. Maksimov G.V.]

The isolation of hexamer PC from cells... was performed according to the methods described in previous studies [150]. Centrifugation was employed to harvest algal cells, which were subsequently resuspended in a phosphate buffer solution with a concentration of 0.002 mol/L (containing 0.004 mol/L sodium aside, pH7.0) and then lysed three times, by freezing and thawing. After centrifugation at 20000g at 4℃, $(NH_4)_2SO_4$ (1.25 mol/l was added to the precipitate and centrifuged again to obtain the crude extract of PC, which was then loaded onto a Macro-Prep Methyl hydrophobic chromatography column. The column was then washed with phosphate buffer containing 1.25, 0.9, 0.5 and 0.2mol/l $(NH_4)_2SO_4$, respectively. The collected eluent (with purity (A620/A280) above 4.0) was concentrated using a 30kDa ultrafiltration tube. Next, the sample incubation medium was changed to phosphate buffer (600mmol/L, pH8.0), and the sample was further purified by centrifugation in sucrose density gradient (0.2~0.5mol/L linear gradient, 600mmol/L phosphate buffer, pH8.0) on a Beckman Coulter l-100x ultracentrifuge for 16h (43,000rpm, 4℃, USA). The sample (with a sedimentation coefficient of about S20) was collected as a hexamer of C-phycocyanin.

In spectral studies (RS and IR studies), powdered PC was used and dissolved in 10x PBS with a concentration of 10mM. The pH of the solution was changed by titration with 1.5% hydrochloric acid and % sodium hydroxide solution to obtain a

protein with a specific pH value.

In the RS and IR analyses, we used powdered PC, which was dissolved in 10x PBS with a concentration of 10mM. In order not to interfere with fluorescence and to get the best results, we chose to measure 0.1mM protein solution (pH=7.0). The pH of 0.1mM phycocyanin solution was measured using a paper pH test. The solution was divided into 4 groups at pH5.5, pH6.5, pH7.0, pH7.5. To obtain suitable solutions with a specific pH value, the pH was measured by titration with 1.5% hydrochloric acid solution and 0.1%、1% sodium hydroxide solution.

2.21 Raman spectral analysis

2.21.1 Synthesis of silver nanostructures

[The joint authors of this paper: Liu W, Hao J, He Y.]

The silver nanostructures were synthesized according to the method developed earlier [152]. First, 2.93g of silver nitrate was dissolved in 40mL of Milli-Q water. In parallel, 7g of NaOH was dissolved in 30mL of water and then added by thin stream under stirring to the silver nitrate solution. The silver oxide precipitate precipitated during the reaction was washed three times with Milli-Q water (100 mL each), then 25ml of Milli-Q and 5mL of concentrated ammonia solution were added under constant stirring. As a result, a clear solution - ammonia complex of silver was obtained. Cover glasses were washed in detergent and held for 5 min in an ultrasound bath, air-dried and placed in a thermally stable glass beaker for 1 litre, which was placed on a pre-warmed surface at 380°C. A solution

of the silver-ammonium complex was poured into the vessel of an ultrasonic atomizer (Albedo PMP, TU 9444-001-49917419-2010, RF) (30ml) and sprayed onto the surface of the cover glasses by slow circular motions when heated to 380°C, pausing for a period of 5 min every 3 min. The distance of the atomizer nozzle to the cover glasses was 1.5-2.0cm. Then the glasses were incubated for 15 min at 400°C, after which they were cooled and packed in light-tight capsules. As a result, complex hierarchical nanostructures of metallic silver were formed on the glasses in the form of intersecting rings with a maximum diameter about 50 μm, covered with spherical particles with diameters ranging from a few units to tens of nm. The obtained nanostructures retained plasmonic properties for several months.

2.21.2 Analysis of DAAO and D-amino acids by Raman spectroscopy

[The joint authors of this investigation: Bochkova Zh. V, Li V.]

GRS spectroscopy was used to study the conformation of the FAD-cofactor of a purified preparation of D-amino acid oxidase isolated from porcine kidney (pkDAAO, Shanghai Haruno Biotechnology Co., Ltd.) in an oxidized state and with the addition of an excess of either D-alanine or D-serine.

The SERS spectra were recorded on a confocal microscope-spectrometer NTEGRA Spectra (NT-MDT, Zelenograd, Russia) coupled to an inverted microscope IX-71 (Olympus, Japan) in the range of 300-2000cm^{-1}, with a measurement step of 0.8cm^{-1}, the recorder was a Peltier-cooled CCD detector at -50℃.

The crystalline preparation of pkDAAO (obtained from pig kidney, Shanghai

yuanye Bio-Technology Co Ltd) was dissolved in sodium phosphate buffer (final protein concentration 1mg/mL). To conduct the experiment, a 20μl solution was carefully placed onto the bottom of a Petri dish that had a glass bottom (Metex). Subsequently, a glass fragment containing silver nanostructures was gently immersed into the liquid droplet, ensuring that the side with sputtered silver nanostructures faced downwards towards the laser beam. The laser beam was then precisely directed towards the liquid layer in proximity to the nanostructured surface using a ×20 lens featuring a numerical aperture of 0.45. This arrangement resulted in a laser spot with an approximate diameter of 800 nm. The laser had a wavelength of 532 nm and its power was carefully regulated to not exceed 1 mW. The accumulation time for signal acquisition varied across different experimental series, with values of either 1 or 60 s being employed.

The reaction of pkDAAO with substrate was initiated by adding an equivalent volume drop of D-alanine (100mM) or D-serine (100mM) solution in sodium phosphate buffer to a drop of solution (1mg/mL). To record the dynamics of the Raman signal from the FAD group of pkDAAO in the presence of substrates, the spectrum was taken every second for the first minute from the time of D-amino acid addition and then at one-minute intervals.

2.21.3 Analysis of Phycocyanin by using Raman spectroscopy

[The joint authors of this investigation: Parshina E.Yu., Li V., Yusipovich A.I., Gvozdev D., He Yang. Maximov G.V.]

Raman spectra of the sample were measured on a combined confocal

microscope-spectrometer Integra-Spectra (NT-MDT, Zelenograd, Russia) and on an InVia Qontor confocal Raman microscope (Renishaw, UK). The spectra were recorded on an Integra-Spectra microscope-spectrometer using an excitation light wavelength of 488 nm, a 600 pc/mm grating, a 20x objective, and a spectrum recording time of 60s. The sample was dried in the form of a drop on a mirror glass, and the spectra were recorded from the edge of the drop.

For registration of spectra on inVia Reflex Renishaw microscope-spectrometer we used excitation light wavelength 785 nm, grating 1200l/mm(vis), objective 50x, spectrum exposure time 5s, laser power 50% (MAX=280mW for 785nm), accumulation 1, spectral range 200-1800nm. The spectra were recorded from a drop of phycocyanin solution (about 10 mM) applied to the foil [153].

NTEGRA-SPECTRA confocal microscope-spectrometer (NT-MDT, Zelenograd, Russia) based on Olympus IX microscope, 5x objective (Olympus, Japan), 40x (Olympus, Japan), 532 nm laser, WITec alpha 300 Raman spectrometer, 5x objective (Zeiss, Germany), 532 nm laser (WITec, Germany), Zetasizer Nano ZS (Malvern, Russia), pH410 pH meter (Akvilon, Russia), Laborfuge 400R centrifuge (Thermo Scientific, USA), Gnome thermostat (DNA -technologies, Russia), solid-state thermostat "Termit" (DNA-technologies, Russia), power supply "Elf-8" (DNA-technologies, Russia), phase-contrast laser interference microscope developed at VNIIOFI on the basis of Linnik's micro-interferometer MII- 4 (FKM) (VNIIOFI, Russia), Spectrum Two IR-Fourier spectrometer (Perkin Elmer, USA), 16-channel time-correlated spectrograph with 45 single-photon counts (PML-SPEC, Becker & Hickl GmbH, Germany), Flame UV/ VIS (Ocean Insight, USA).

2.21.4 Raman spectroscopy of β-carotene

We conducted a study on Raman scattering of β-carotene using an in-via Basis spectrometer (Renishaw, Great Britain). To excite the sample, a laser emitting radiation at a wavelength of 532nm and a power of 100mW was employed, along with a 50× objective. Raman scattering was detected by a CCD detector (1024 × 256 pixels) equipped with Peltier cooling to -70°C. The grating used had 1800 lines/mm. Prior to analysis, we visually identified the location of the Raman scattering nano-structured substrates (coatings) using a Leica class microscope. For analyzing carotene, we focused on the characteristic bands within the Raman spectrum, specifically within the range of 600 to 2000cm^{-1}.

2.21.4 The preparation of nanostructures for SERS [153]

In this study, we used substrates with a silver-based nanostructured coating, onto which carotene samples were applied (2 — 0.02μ/ml or 37nMol/L — 3.7nM/L). Substrates were obtained by nano-structuring using the technique outlined in [154]. An aqueous solution of sodium hydroxide (0.1M NaOH, high purity water, Milli-Q, Millipore) was added dropwise to a freshly prepared solution of 0.01M aqueous silver nitrate until a black-brown oxide of silver (I) was completely precipitated. The prepared oxide was washed thoroughly with deionized water and dissolved in a twofold molar excess of a 10 % aqueous solution of ammonia to have a solution of 0.01M of a silver complex (I). The resulting clear silver complex

solution was filtered through filter units driven by Millex-LCR syringes (Millipore, 0.45 microns pores). This initial ammonia solution of silver (I) oxide was then nebulized into mist and 1–5micron droplets were poured onto 'warm' glass, alumina, or microporous silica substrates (270°C) over the course of 40–60 min (possible 250°C, deposition thickness 45nm).

2.22 Registration of proteins infrared spectra (IR)

[The joint authors of this investigation: Parshina E.Yu., Li V., Yusipovich A.I., Gvozdev D., He Yang. Maksimov G.V.]

Infrared spectra of the sample were recorded on a Spectrum Two FT-IR spectrometer (Perkin Elmer, USA) with an incomplete internal reflection attachment (ATR-FTIR). A drop of protein solutions in buffer with different pH values was applied to a zinc selenide window, the signal was recorded in the range 550 - 4000cm^{-1} with a scanning step of 4cm^{-1} in 4 repetitions, 3 spectra were measured from each drop. The obtained spectra were processed in the program Unscrambler X 10.4 (CAMO, Nedre Vollgate, Norway). The spectra were presented as a dependence of absorbance on the wave number; to eliminate the impact of the water spectrum and the distinctive bands of buffer components, the protein solution's spectra were adjusted by subtracting the buffer spectrum. Additionally, the spectra were normalized to the amplitude of the broad band located in the 2000cm^{-1} region.

In order to analyze the protein's secondary structure, the Gaussian curve fitting approach was employed for the Amide I band within the 1600-1700cm-1

region. The algorithm [155] was utilized for this purpose. The precise location of the band's peak was determined by smoothing the spectrum, calculating the second derivative, and subsequently subtracting the baseline. The Peak Analyzer module of the OriginPro 2022 program was employed for fitting the spectra. Gaussian curves were employed to approximate the various bands [155].

For the DAAO protein, the following ranges were observed for different structures: α-helices: 1656 ± 2.0, 1663 ± 3.0cm^{-1}; single-chain protein structures: 1624 ± 1.0, 1627 ± 2.0, 1633 ± 2.0, 1638 ± 2.0, 1642 ± 1.0 ,1691 ± 2.0, 1696 ± 2.0cm^{-1}; β-helices: 1667 ± 1.0, 1675 ± 1.0, 1680 ± 2.0, 1685 ± 2.0cm^{-1}; undetermined structure: 1.648 ± 2. 0cm^{-1}.

2.23 Absorption and fluorescence spectra of phycocyanin (PCs) and DAAO.

[The joint authors of this investigation: Parshina E.Yu., Li V., Yusipovich A.I., Gvozdev D., He Yang. Maximov G.V.]

The absorption spectra of phycocyanin (PCs) were obtained by utilizing a MayaPro spectrophotometer, specifically from Ocean Optics located in the United States. To achieve this, we utilized a stabilized white light source equipped with an SLS201L tungsten lamp provided by Thorlabs, also from the United States. For fluorescence spectra analysis, we used a Flame spectrophotometer from Ocean Optics, again, in the United States. To perform fluorescence excitation, we utilized a PLS-510 LED laser manufactured by InTop, a company based in Russia, with a specific wavelength of 510nm. During the measurements, we maintained a

constant temperature of 25°C using a thermostatted Qpod 2e cuvette holder from Quantum Northwest, United States, along with magnetic stirring at a rate of 500 rpm. Furthermore, the measurements were conducted in a quartz cuvette with a capacity of 1ml.

The absorption characteristics of D-amino acid oxidase solutions were observed using a two-beam scanning spectrophotometer, Specord UV VIS (manufactured by Carl Zeiss Jena in Germany). The measurements were conducted within the wavelength range of 400-600 nm. Plastic cuvettes with a path length of 1cm were employed for these observations. The absorption spectrum exhibited a peak at 450 nm. During the measurements, the enzyme concentration was set at 5.7μM ($\varepsilon 445 = 11300 M^{-1} \cdot cm^{-1}$, 158). Specifically, 18.5μl of the enzyme stock solution was mixed with 1 ml of the buffer solution.

Prior to recording the absorption spectra, a baseline measurement was taken using the buffer solution (20mM Na-PB, pH6.5). After each measurement of enzyme solution was monitored by addition of crystallized D-alanine to a concentration of 5mM enzyme solution, with an incubation time of at least 5min. Finally, to 1 ml mixture of pkDAAO enzyme and alanine solution add 2mg of the strong reducing agent, crystalline sodium disulfide phosphate.

To record the absorption spectra, the baseline was first measured against the buffer solution (20mM Na-PB, pH6.5). Afterward each measurement of the enzyme solution was followed by the addition of crystallized D-serine to a concentration of 5mM enzyme solution, with an incubation time of at least 5min. Finally, to 1 ml mixture of pkDAAO enzyme and alanine solution add 2mg of the

strong reducing agent, crystalline sodium disulfide phosphate.

2.24 Measurement of the attenuation kinetics of fluorescence anisotropy of PC.

[The joint authors of this investigation: Parshina E.Yu., Li V., Yusipovich A.I., Gvozdev D., He Yang. Maximov G.V.]

Fluorescence anisotropy experiments were performed on a standard fluorescence setup with 90° excitations (L-configuration). To excite the fluorescence of PCs, a PLS-510 LED laser (InTop, Russia) was used in pulse mode (pulse duration 25ps, pulse repetition rate 50MHz). The excitation light used was polarized using a broadband polarization filter (Thorlabs, USA). Fluorescence attenuation kinetics of PCs with picosecond time resolution was recorded on a SimpleTau-140 (Becker & Hickl, Germany). The fluorescence signal was passed through a ML 44 monochromator (Solar laser systems, Belarus) in the 640nm range and recorded with a hybrid HPM-100-40 detector (Becker & Hickl, Germany) with an emission polarizer in vertical and horizontal positions. The emission polarizer was rotated using a motorized support (K10CR1/M, Thorlabs, USA), the rotation angle was set using APT software (Thorlabs, USA).

2.25 Determining the Size of Protein Molecules by Dynamic Light Scattering (DSL)

[The joint authors of this investigation: Parshina E.Yu., Li V., Yusipovich A.I., Gvozdev D., He Yang. Maximov G.V.]

Dynamic Light Scattering the method of dynamic light scattering (DRS,

(photon correlation spectroscopy, quasi-elastic light scattering) is used in laser correlation spectroscopy to determine the diffusion coefficient of dispersed particles in a liquid. The essence of the method is to measure local in homogeneities of the refractive index of the medium, which arise due to the chaotic The size of the particles must be of the same order as the wavelength of the scattered light - only in this case is it possible to scatter light on the particles 1 ml of the resulting solution was placed in a disposable polystyrene DTS0012 cuvette for measuring dynamic light scattering (Malvern, UK) with an absorbing layer thickness of 12 mm. Adaptation of the sample to temperature - 60 seconds, the number of measurements taken - 100. Each measurement was carried out at least five times. The results were processed using the Malvern software supplied with the Zetasizer Nano ZS instrument and MS Excel (2010).

The size of protein molecules was determined using a Zetasizer Nano ZS (Malvern, UK). The experiments were conducted in a temperature-controlled cell at a temperature of +25°C. It took the samples approximately 60 seconds to adapt to this temperature. A total of 100 measurements were recorded during the experiment. Each measurement was executed no fewer than five times. The obtained data were analyzed using the Malvern software that accompanies the Zetasizer Nano ZS apparatus, as well as MS Excel.

2.26 Picosecond fluorescence of tryptophan.

The conformational state of DAAO was diagnosed using time-correlated

single-photon counting (TCSPC) of tryptophan (Trp) fluorescence (τfl Trp) in the 340nm range (pulsed ultraviolet LED (EPLED 265nm) fluorescence excitation at 261nm). PML-SPEC, Becker & Hickl GmbH, Germany))[156].

3. RESULT AND DISCUSSION

3.1 DAAO gene analysis of the yeast Hasenula polymorpha

3.1.1 Comparison of AK after-treatment of DAAO genes of *H. Polymorpha*.

The genes HP02082, HP2165, HP2194, HP2400 in the DL1 strain encode proteins ranging in size from 332 to 359 a.c. and are members of the FAD-dependent oxidoreductase superfamily based on the annotations.

The degree of sequence similarity of these proteins in pairwise alignment ranges from 44 to 50%. Multiple alignment of all 4 sequences with the DAAO sequences of the yeast *Pichia pastoris* can easily reveal several conserved motifs. Earlier in our group, Ekaterina Lobanova obtained knockouts for 2 of the 4 genes (Fig. 12).

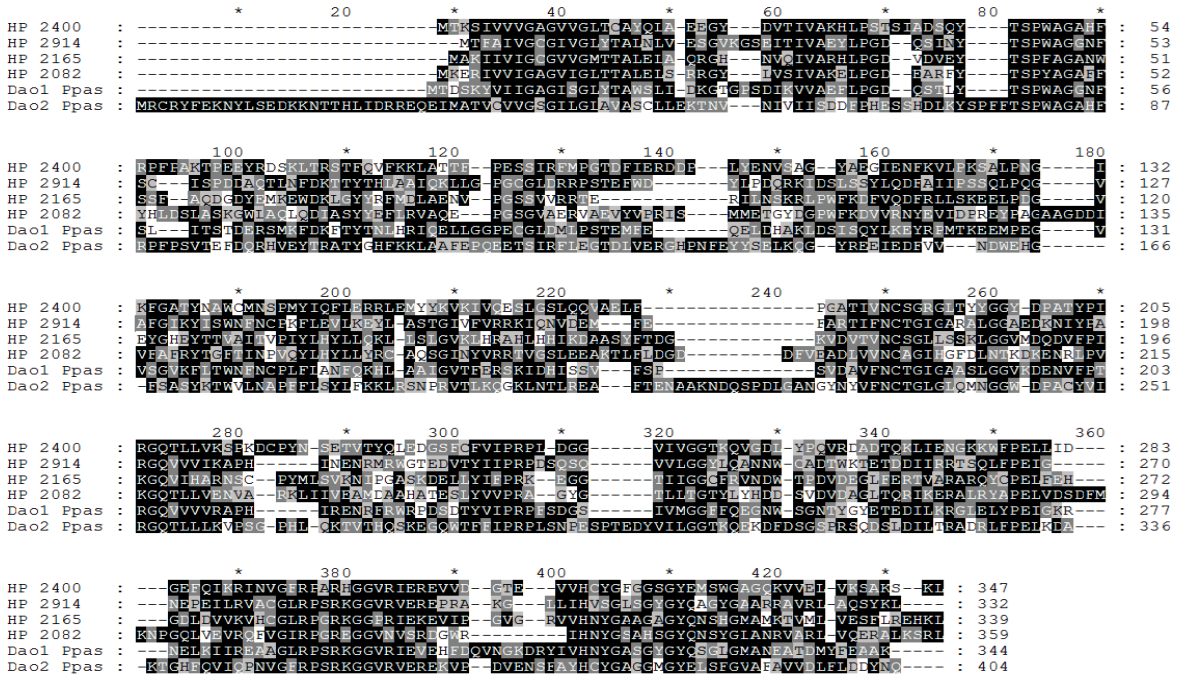

Fig. 12 Multiple alignment of DAAO genes in strain DL1

3.1.2 Construction of plasmids for genetic inactivation of DAO genes from the yeast Hansenula polymorpha

3.1.2.1 Design and construction of a vector to produce a knockout on the HP_2082 gene.

To search for suitable restriction sites, the sequence of the HP_2082 locus with flanking sites extracted from the NCBI database was analyzed using the NEB cutter program to identify double sites located 0.7-1.5 tpn from the beginning and end of the HP_2082 OPC that are absent in the pAM773 vector.

Suitable SalI sites were found at positions 77 and 3702 of the *H. Polymorpha* chromosomal DNA region to the left and right of the HP2082 gene shown in Fig. 13. The matrix for cloning the flanking fragments was obtained after hydrolysis of

genomic DNA using SalI and subsequent ligation. The primers 2082L_Bgl2 and 2082R_Spe1, selected using Ugene software, included the flanking restriction sites BglII and SpeI, which are part of the two MCSs of the pAM773 vector and are absent in the two flanking sequences (between the SalI sites and the primers).

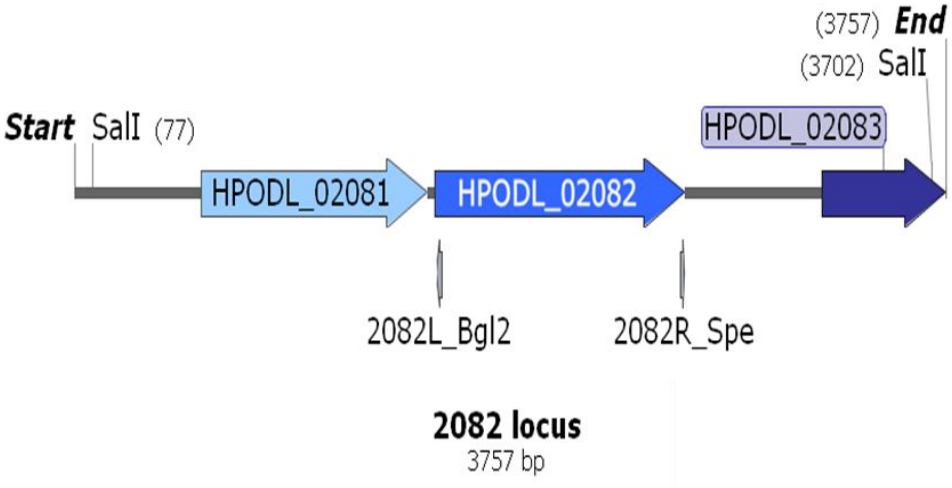

Fig. 13 Schematic of the HP2082 locus and flanking sites.

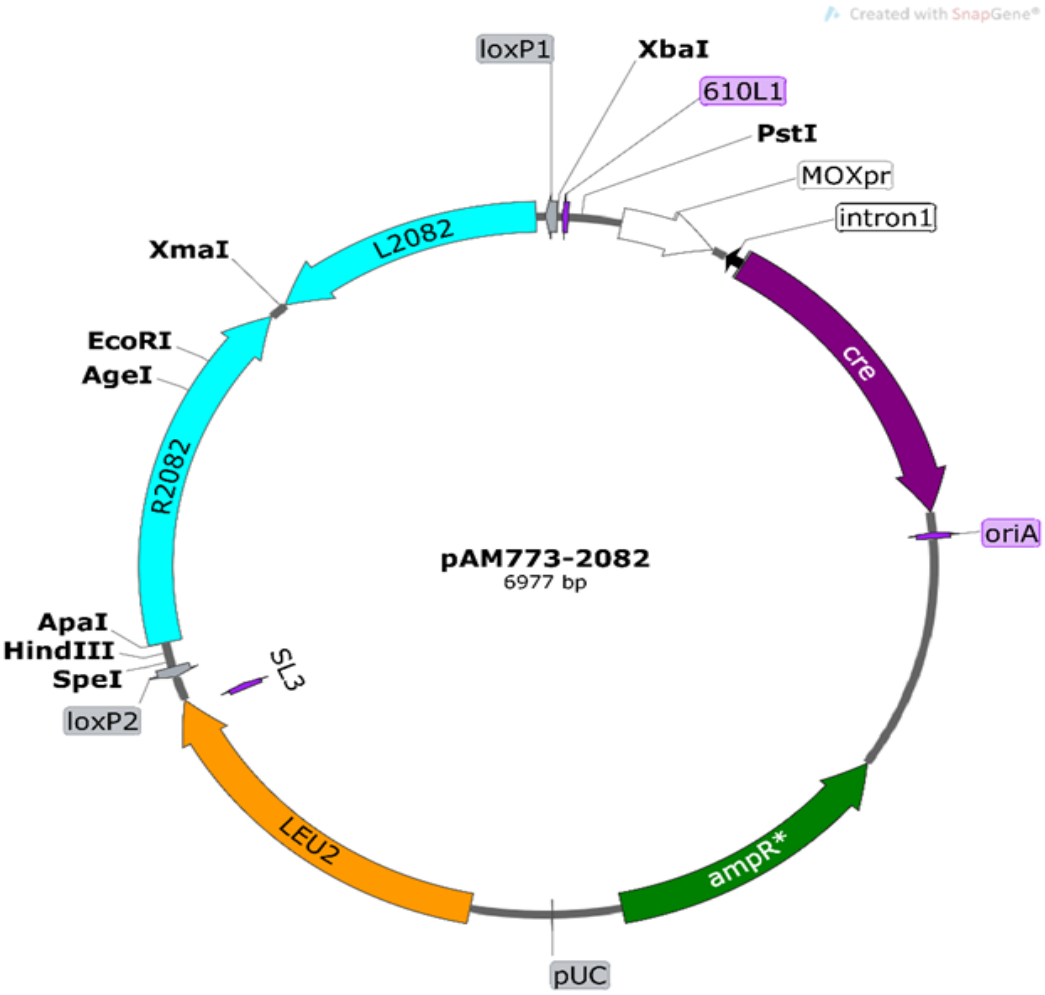

Fig. 14 **S**chematic diagram of plasmid LW2082

The obtained preparation was used as a matrix for PCR with primers 2082L_Bgl2 and 2082R_Spe1, specifically annealing at the ends of the cloned fragment and carrying flanking restriction sites BglII and SpeI.

After PCR, a 2500 bp fragment was obtained on the resulting matrix using Phuzion polymerase, which was cloned into the pAM773 vector after SpeI/BglII hydrolysis, and the resulting plasmid was designated LW2082 (Fig. 14)

3.1.2.2 Design and construction of a vector to produce a knockout for the HP_2400 gene.

Using the NEB cutter program, suitable BglII restriction sites were found at positions 172 and 2145 of the *H. Polymorpha* chromosomal DNA region to the left and right of the HP2400 gene (Fig. 15).

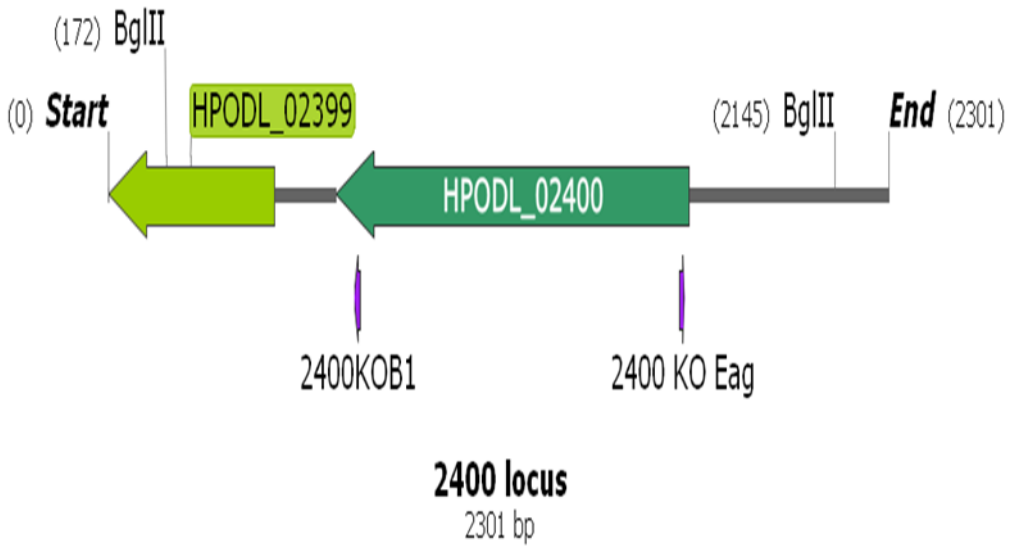

Fig. 15 Schematic of the HP2400 locus and flanking sites.

The obtained preparation was used as a matrix for PCR with primers 2400KOB1 and 2400KOEag, flanking restriction sites BamHI and EagI (absent in the two flanking sequences) were introduced, specifically annealing at the ends of the cloned fragment and carrying flanking restriction sites BamHI and EagI. The 900 bp PCR product was hydrolyzed at the EagI/BamHI sites and inserted into the pAM773 vector at the EagI and BamHI sites. The resulting plasmid was designated as LW2400 (Fig. 16)

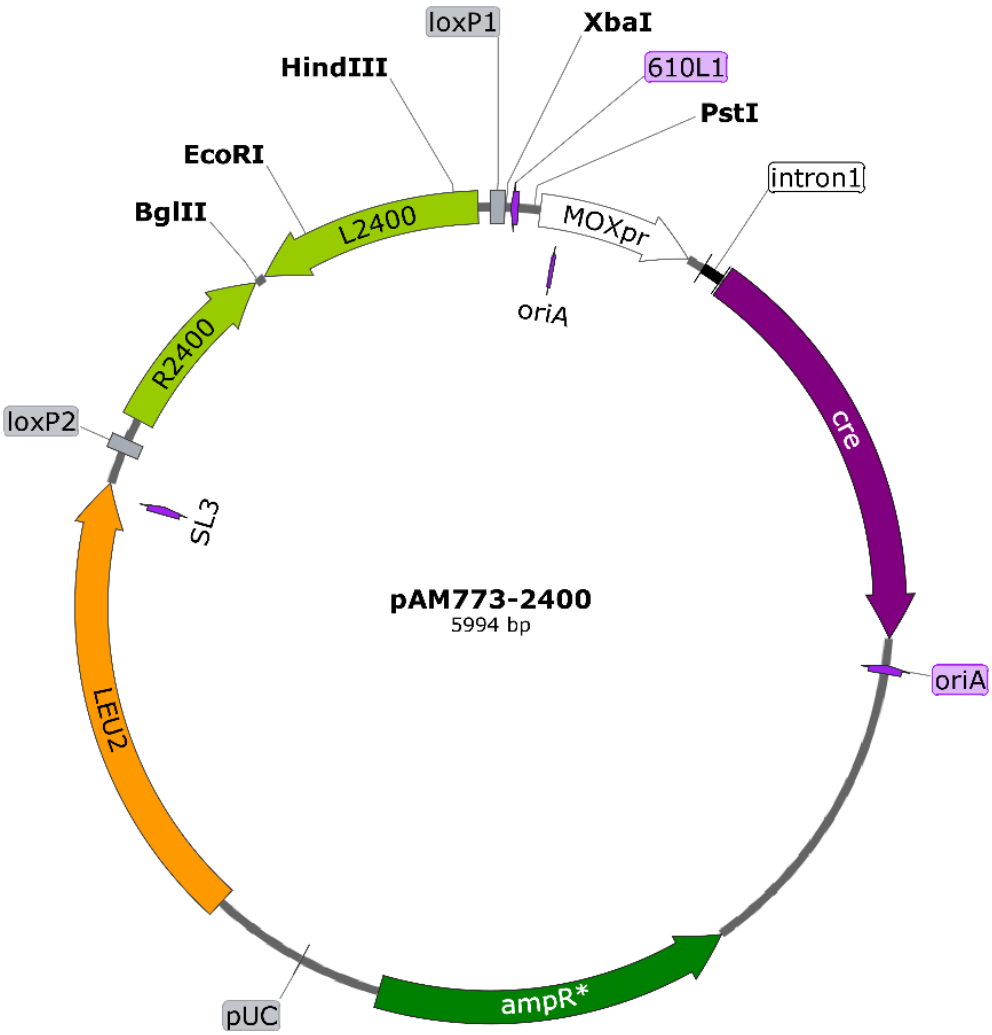

Fig. 16 Schematic diagram of plasmid LW2400.

3.1.2.3 Design and construction of a vector to obtain a knockout of the HP_2165 gene.

Using the NEB cutter program, suitable XmaI restriction sites were found at positions 127 and 3371 of the *H. Polymorpha* chromosomal DNA region to the left and right of the HP2165 gene shown in Fig. 17.

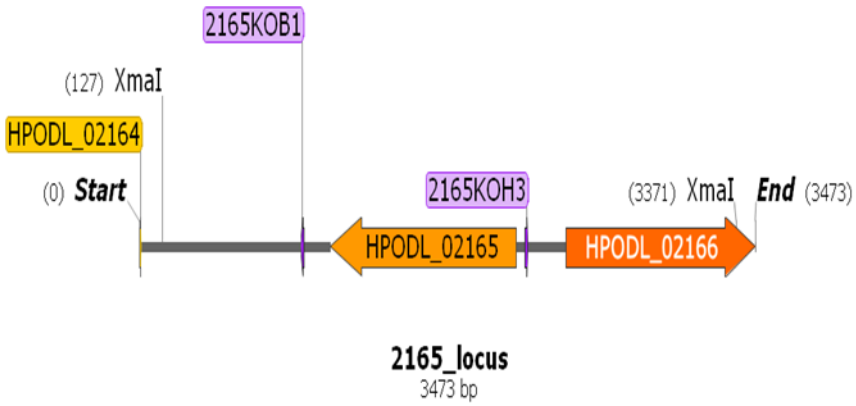

Fig. 17 Schematic of the HP2165 locus and flanking regions.

To clone the HP2165 gene, the genomic DNA was hydrolyzed using XmaI restrictionase, followed by ligation to form ring structures. The obtained product was used as a matrix for PCR with primers 2165KOB1 and 2165KOH3 specifically annealing at the ends of the cloned fragment and carrying flanking restriction sites BamHI and HindIII. The 2100 bp PCR product was hydrolyzed at the HindIII and BamHI sites and inserted into the pAM773 vector at the HindIII and BglII sites. The resulting plasmid was designated as LW2165.(Fig. 18)

3.1.3. Preparation and characterization of transformants with HP2400 gene knockout.

2µg of LW2400 plasmid DNA was hydrolyzed by BglII restrictionase, the product was purified using CleanUp Mini kit (Eurogen) and eluted in a volume of 12µl. For transformation of strain DL1, 5µl of sample was used. The transformation resulted in 45 clones, 12 were used for analysis.

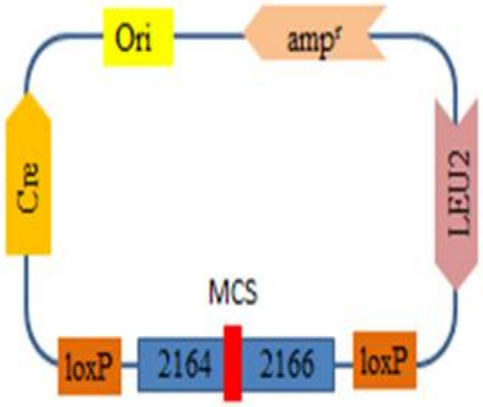

Fig. 18 Schematic diagram of plasmid LW2165. Where Cre, Cre-encoding ORF with intron; ori, bacterial replication source; ampr, bacterial marker of ampicillin resistance with deleted ScaI site; LEU2, S. cerevisiae Gene LEU2 with deleted EcoRI, EcoRV and KpnI restriction sites having wild-type promoter or modified to work better in *H. Polymorpha*; MCS, multiple unique cloning sites[157].

To confirm the accuracy of the integration border on the left, PCR analysis of the isolated DNA was performed using primer pair 2400LF1/610, which expected an 800bp fragment. This fragment was found in 12 of 12 samples. (Fig. 19).

To check the correctness of the left integration boundary, we performed PCR analysis of the isolated DNA with primer pair 2400RFl/SL3, expecting fragments of 900 bp in size. Such fragments were detected in 11 out of 12 samples. (Fig. 20)

For induction of excision, the transformant inserts were transferred to medium with methanol. The resulting leu clones are currently being analyzed.

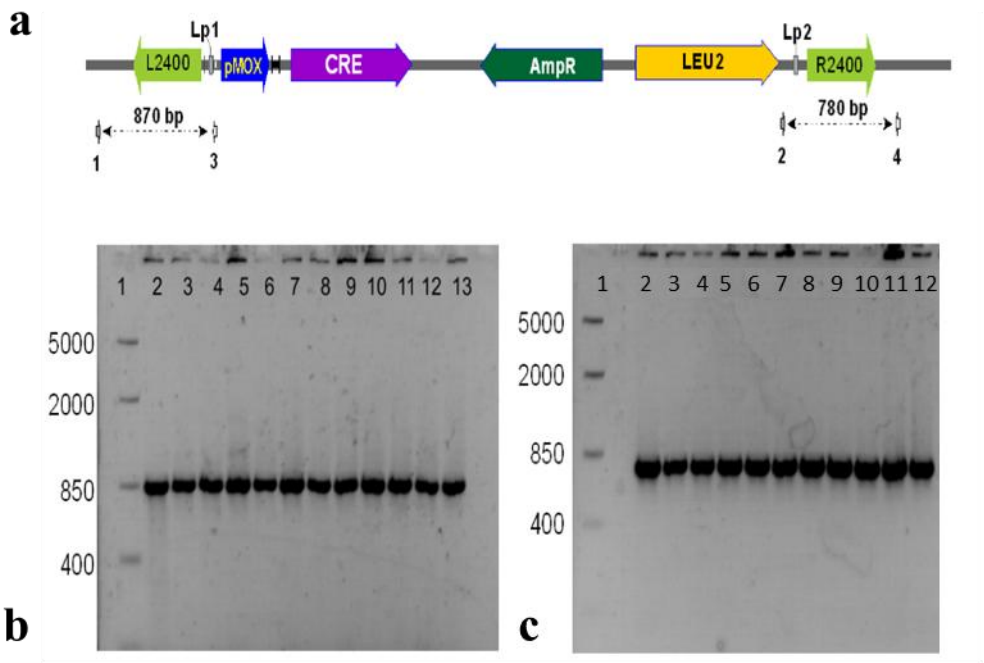

Fig. 19 Schematics of the HP2400 locus cassettes and din fragments on the right and left sides. a - Schematics of HP2400 locus cassettes and fragments on the right and left sides; b - PCR analysis confirming the presence of the target locus L2400 sequence. 1- marker 5 kb DNA ladder, 2-13 restricted locus L2400 - BglII on the left side with primer pair 2400LF1/610; c - PCR analysis confirming the presence of the target locus R2400 sequence. 1- marker 5 kb DNA ladder, 2-12 restricted locus R2400 - BglII on the right side with primer pair 2400RFl/SL3.

3.1.4 Characteristics of the genotypes of the obtained knockouts.

In total the following knockout strains were obtained: Single-knockout: D2400::loxP, Double-knockout: D2165::Zeo D2082::loxP, D2914::Zeo D2400::loxP, D2400::loxP D2082::loxP , triple knockout: D2914:: loxP: Zeo, D2400::loxP D2082::loxP.

To investigate the biochemical and physiological characteristics of the obtained strains, we used the collection created in conjunction with the previously obtained D2165::Zeo D2914::Zeo strains.

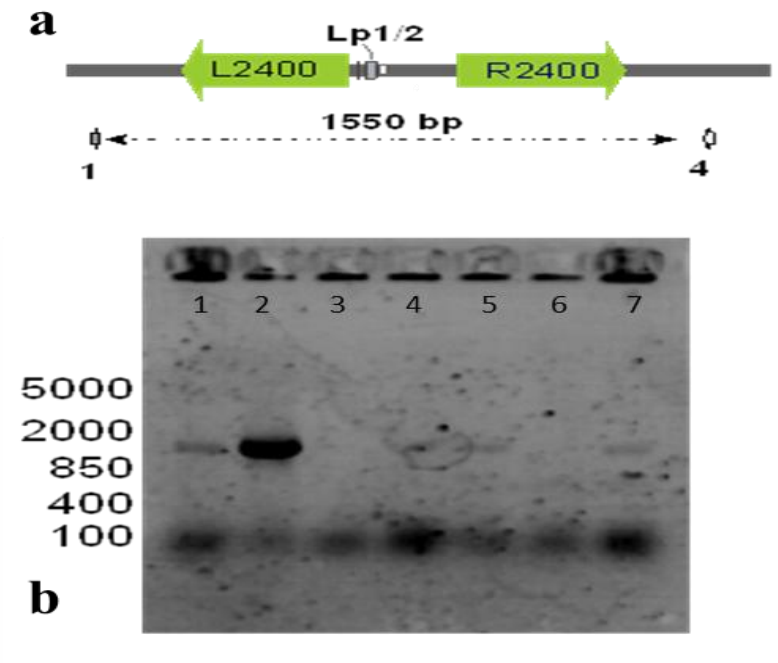

Fig. 20 Separation electropherogram in 1.7% agarose gel of PCR products obtained during screening of DL1/LW2400 knockout clones with primers 2400RFl/SL3. a - Schematic of the HP2400 knockout locus and its fragment length ; b- PCR analysis to verify the knockout of *H. Polymorpha* clones. 1- marker 5 kb DNA ladder, 2-7 DNA ligation. 2-7 checks of "knockout" *H. Polymorpha* clones at locus 2400, of which 2- successful, 3-7 unsuccessful shifts.

3.1.5 Culture properties of the strains

3.1.5.1 Cultivation of knockout strains in liquid and dense YNB media with different nitrogen sources

A series of experiments revealed that the introduced genetic modifications did not result in growth retardation compared to the original - DL1 recipients and previously obtained single knockouts D2165::Zeo, D2914::Zeo. The result was obtained by analyzing the growth pattern of cultures on 1xYNB liquid media (without amino acids and ammonium sulfate, 0.17% w/v) using 2% glucose or 1% methanol as a carbon source.

The method of serial dilutions was used for rapid assessment of growth parameters and the degree of stress resistance of strains. As a result, 3 μl of dilutions (10-4,10-3,10-2,10-1) were applied to dishes with dense YNB medium with different sources of nitrogen (ammonium sulfate, D-alanine, D, L-alanine), carbon, with the addition of 0.5 M sodium chloride (resistance to osmotic stress), 2 mM hydrogen peroxide (resistance to oxidative stress) (Fig.5). Differences in the character of growth of strains on solid medium were observed, as well as differences in the degree of sensitivity of strains to osmotic stress (growth on cups with 0.8 M NaCl), oxidative stress (growth on cups with 2.5 mM hydrogen peroxide).

This study revealed differences in the growth rate of strains on dense media with D, L-alanine. Double knockout experiments with D2165::Zeo D2082::loxP (Δ2082/2165) and D2400::Zeo D2082::loxP (Δ2082/2400) showed increased

growth compared to the other strains. In the Δ2082/2165 strain, the 2082 and 2165 genes were missing, while the 2914 and 2400 genes were retained; in the Δ2082/2400 strain, the 2082/2400 gene was knocked out, while the 2165/2914 gene was retained.

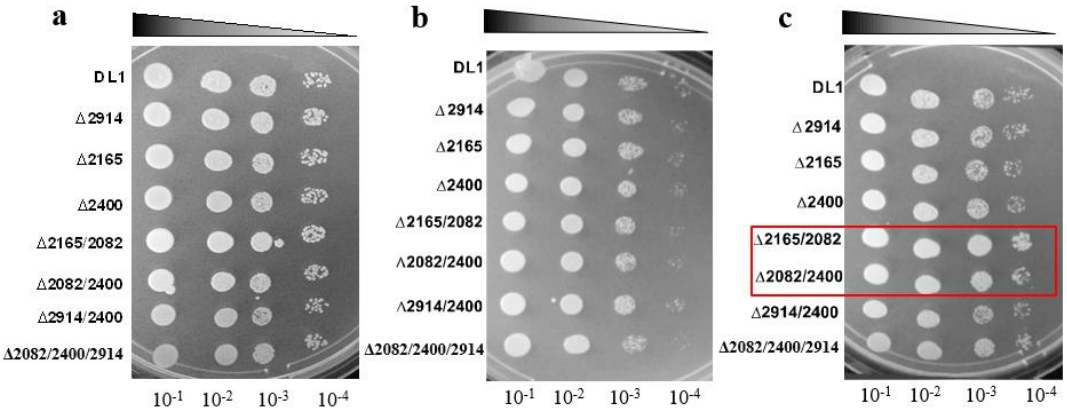

Fig. 21 Анализ роста штаммов в стандартных условиях YNB с разными источниками азота. **a** - YNB + AS/2% Glu; **b** – YNB + AS/1% Gly/1% Met; **c** - YNB + DL-ala/ 1% Gly/1% Met d - Table name of knockout and its gene residue. Where AS - 0.5% ammonium sulfate; DL-Ala - 30mM DL-alanine; 2% Glu - 2% glucose; 1% Gly 1% Met - 1% glycerol1% methanol

Therefore, the activity of all three major DAAOs of H.polymorpha (as 2165, 2400 and 2914) was able to induce by D-alanine combined with 1% glycerol and 1% methanol. Compared with other strains in the same group, strains with 2914/2400 gene (Δ2082/2165) and 2165/2914 gene (Δ2082/2400) grew better, of which Δ2082/2165, which with 2914/2400 gene, grew even better. Therefore, it can be assumed that D-alanine combined with 1% glycerol and 1% methanol induces the

expression of HP2165 and HP2914 genes. Since the HP2914 gene is not affected in these strains, it can be assumed that this gene is important for the oxidation of D-alanine (**Ошибка! Источник ссылки не найден.**).

3.1.5.2 Growth of strains on different cultures with sources of nitrogen and carbohydrate

The difference in strain growth parameters was more dramatic with prolonged culture on liquid media. Fig.22 showing the ratios of the densities of cultures grown for 72 hours in liquid medium under the same conditions on medium with D-alanine and a mixture of glycerol and methanol as well as medium with ammonium sulphate and glucose. The recipient DL1, HP2165, HP2400 and triple knockout strains had much better growth on medium supplemented with DAla-glycerol-methanol, whereas the HP2914 gene knockout strain, in contrast, grew best on medium supplemented with ammonium sulphate and glucose. This led to the suggestion that the HP2914 gene encodes an oxidase that is important for growth on this substrate.

3.1.5.3. Carbon and nitrogen sources to induce oxidase activity

We analyzed the relation between oxidase activity in cells of strains grown on different media. It turned out that in strain DL1 grown on medium with D-ala and 1% glycerol and methanol the activity towards three different substrates - D-Ala, D-Asp, D-Phe - was increased 10-25 times. In this case, in the double mutant d2400-2914 the activity to D-Ala and D-Asp was weakly expressed to D-Ala and

D-Asp

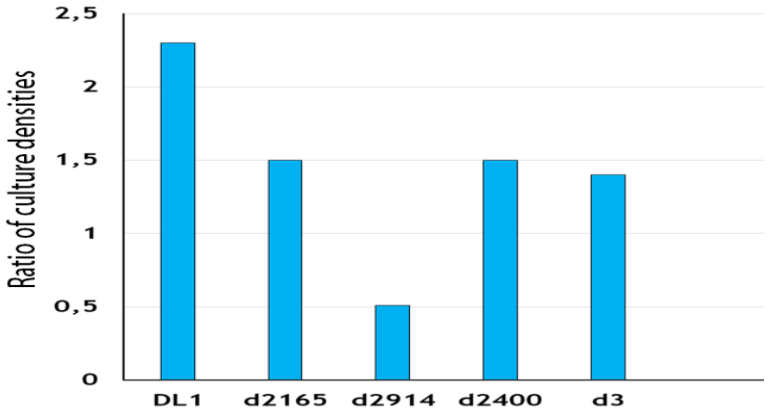

Fig. 22. Differences in the growth parameters of strains grown on media with different sources of nitrogen and carbon. (The culture density ratio is the ratio of the growth of the strain on a medium containing a mixture of 1% glycerol and 1% methanol with D-Ala as the nitrogen source to the growth on a medium containing ammonium sulfate and 2% glucose.).

and more sharply to D-Phe, in the double mutant d2165-2082 - weakly to D-Phe and expressed to D-Ala and D-Asp, in the triple mutant the activity to D-Ala was best induced. (Fig. 23).

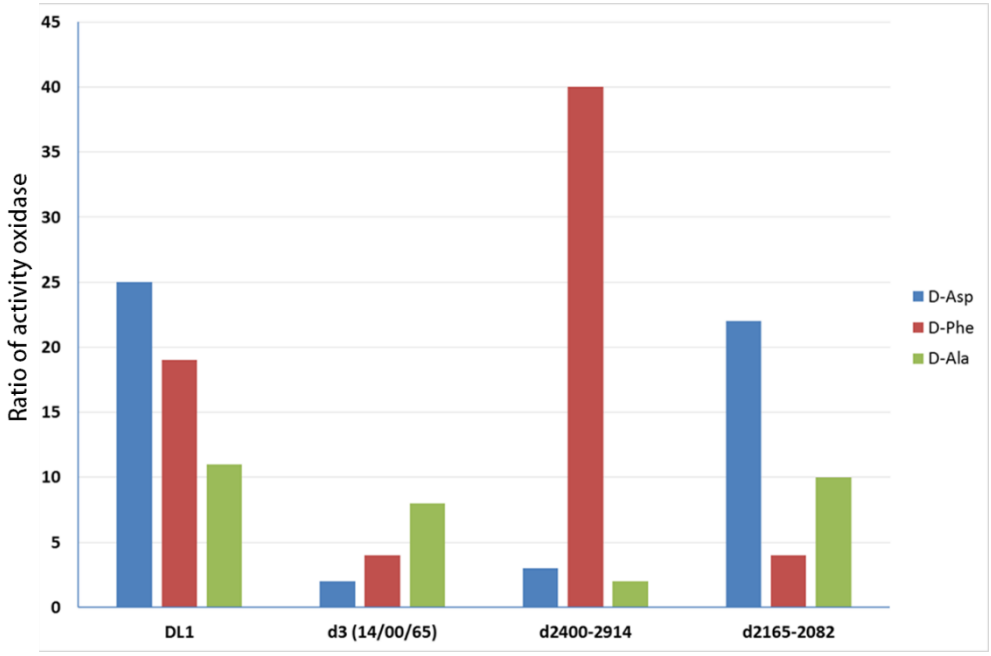

Fig. 23 Carbon and nitrogen sources to induce oxidase activity. (The ratio of oxidase activity is equal to the ratio of the growth of the strain on medium with D-Ala as nitrogen source and a mixture of 1% glycerol and 1% methanol to the growth on medium containing ammonium sulfate and 2% glucose)

3.1.5.4 Substrate specificity of oxidases as determined using knockout strains

Our partners from the Department of Chem Enzymology carried out work on obtaining functionally active recombinant oxidases HP2165, HP2914, HP2400 in *E. coli* cells. Substrate specificity analysis showed that the HP2914 gene encodes a 1-type oxidase most specific for D-Ala and other "small" a.c.o., the HP2165 gene encodes a 2-type oxidase most specific for D-Phe, the HP2400 gene encodes an aspartate oxidase strictly specific for D-Asp, D-Glu. These data are well supported by activity assays on intact cells in the knockouts obtained. Here we present the ratio of activities to different substrates in the original and knockout strains determined on cells obtained when cultured under optimal induction conditions. In

the double knockout of HP2914-2400, which the remaining gene HP2165, the predominant activity is driven by D-Phe; in the double knockout HP2082-2400, activity is driven by the ratio of D-Ala to D-Phe; on the HP2082-2165 double knockout, the activity is determined by D-Asp; and on the triple knockout, the activity is determined by the ratio of D-Ala. One possible explanation for the stimulation of activity in the knockouts relative to the remaining non-deletion gene is the greater availability of the -FAD cofactor for the formation of the holoenzyme due to reduced competition from other oxidases. The residual activity may be due to both the action of the major DAAO and the activities of racemase and L-amino acid oxidase whose genes have not yet been identified (Fig. 24).

3.1.5.5 Comparative role of nitrogen and carbon sources in the induction of oxidase activity

Dao1 gene expression in the yeast *Rhodotorula gracilis* is induced by D-Ala, inhibited by L-Ala, and likely to be repressed by glucose [158]. We compared the pattern of induction of activity towards D-Ala when strain DL1 was grown on media with different nitrogen (D-Ala, DL-Ala, ammonium sulfate) and carbon sources (Fig. 25). The role of D-Ala as an efficient inducer of DAAO activity during growth on glycerol-and methanol-containing medium was further supported. Glucose and

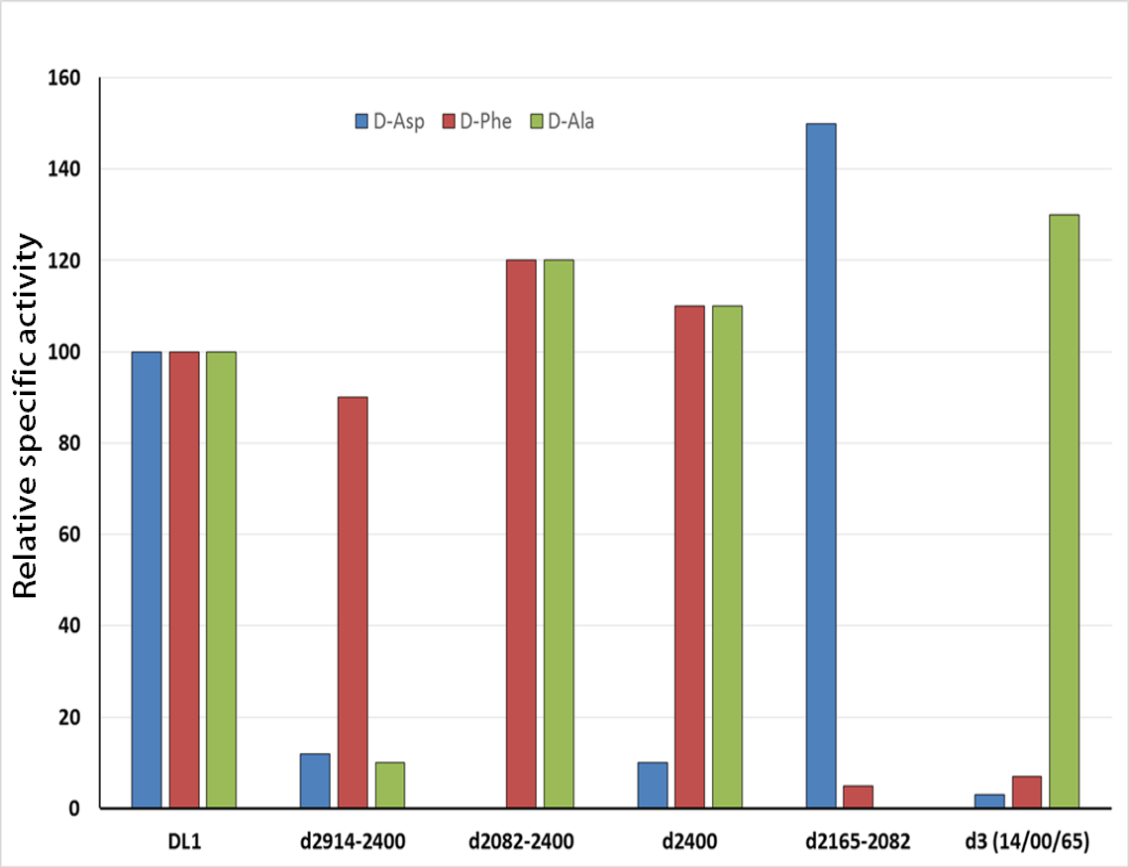

Fig. 24 Substrate specificity of oxidases determined using knockout strains (specific activity ratio is the ratio of the number of strains grown on medium with D-Ala as a nitrogen source and a mixture of 1% glycerol and 1% methanol to the number of strains grown on medium with ammonium sulfate and 2% glucose.).

ammonium sulfate inhibited DAAO activity. On medium with glucose, DL-Ala is a weak inducer of DAAO. Thus, the character of DAAO activity induction in *H. Polymorpha* and R. gracilis was similar.

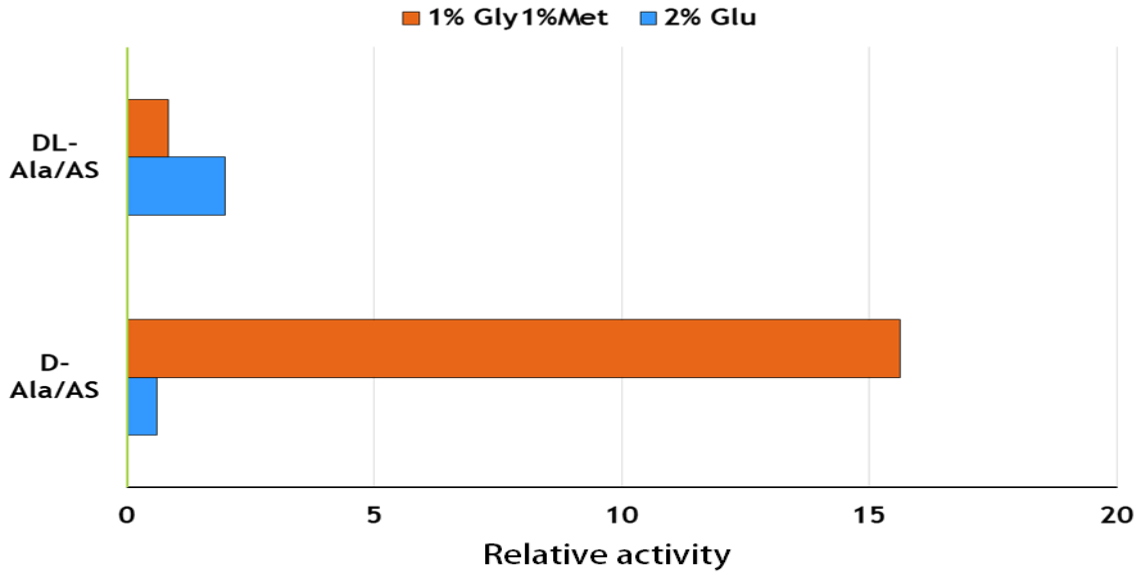

Fig. 25 Relative activity of strain DL1 grown for 72 h on medium with different sources of nitrogen and carbohydrates. Where **DL**-Ala/AS is the substrate DL-alanine and ammonium sulfate; **D**-Ala/AS is the substrate D-alanine and ammonium sulfate.

3.1.5.6 RT-PCR analysis of DAAO gene expression

To investigate the nature of the transcriptional regulation of the DAAO genes, we analyzed their expression by RT-PCR during growth of the DL1 strain on media with different nitrogen and carbon sources (Fig. 26). Growth on medium supplemented with D-Ala and a mixture of glycerol and methanol was shown to induce the expression of the genes HP2914, HP2165. These data indicate the similarity of the nature of regulation of DAO gene expression in yeast *H. Polymorpha* and *R. gracilis*. Growth on medium with DL-ala induces the expression of HP2082 gene. The recombinant HP2082 protein obtained in *E. coli*

cells has very weak oxidase activity, so the contribution of this gene to the total DAO activity of *H. Polymorpha* cells is still unclear.

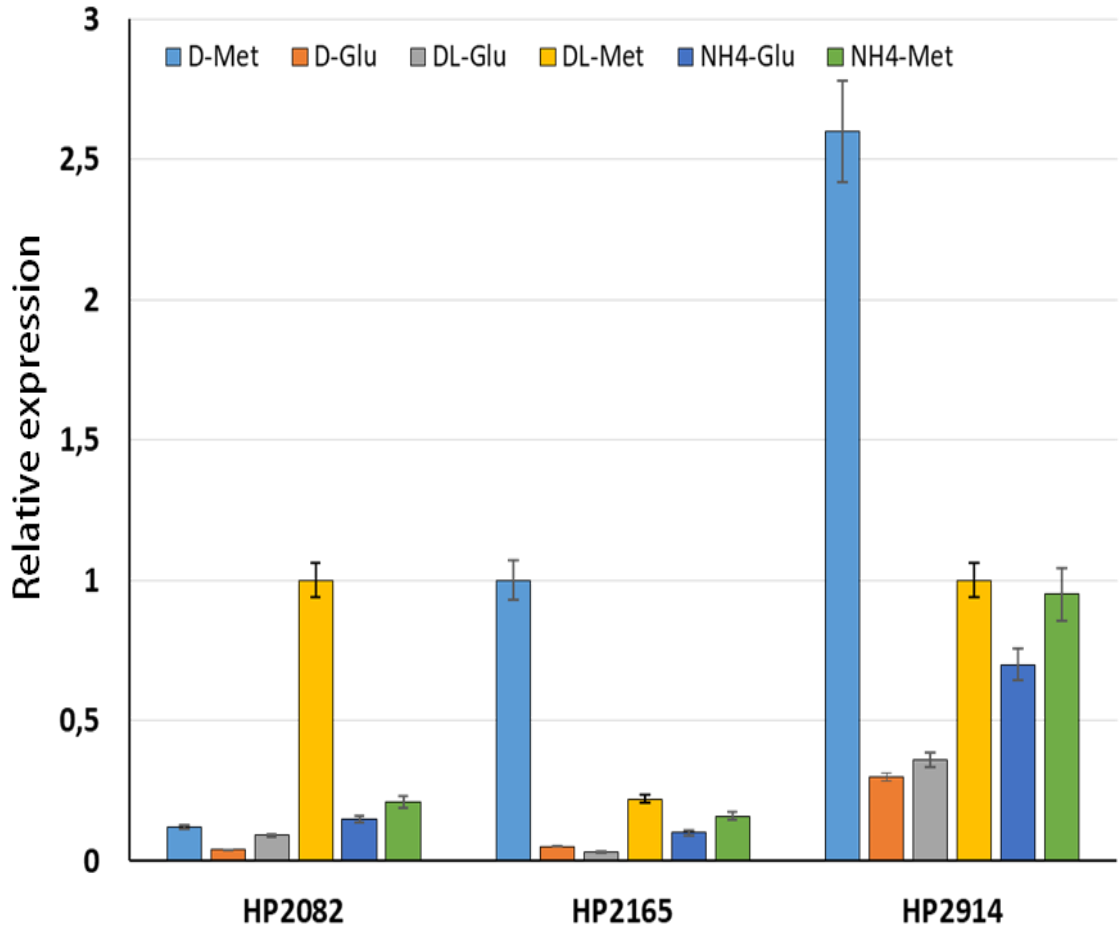

Fig. 26 RT-PCR analysis of DAAO gene expression

3.2 Development of biophysical approaches to study protein molecular changes

In this part of the dissertation, we will present the results of original studies of biological molecules using new technologies and some optical methods, which we

will later use to study the physicochemical changes in a protein molecule during activation of the DAAO enzyme. We believe that such a preliminary study will improve the efficiency and quality of work with the DAAO enzyme.

3.2.1 Development of a Raman signal amplification technique for studying the conformation and content of biological molecules.

[The joint authors of this paper: Liu W, Hao J, He Y.]

The purpose of this set of experiments was to test the method of using silver nanoparticles to enhance the Raman signal on the example of carotenoid molecules. The basis for the Raman line vibrational assignments of the carotenoids is taken from equation [159]. Inspection of the plot in Fig. 27 reveals strong lines at 1522, 1160, and 1004cm^{-1} that represent the marker bands for the β-carotene molecules [160, 161]. For example, the line at 1522cm^{-1} can be attributed to a collective stretching mode at C=C, the frequency of which is a function of the effective conjugation length along the backbone of the β-carotene molecule (for details see [154,162] and references).

The effects of Resonance selectively enhance β-carotene Raman signals even though they are a minor component of the blood, given that the wavelength of the laser line at 514nm is very close to the absorption maximum in the electronic UV–vis spectrum of the β-carotene [154].

In the course of the study, to determine the sensitivity of this approach and the potential for its further use in DAAO experiments, Raman spectra were acquired at

a range of carotene concentrations (Fig. 27). Raman spectroscopy intensity with increasing concentration of carotene (in the range from 0.02 to 20mg/ml or 37μmol/l - 37mmol/L) was found to increase in the presence of the compound, and the maximum changes were found to be in the linear region (from 0.25 to 5mg/ml (466μm/l - 931μm/L). The results of this study are shown in Fig. 28. For example, the sensitivity of Raman spectroscopy to record the concentration of carotene in solution is found to be 0.02mg/ml (37μmol/l).

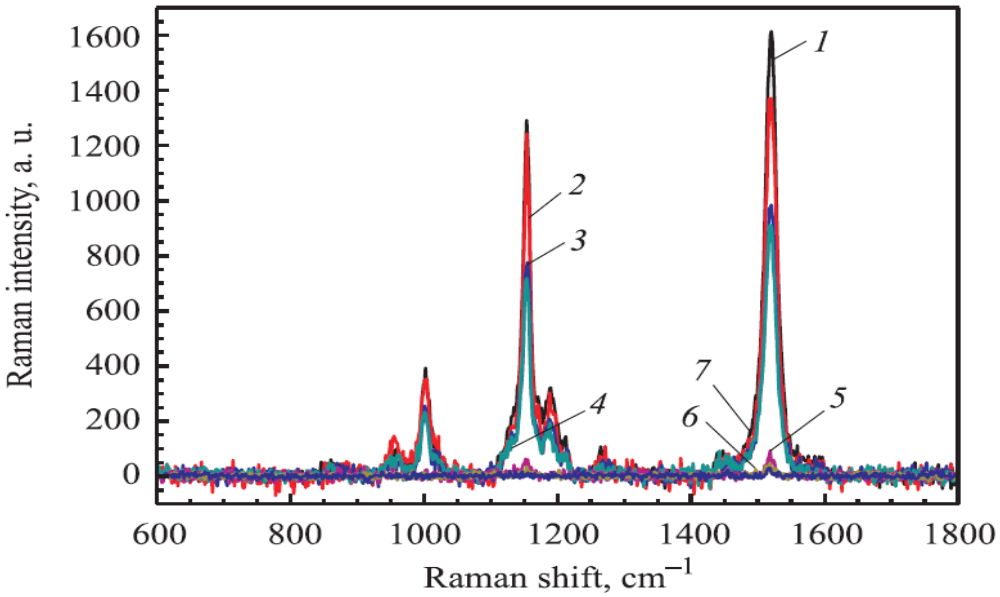

Fig. 27 Raman spectra obtained at a range of β-carotene concentrations in the sample were as follows: 1— concentration of β-carotene in the sample at 20 mg/ml (37.2mmol/l); 2 —4mg/ml (7.4mmol/L); 3 —2mg/ml (3.72mmol/l); 4 —0,4mg/ml (740μmol/l); 5 —0.2 mg/ml (372μmol/l); 6 —0.04 mg/ml (74μmol/l); 7 — 0.02mg/ml (37.2μmol/l).

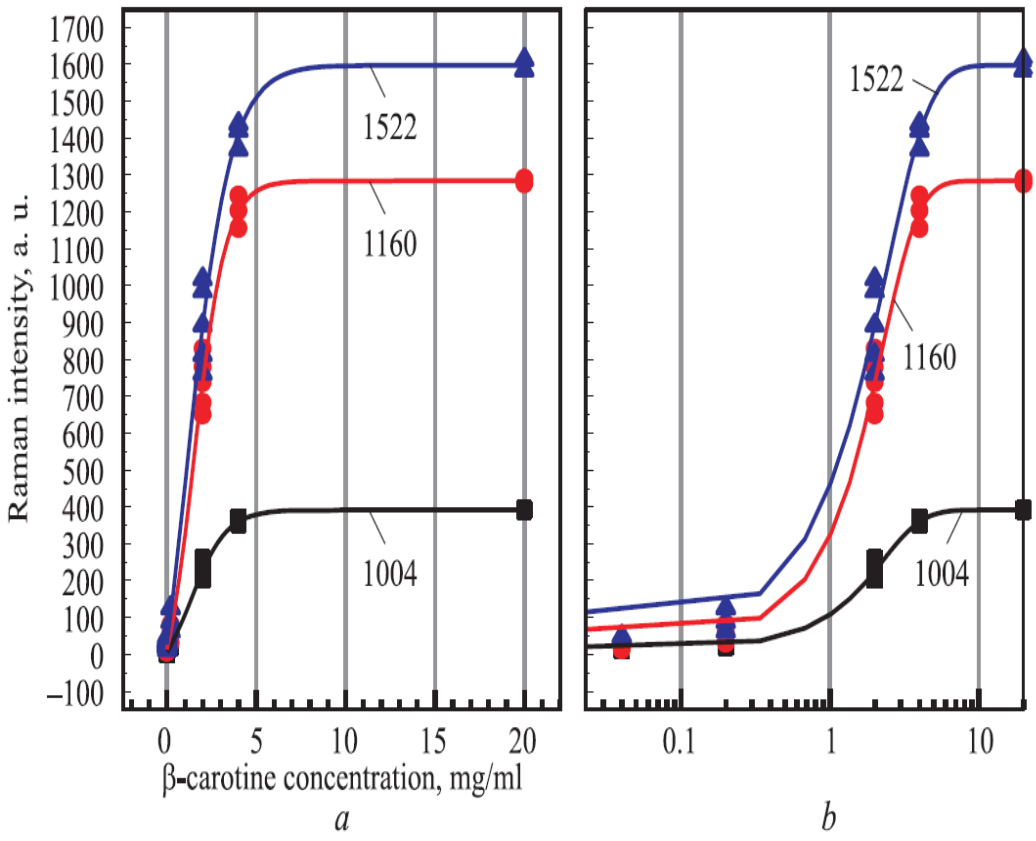

Fig. 28 Calibration plot to determine β-carotene concentration: a) direct relationship; b) decimal log.

The ability of the resulting nanostructured substrates to increase the Raman signal from carotene was investigated in the next set of experiments (Fig. 29). The use of a substrate has been found to enhance the Raman signal when the sample is diluted by a factor of 10^5–10^6, when the concentration of the material is 10–9 mol/L (see Fig. 29, Table. 4).

The use of nanostructured silver substrates therefore allows the Raman scattering of the individual carotene molecules to be enhanced, which is important for determining the sensitivity of this approach as well as the potential for its further use in DAAO experiments.

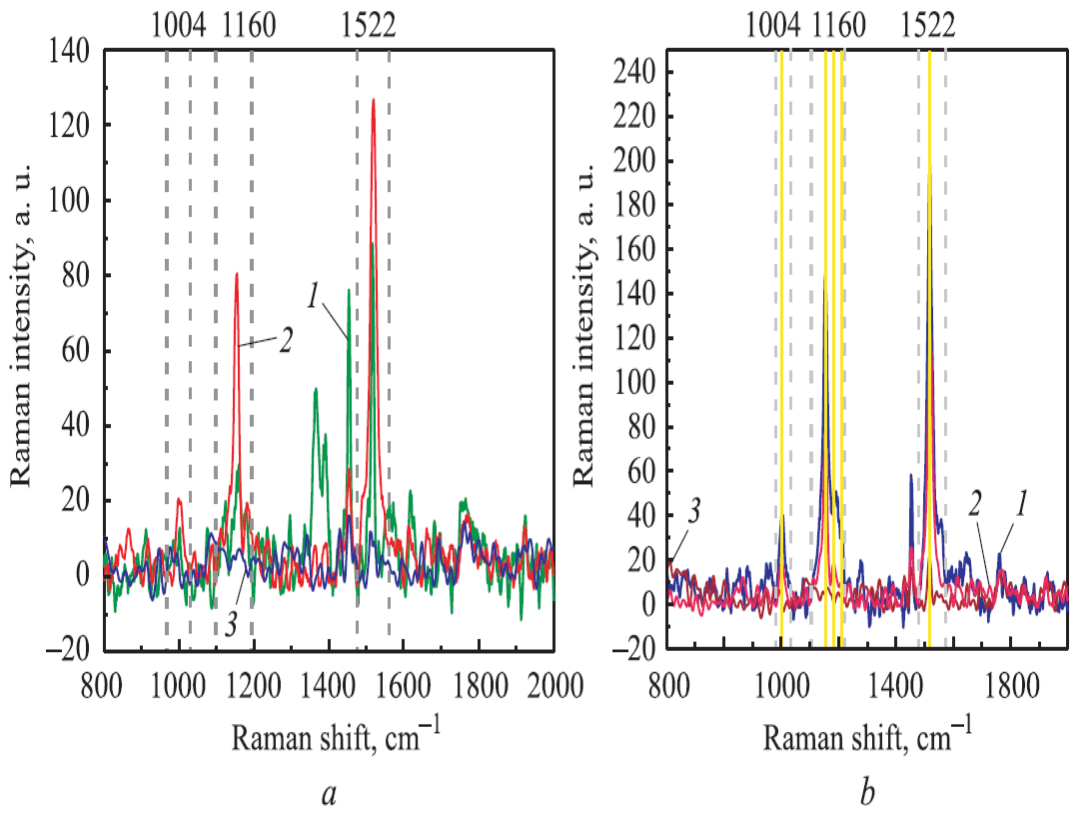

Fig. 29 Comparison of Raman spectra under different conditions. The samples were diluted 10^6 (a) and 10^5 (b) times, respectively, and observed on silver substrates (1), when the samples were diluted 100 times (2), and without substrates (coatings) (3).

The morphology, size, and localization of silver nanoparticles on a nanostructured substrate have been found to affect the interactions and optimal conditions for enhancing Raman scattering [163,164]. In this study, we investigated the relationship between the Raman signal and the concentration of carotene in solution, as well as the substrate. The Raman signal was evaluated by the ratio of characteristic bonds in the Raman spectrum, namely I_{1522}/I_{1160} (to assess the contribution of stretching vibrations of double bonds in the polyene chain), I_{1160}/I_{1004}, and I_{1522}/I_{1004}. The signal was normalized using an "intramolecular

reference" (Fig. 29).

Table. 4 Differences in gain factors of β-carotene at different concentrations.

Raman band intensity-1004cm^{-1}	Raman band intensity -1160cm^{-1}	Raman band intensity -1522cm^{-1}
Dilution 100,000 times, final concentration β-carotene 0.0002mg/ml		
7 702	6 444	10 617
6 935	4 678	8 655
12 849	12 819	14 527
9 954	9 550	13 454
11 869	10 912	15 822
15 103	11 496	15 877
10 735	9 316	13 159
Dilution 1,000,000 times, final concentration of β-carotene 0.00002mg/ml		
-	38 716	47 056
-	46 879	47 801
Raman band intensity-1004cm^{-1}	Raman band intensity -1160cm^{-1}	Raman band intensity -1522cm^{-1}
Dilution 1,000,000 times, final concentration of β-carotene 0.00002mg/ml		
59 491	44 380	59 324
-	21 624	-
-	33 210	-
-	29 430	-
–	53 297	-
–	54 041	85 642
–	30 006	71 878
–	30 437	54 382
59 491	38 202	62 457
EF= (I_{SERS} / I_{cr}) (C_{cr} /C_{SERS}).		

The morphology, size, and localization of silver nanoparticles on a nanostructured substrate have been found to affect the interactions and optimal conditions for enhancing Raman scattering [163,164]. In this study, we investigated the relationship between the Raman signal and the concentration of carotene in solution, as well as the substrate. The Raman signal was evaluated by the ratio of characteristic bonds in the Raman spectrum, namely I_{1522}/I_{1160} (to assess the contribution of stretching vibrations of double bonds in the polyene chain), I_{1160}/I_{1004}, and I_{1522} /I_{1004}. The signal was normalized using an "intramolecular reference"

3.2.2 The utilization of nanostructured substrates has been employed to improve the Raman signal of carotenoids in blood plasma

[The joint authors of this paper: Liu W, Hao J, He Y.]

As mentioned earlier, the resonant Raman spectrum primarily exhibits lines associated with β-carotene. In comparison to previous studies, the SERS spectrum presented in this research displays clearer and more detailed lines.

The next set of experiments was designed to record the Raman signal from carotene in blood plasma, diluted between 10 and 100 times, and then fixed onto a nano-structured substrate (Fig. 31). Dilution of the plasma by an amplification factor of 100 has been found to identify and score key parameters (intensity of band, the position of the band in the spectrum, the ratio of the major bands) from the Raman spectrum of plasma carotene. Thus, using Raman it is possible to control for changes in the concentration and conformation of the molecule of carotene, by recording both the amplitude of the Raman intensity as well as the ratio of band intensities in the Raman spectrum of the carotene compound. When carotene molecules are attached to a nanostructured substrate, the sensitivity of the method is significantly enhanced (the amplification factor reaches 10^4), and enables the Raman spectra of carotene to be recorded in blood plasma, which is important for clinical diagnosis.

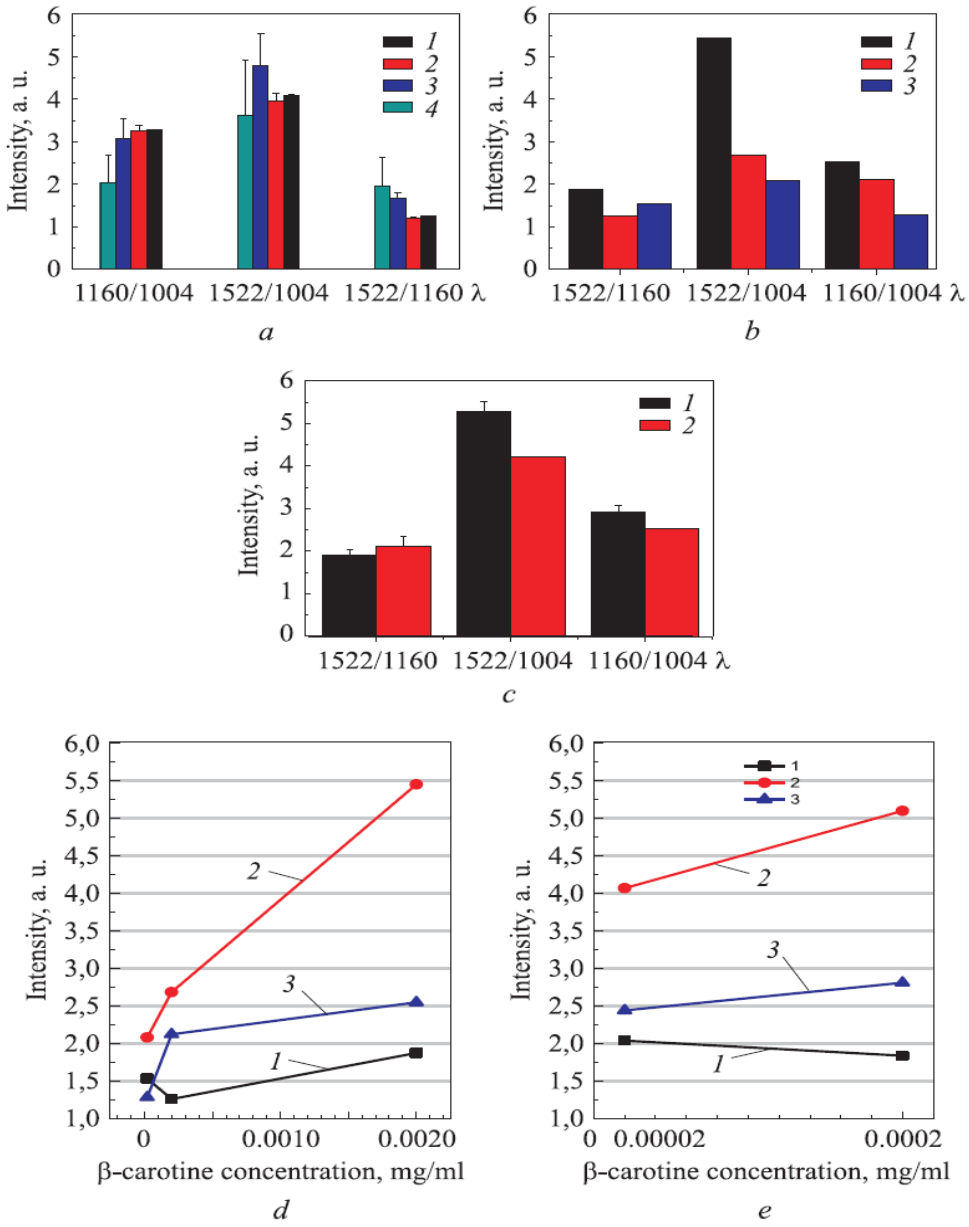

Fig. 30 Peak ratios for β-carotene were measured under different conditions: a) in aqueous solution at concentrations of 20mg/ml (1), 2mg/ml (2), 0.2 mg/ml (3), and 0.02mg/ml (4); b) on a silver support with a dried sample at concentrations of 0.002 mg/ml (1), 0.0002 mg/ml (2), and 0.00002 mg/ml (3); c) on a silver support with an aqueous solution at concentrations of 0.0002 mg/ml (1) and 0.00002 mg/ml (2); d) is the same as b); e) is the same as c); peak ratios is 1 - I_{1522}/I_{1160}, 2 - $I1_{522}/I_{1004}$, and 3 - I_{1160}/I_{1004}.

The results of the present study indicate that Raman spectroscopy with excitations at λ= 534nm can be used as a probe specific for β-carotene present in blood and implicated in human functional changes [165–167]. The analysis of the Raman and SERS spectra recorded at 534nm has revealed that, using the same excitation line and Raman equipment, it is possible to selectively investigate β-carotene based on the preparation of the blood sample.

In SERS conditions, when silver colloids are mixed with a blood sample, hem markers become visible. On the other hand, in normal Raman conditions, resonance enhancement enables the direct observation of β-carotene features. This demonstrates the versatility of the Raman technique and its potential for determining the sensitivity of this approach. Moreover, it opens possibilities for its future utilization in experiments involving DAAO (Fig. 32).

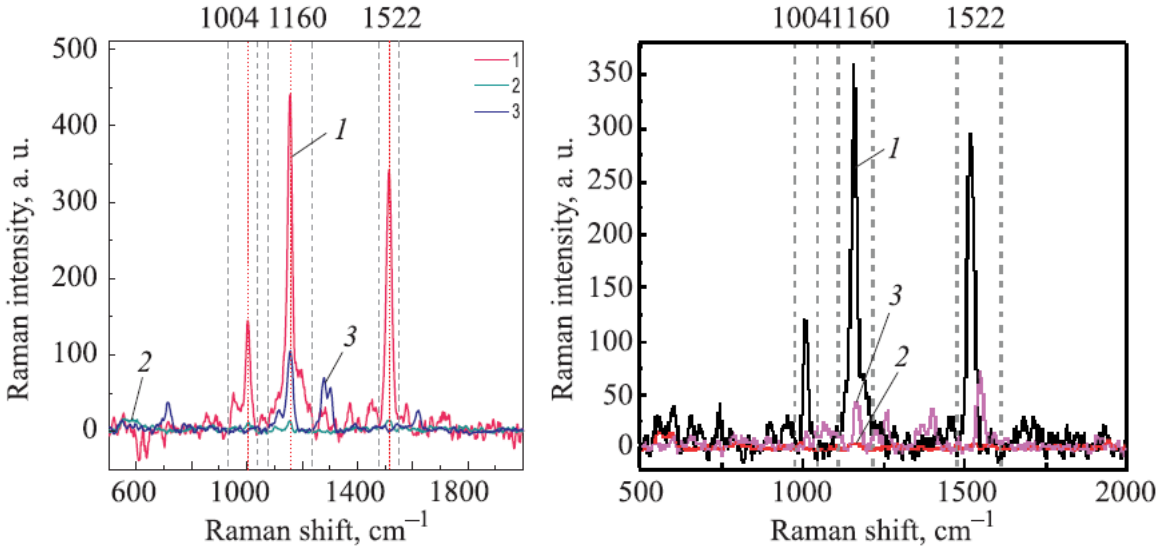

Fig. 31 Raman spectra from plasma samples under different conditions: a) a 10-fold dilution in solution, and b) a 100-fold dilution followed by drying. The spectra were recorded for three scenarios: 1) blood plasma, 2) diluted sample, and 3) diluted sample deposited on a silver substrate.

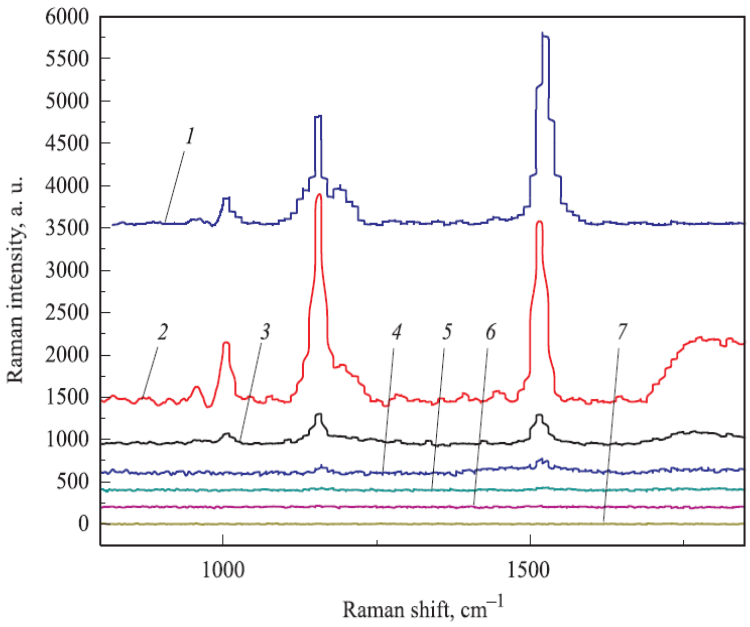

Fig. 32 Raman spectroscopy spectra of carotenoids were obtained from various objects: 1 - apple (λ=473nm); 2 - undiluted plasma dried on a glass slide; 3 - whole plasma; 4 - plasma diluted with Alena's buffer 2 times; 5 - plasma diluted with Alena's buffer 10 times; 6 - plasma diluted 100 times; 7 - plasma diluted 1000 times (λ = 532 nm). The 1520 - 1526cm^{-1} band corresponds to stretching vibrations of the C=C bond in the polyene chain, the 1160cm^{-1} band corresponds to stretching vibrations of C-C in the polyene chain, and the 1008cm^{-1} band corresponds to stretching vibrations of the C-CH_3 bond between the carbon of the polyene chain and a carbon of a pendant methyl group.

3.2.3. pH dependence of the protein, phycocyanin, absorption and fluorescence spectra.

[The joint authors of this paper: Liu W, He Yang]

The goal of this series of experiments was to develop an approach to study the

conformation of an enzymatic protein, DAAO using optical search methods. The purpose of this study was to determine the position dependence of the absorption and fluorescence spectrum of the protein, phycocyanin (PC) on pH. In the absorption spectrum of PC. (Fig. 33) absorbance of the protein can be distinguished with a maximum at 280nm, along with a strong chromophore absorption band in the visible part of the spectrum (with a maximum of about 620nm). The fluorescence of the chromophore peaks at 645nm (Fig. 34).

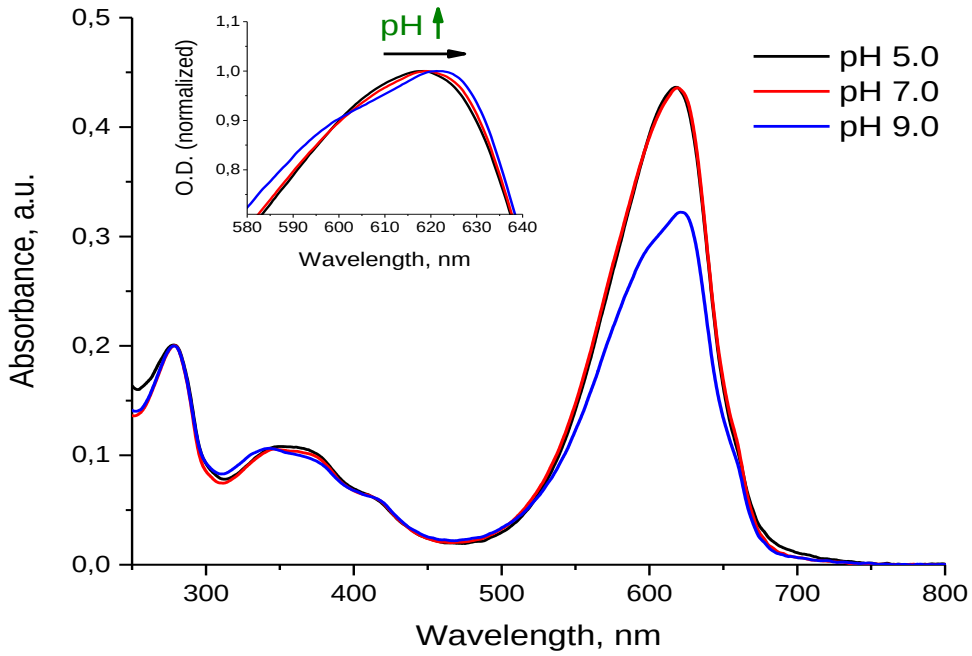

Fig. 33 Absorption spectra of phycocyanin in buffer solutions with different pH values. Normalization by absorption at a wavelength of 280nm. The spectra were normalized to the absorption at 280nm. The pH-dependent shifts of the long-wavelength absorption band of a chromophore are shown in the inset.

According to the obtained results, the higher the pH, the stronger the shift of

the chromophore absorption spectrum to the long wavelength region, and the spectrum of fluorescence -in contrast, in the short wavelength region (Fig. 33, Fig. 34, insets). Consequently, a decrease in the Stokes shift is observed with increasing pH.

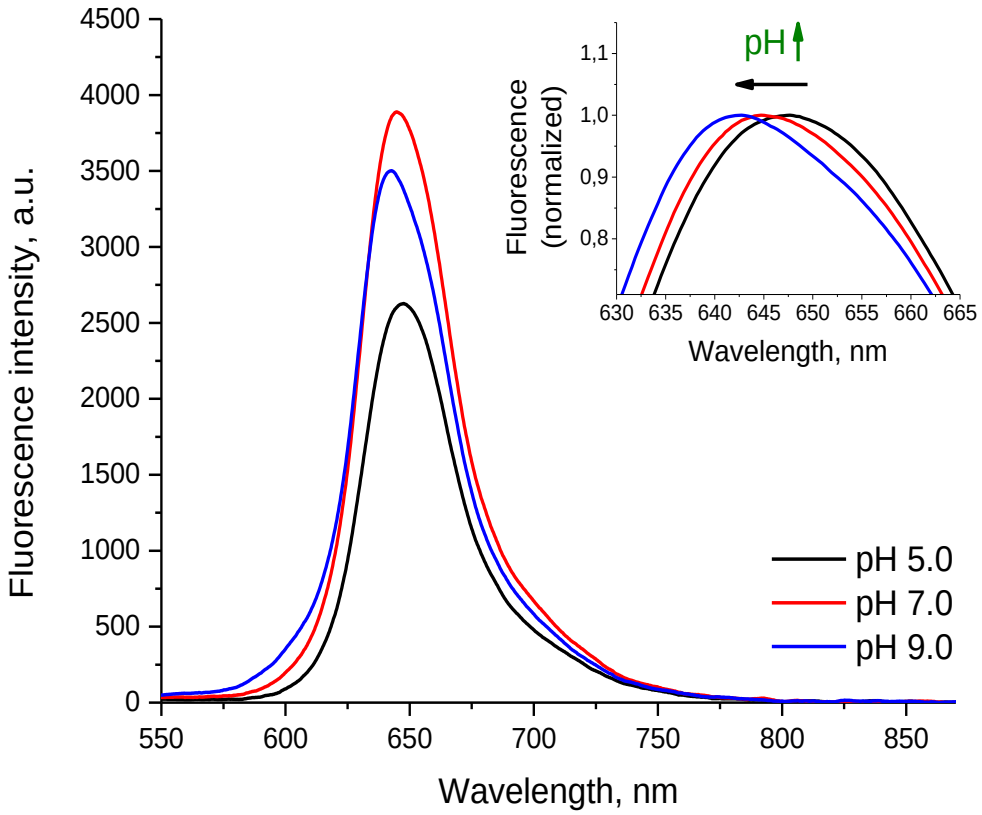

Fig. 34. Fluorescence spectra of PC (0.5μM) in solutions with different pH values. Excitation at a wavelength of 510nm. The inset shows the location of the peak of the PC fluorescence spectrum as a function of pH.

The greater the influence of the chromophore's microenvironment on the positioning of its energy levels, the greater the magnitude of the Stokes shift is known. When absorbing a quantum of light, the molecule appears in a "no

equilibrium" excited state, when the more inert nuclei of atoms of the molecule itself, as well as the nearest molecules of the microenvironment, have not yet had time to rearrange themselves when the electronic state changes. After the corresponding rearrangement, the energy of the excited state S1 decreases, which is the cause of the Stokes shift. The Stokes shift is typically minimal in a highly viscous environment. Therefore, it can be inferred that the rate of rearrangement of the microenvironment surrounding the chromophore molecule increases as the pH decreases. Such effect can be explained by partial denaturation of the protein, or changes of its oligomeric state, when chromophores become more accessible for water molecules A pH dependence of the latter process is proved that, at a certain pH value, $(\alpha\beta)_6$ hexamers of C-PC dissociate into (αβ) monomers and separate subunits[168], and; this process is accompanied by the bathochromic shift of the absorption spectrum [169] in published article by Neufeld, Glazer et al..

If we evaluate the fluorescence intensity of equimolar solutions of PC in solutions with different pH values, we can notice that the fluorescence intensity differs little at pH9.0 and 7.0 (by 2.5 % when normalizing the samples to D510), but significantly decreases (25%) at acidic pH. This sharp drop in fluorescence intensity can also be attributed to thermal quenching of excited states of the chromophore by solvent molecules.

Interestingly, the ratio of the maximum intensity values 620/280nm absorption bands of the protein at pH5.0 and 7.0 does not change, but at pH9.0 a hypochromic effect in the absorption region of the chromophore is observed. Although this behaviours is usually observed during protein aggregation, we do not

see a significant contribution of scattering to the absorption spectrum of samples at alkaline pH. At the same time, association of (αβ) monomers into an $(\alpha\beta)_6$ hexamer results in an increase of the molar absorption coefficient[169].

Thus, at alkaline pH it can be assumed that changes in the conformation of the protein led to a decrease in the molar extinction coefficient of the chromophores.

3.2.4 Evaluation of phycocyanin chromophore mobility in solutions with different pH.

[The joint authors of this paper: Liu W, He Yang]

The method of time-resolved anisotropy of fluorescence allows the evaluation of the different rotational motions of a chromophore possessing fluorescence. In the experiment, the sample is excited by vertically polarized light, which is absorbed only by those molecules whose absorption dipole moment is co-directional with the excitation light. After the light flash is turned off, the excited molecules relax to the ground state with the emission of a quantum of polarized fluorescence; the fluorescence anisotropy is a characteristic that allows the estimate of the mutual orientation of the dipole moment transitions in the molecule. If the molecule is in the liquid phase, during the lifetime of the excited state a rotation of the molecule may occur, which causes a decrease in the fluorescence anisotropy.

The attenuation kinetics of the anisotropy attenuation of the fluorescence anisotropy of PCs are shown in Fig. 35. At neutral pH, we can distinguish two temporal components (Table 5). Neither of them can be interpreted as the rotation

of the whole hexamer; protein complexes of the corresponding mass are characterized by rotational correlation times making tens of nanoseconds[170]. The fast component (of the order of hundreds of picoseconds) was interpreted as the result of depolarization due to the homo-transfer of energy. It is known that radiation-free energy transfer (including FRET) leads to rapid relaxation of fluorescence anisotropy[171]. In hexamer, such energy transfer is possible between individual chromophore molecules, since these molecules are close to each other and have a significant overlap region of absorption and fluorescence spectra. The slow component (of the order of nanoseconds) can be related to the local rotation of protein domains that are microenvironment for chromophore molecules.

As pH decreased from 9.0 to 5.0, a decrease in the contribution of the slow component was observed, while its magnitude remained unchanged (**Ошибка! Источник ссылки не найден.**, Fig. 35). Indeed, a C-PC existence in the form of $(\alpha\beta)_3$ trimers and $(\alpha\beta)_6$ hexamers at neutral and alkaline pH has no effect on the microenvironment of chromophores within a protein globule. A partial monomerization of C-PC trimers at acidic pH should lead to the chromophore exposure to a solution, where the retardation of its movements is removed. On the contrary, within the pH range of 9.0–5.0, the fast component becomes dominant. First, ($\alpha\beta$) monomers keep the possibility of a nonradiative energy transfer. Second, the exposure of a chromophore molecule to a solvent result in an appearance of its own fast rotation, which magnitude is comparable to that of the time of relaxation caused by energy transfer; therefore, these two processes are difficult to separate during the approximation process.

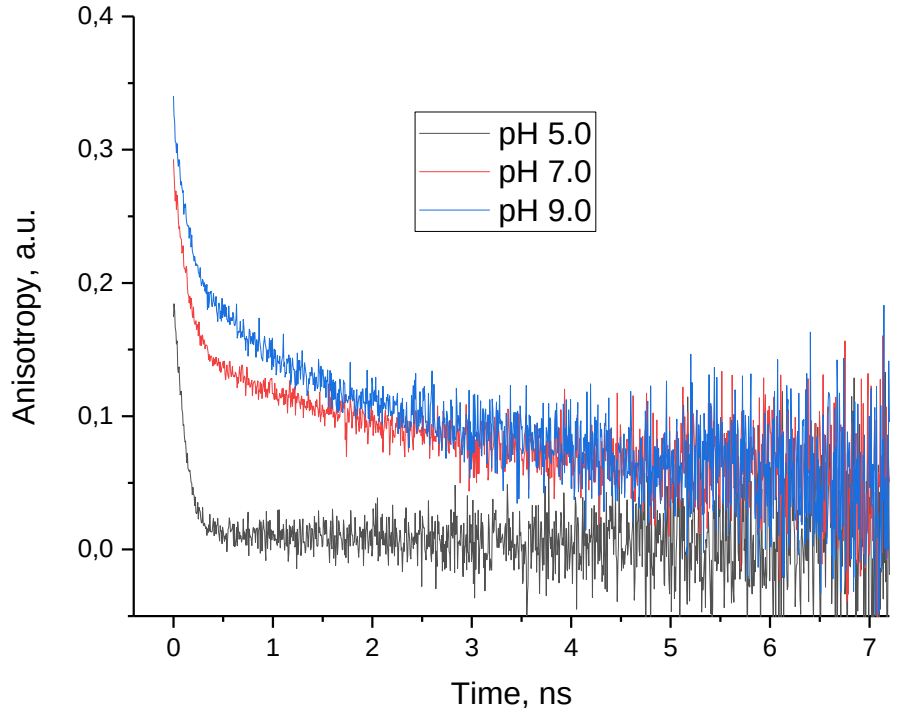

Fig. 35. Anisotropy attenuation curves of phycocyanin (50nM) in buffer solutions with different pH. Excitation at 510 nm, fluorescence registration wavelength 640 nm.

Table. 5 Parameters of approximation of kinetics of fluorescence kinetics of PCs

	θ_1, ns	θ_2, ns	A_1, %	A_2, %
pH 5.0	0.122±0.01	–	100 (0.187±0.02)	–
pH 7.0	0.148±0.02	2.86±0.34	58.2 (0.142±0.09)	41.8 (0.102±0.01)
pH 9.0	0.196±0.03	2.92±0.3	48.1 (0.138±0.01)	51.9 (0.149±0.01)

In the next experiments the size of phycocyanin (50nM) in buffer solutions with different pH was determined using a Zetasizer Nano ZS (Malvern, UK) (Fig.

36). We proposed that changes in pH could disrupt the quaternary structure and size of a given protein. The measurements were conducted in a thermostatic cell at a temperature of +25°C. The samples were allowed to adapt to the temperature for 60 seconds before the measurements were taken. A total of 100 measurements were recorded. Each measurement was performed at least five times. The results were processed using the Malvern software supplied with the Zetasizer Nano ZS instrument and MS Excel.

During this study, changes in the amount of protein are not detected. This may be due to the sensitivity of the chosen research method.

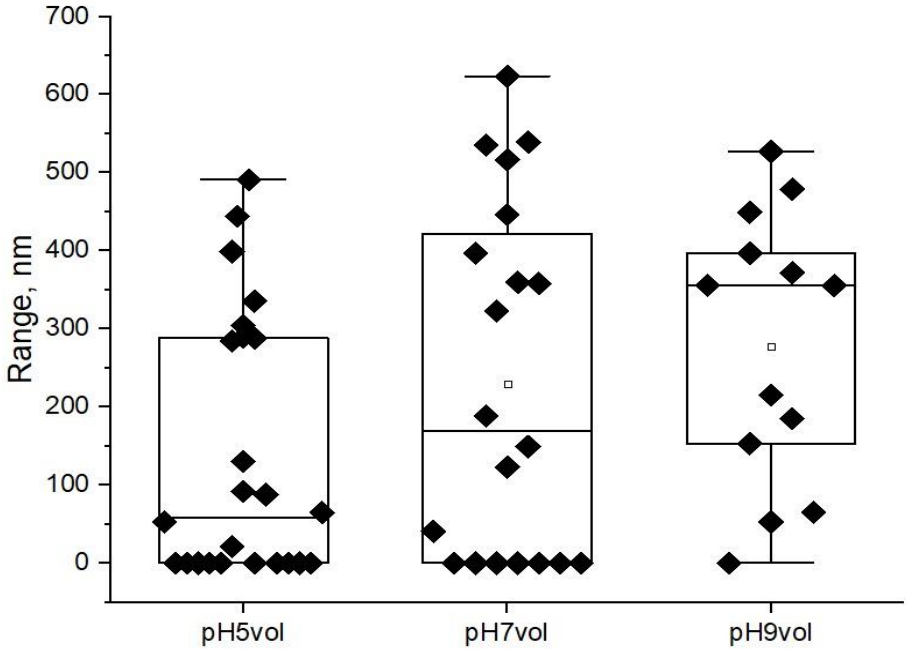

Fig. 36 The dependence of phycocyanin size on pH

3.2.5 Study of a pH dependence of the chromophore conformation and the secondary structure of a phycocyanin protein using the Raman spectroscopy.

[The joint authors of this paper: Liu W, He Yang]

The conformation of the chromophore and protein part of PC was investigated by vibrational spectroscopy. Raman spectroscopy (spectroscopic technique based on Raman scattering) predominantly offers insight into the chromophore's structure and, to some degree, the protein's structure. Since C-PC is characterized by a significant absorption within the visible range, excitation of a Raman scattering causes an intensive fluorescence. To avoid this, we chose excitation light in a region far from the absorption maximum: the near-infrared region (785 nm) and the blue region (488 nm).

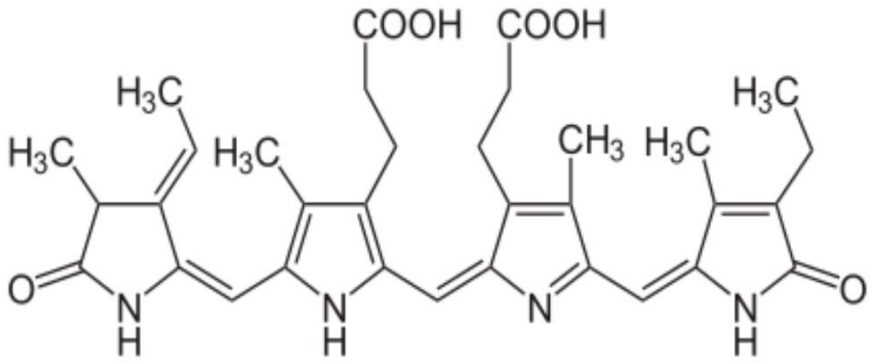

Fig. 37 Structure of phycocyanin

In Fig. 38 shows the RS spectra recorded at 785nm excitation, one can see well resolved spectra in the region close to normal pH values (6-7.5). The spectrum band near 1635–1645cm^{-1} corresponded to vibrations of a methine bridge (v(C=C))[172] in an extended chromophore conformation[173]. When the pH is reduced to 5.5, this band shifts to the 1625cm^{-1} region, which corresponds to the folded

conformation of the chromophore formed upon denaturation[173]. We can also note the appearance of a second peak in the lower frequency region near the 1639cm^{-1} band at pH values of 6-7.5, which may indicate a partial change in the conformation of the chromophore from extended to folded. The band at 1585cm^{-1} corresponded to vibrations of double bonds in pyrrole rings, while the band at 1460cm^{-1} corresponded to deformation vibrations of methylene groups[172,173]. The band, which always present in the spectra at 1365–1380cm^{-1}, can be referred to the vibrational mode ν_4 of a pyrrole ring [172] and may include deformation vibrations of C–H bonds like the band at 1320cm^{-1} [173]. Two maxima corresponding to the vibrations of the Amide III band of the protein part of C-PC presented in the region of 1240–1280cm^{-1}; the band at 1241cm^{-1} was referred to the Amide III vibrations of the disordered protein structure, and the second band at 1275cm^{-1} corresponded to the Amide III vibrations in α-helices. The bands at 980cm^{-1} correspond to antisymmetric stretching of O–P–O bonds in the phosphorylated head group (probably the component of buffer solution)[174], 815cm^{-1} seemed to correspond to valence vibrations of C–C bonds and those of the C–C bonds in a carbon chain; the band at 666cm^{-1} corresponded to vibrations of the S–C bond within disulfide bridges binding a chromophore to cysteine residues of a protein part of C-PC [173].

If medium pH changed towards acidic values (pH5), the intensity of Raman spectra significantly decreased (Fig. 38) that can be explained by a partial protein denaturation and/ or increased absorption of a sample in a near infrared region. To study the chromophore structure at pH values significantly differing from normal pH, we used exciting light from the blue part of the spectrum. In this case, spectra

of about the same intensity were registered for the whole pH range from 5 to 9 (Fig. 39). At the same time, excitation at 488nm did not cause a reliable shift of the band at 1640cm^{-1} for acidic pH values (which could indicate denaturation). It is possible that denaturation observed in the experiments with excitation at 785nm was also caused by a partial absorption of the exciting radiation and the heating of a sample. In the case of excitation at 488nm, a medium-intensity band was observed at 1264cm^{-1}; it probably corresponded to the Amide III vibrations within α-helices[173]. According to some data, the presence of this band makes it possible to distinguish C-PC and allophycocyanin spectra [172]. It was also shown that the intensity of the Amide III band significantly increased at pH7 and pH9 compared to pH5 (Table. 6) that evidenced an increase in the fraction of α-helices.

Raman spectra recorded at the exciting wavelength of 488nm provided a detailed image of the band at 1637cm^{-1}. In the case of alkaline pH, a significant shoulder increase (peak appearance) was observed at 1602cm^{-1}; moreover, the area of a peak at 1587cm^{-1} also changed. This fact can be interpreted as a partial shift of a 1637cm^{-1} band towards low frequencies that evidences the appearance of chromophore molecules in a folded conformation. Such peak shift at low pH (Fig. 38) may be associated with a protein denaturation; however, the shift recorded in our experiment may indicate changes in the chromophore extending degree, which were not associated with denaturation. Other peaks presented in Fig. 38 and Fig. 39(excepting those mentioned in Table. 6) did not show significant pH-associated shifts.

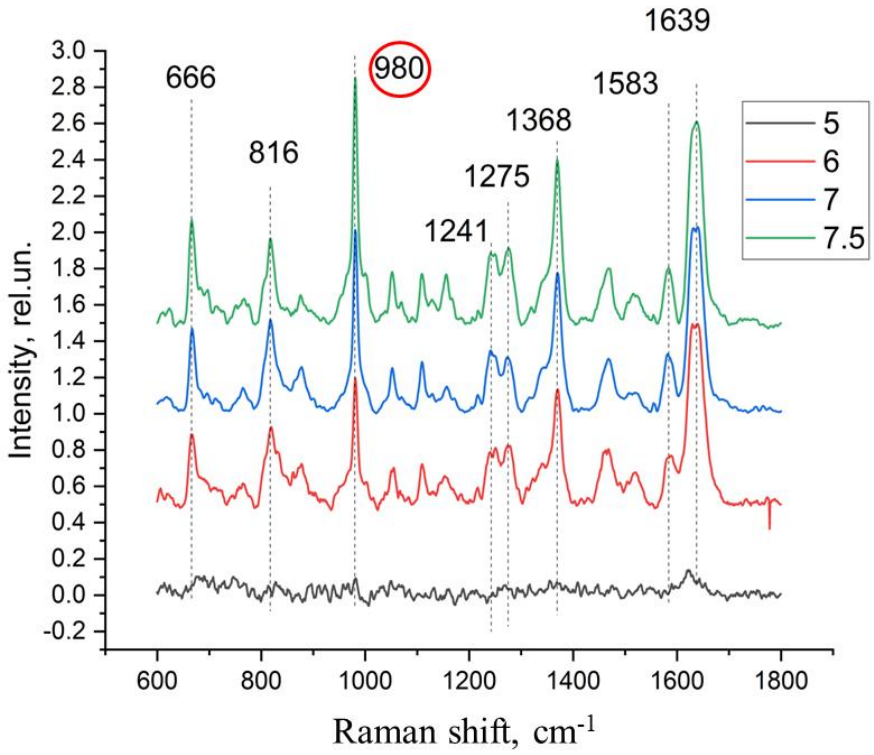

Fig. 38 Typical C-phycocyanin Raman spectra were recorded at the exciting wavelength of 785nm and different pH values (the spectra obtained for pH6 - 7.5 are normalized to the intensity of a band at 1639cm^{-1}). Registered bands are indicated with dotted lines.

Table. 6 Intensity of bands at 1264 and 1602cm^{-1} in the Raman spectrum at the excitation wavelength of 488 nm and different pH values.

pH	Band at 1264 cm^{-1}, rel. units Medium ± STD	Band at 1602 cm^{-1}, rel. units Medium ± STD
5	13.950 ± 2.376$^{\#}$	0.0 ± 0.0$^{\#}$
7	14.340 ± 1.095$^{\#}$	0.0 ± 0.0$^{\#}$
9	19.750 ± 1.524	12.63 ± 6.00
Meaning	Increased fraction of α-helices at neutral and alkaline pH	Denaturation-independent change in the level of a chromophore folding at alkaline pH

#Significant difference between the area of the corresponding bands of samples at the standard and alkaline pH (pH9). The data were calculated using a one-way

ANOVA and a posterior Tukey criterion, $p < 0.05$.

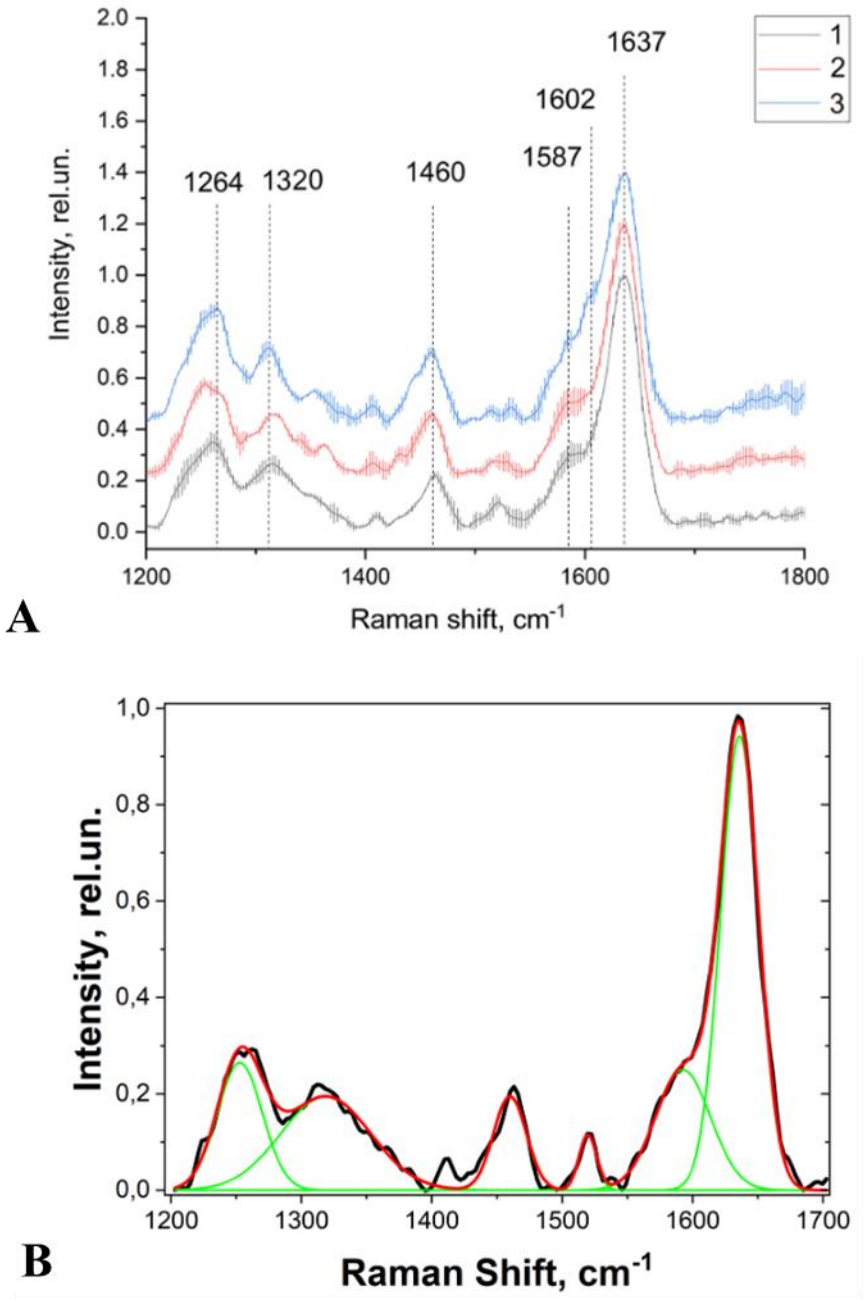

Fig. 39. Raman spectra of C-PC at different pH and 488 nm exciting light (the spectra are normalized to the intensity of a band at 1639cm^{-1}). A-Averaged Raman spectra of C-PC at different pH: (1) pH5; (2) pH7; (3) pH9. Significant bands are shown by dotted lines. B-Example of a deconvolution of phycocyanin Raman spectrum at pH5.

3.2.6 IR spectroscopy study of the structure of a protein part of C-PC at various pH.

[The joint authors of this paper: Liu W, He Yang]

The ATR-FTIR absorption spectra of C-PC solutions characterized by different pH are shown in Fig. 40. The spectra included clear bands corresponding to group vibrations of the protein part of a molecule, while bands corresponding to the chromophore vibrations were absent. The band at 1652cm^{-1} corresponded to group vibrations of peptide bonds in protein molecules (Amide I) with the maximum contribution from vibrations of the carbonyl group (C=O) of the peptide bond. The band maximum is typical for the α-helix structure[175–177]. The band at 1548cm^{-1} corresponded to group vibrations of Amide II peptide bonds, which included deformation and valence vibrations of N–H and C–N bonds, respectively[176] , and had a shoulder near 1524cm^{-1} that might evidence the presence of an α-helix structure[177]. A certain shift of the maximum of the Amide II band towards lower wavenumbers was observed at pH5 and pH9 that could indicate a larger contribution to this absorption band corresponding to β-sheets (~1530cm^{-1} according to[177]). There was also a low-intensity peak at 1740cm^{-1}, which apparently corresponded to vibrations of C=O bonds in amino acid residues of glutamic and aspartic acids. The band at 1450cm^{-1} is usually referred to deformation vibrations of methylene groups in side chains of amino acids.

An example of a fitting of the second spectrum derivative in the region of the

Amide I band is shown in Fig. 41. The results of the Amide I band deconvolution are shown in a histogram (Fig. 42) and in Table 4. The content of α-helices in the secondary C-PC structure at pH7 was ~ 65% that corresponded in general to the data obtained by the FTIR spectroscopy in other studies[178,179]. A circular dichroism (CD) spectroscopy showed about the same content of α-helices (47–67%) as in our study, but a lower content of β-structures (0–10%; Table. 7).

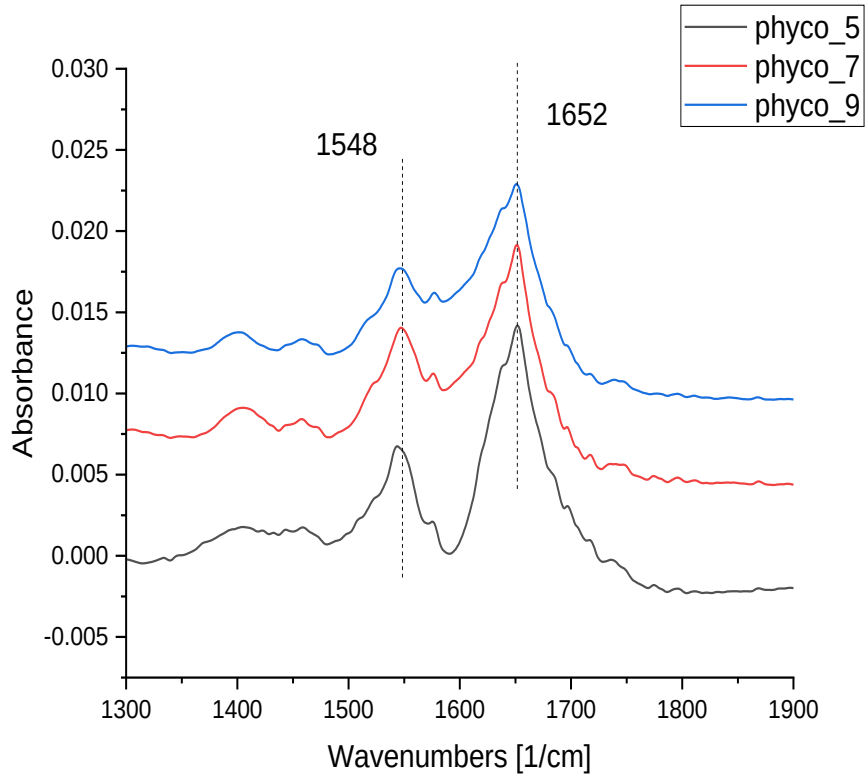

Fig. 40 Typical ATR-FTIR absorption spectra measured at different pH within a range of 1300-1900cm^{-1}. Positions of the Amide II and Amide I bands are indicated with dotted lines.

However, the number of β-structures determined by CD spectroscopy was lower than in the case of a FTIR spectroscopy, whereas the situation for α-helices

was quite opposite. At the same time, the number of β-structures determined by the FTIR spectroscopy was comparable with the data of the X-ray structure analysis [180].

Table. 7. Secondary structure of C-phycocyanin.[181–187]

	Source	α-helix, %	β-sheet, %	β-turn, %	Undetermined structure, %
Theoretical calculations	α-subunit	50.0	0	36.42	13.58
	β- subunit	54.07	0	36.63	9.03
X-ray structure analysis	β- subunit	57.6	0	42.4	–
	β- subunit	51.5	0	48.5	–
	β- subunit	52.4	0	47.6	–
Circular dichroism study	from Zhejiang Binmei Biotechnology Co., Ltd	~66	0	~12	~22
	C. caldarium	47.5±2.2	14.6±4.5	20.3±1.8	17.3±3.2
	P. luridum	67.1±8.9	5.7±0.9	14.6±3.4	14.6±3.4
	Synechococcus lividus (SyI)	54.7	10.5	19.0	16.9

Table. 8. Percentage of different types of secondary protein structures in C-phycocyanin determined at different pH.

Peak, cm^{-1}	1624	1633	1638	1656	1667	1685	1691
Structure,%	Single-chain fragment	Single-chain fragment	Single-chain fragment	α-helix	β-turn	β-turn	Single-chain fragment
pH							
5	15.52±1,40	10.32±3.77	4.77±4.13	58.19±1.04	2.86±0.04	7.44±1.00	0.89±0.54
7	8.26±3,19*	10.31±0.67	0.00	65.43±4.33	2.11±0.42	12.18±0.71*	1.71±0.58
9	3.83±2,54*	8.74±1.93	1.95±3.38	71.07±5.33	1.94±1.41	12.02±1.23*	0.45±0.25

* The value significantly differs from that obtained at pH 5. The data were calculated using a one-way ANOVA with a posterior Tukey's criterion ($p < 0.05$

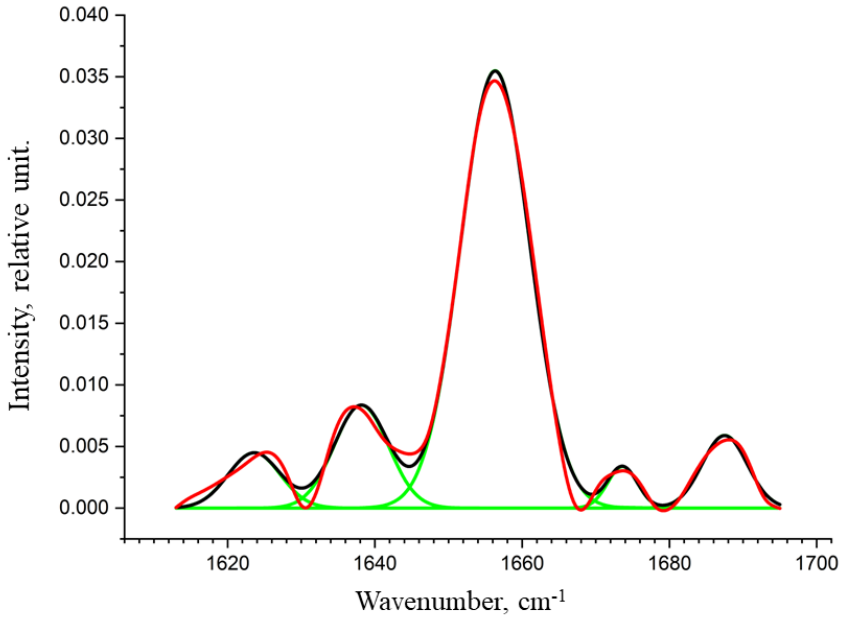

Fig. 41. Example of a deconvolution of the second spectrum derivative in the region of the Amide I band of phycocyanin at pH 7.

In our study, we revealed a significant increase in the percentage of α-helices and β-turns and a decrease in the percentage of single-chain protein segments associated with a pH increase from 5 to 9 (Fig. 42). In the case of single chain segments, significant changes were observed only in the region of 1624cm^{-1} (Table. 8). An increase in the percentage of α-helices in alkaline solutions corresponded to the results obtained by the Raman spectroscopy a well as assumptions about structural changes, which were made based on the shift of the maximum of the Amide II band.

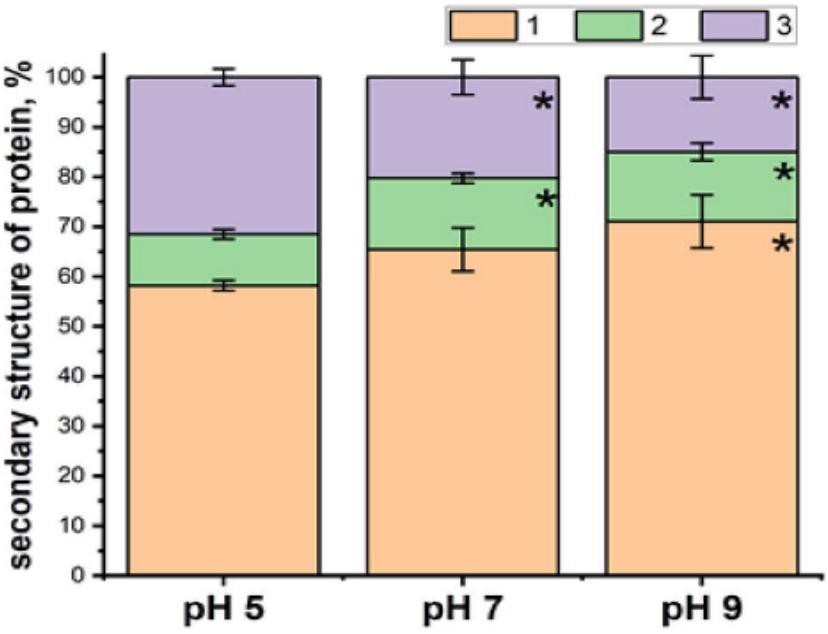

Fig. 42. Percentage of different types of protein secondary structures: 1, α-helix; 2, β-turns; 3, single-chain protein structures. The values significantly different from those obtained at pH 5 are indicated with the asterisk. The data are calculated using a one-way ANOVA and a posterior Tukey's criterion ($p < 0.05$)

According to the existing data, pH decreases or thermal treatment of proteins (such as human serum albumin) results in an increased number of β-structures, especially intermolecular β-sheets; in addition, a certain aggregation between protein globules occurs, which may probably cause the observed increase in intermolecular β-structures[188]. Probably, the similar situation occurs in C-PC in relation to single-chain protein structures. Thus, the analysis of the secondary structure of C-PC by FTIR spectroscopy showed that pH increase towards an alkaline environment causes significant changes associated with an increased content of α-helices and β-turns and decreased percentage of single-chain protein segments.

3.3 Biophysical analysis physical and chemical properties of DAAO

3.3.1 Study of DAAO absorption depending on the reducing agent

Sodium dithionite ($Na_2S_2O_4$) as a strong reducing agent in chemistry can give other substances an electron. The absorption spectrum remained unchanged when the enzyme sample was subjected to spectroscopic analysis. Upon introduction of alanine, no significant alterations were observed in the absorption spectrum. On the other hand, after incorporating sodium dithionite, the enzyme transformed into its completely reduced state (violet curve) (Fig. 43)

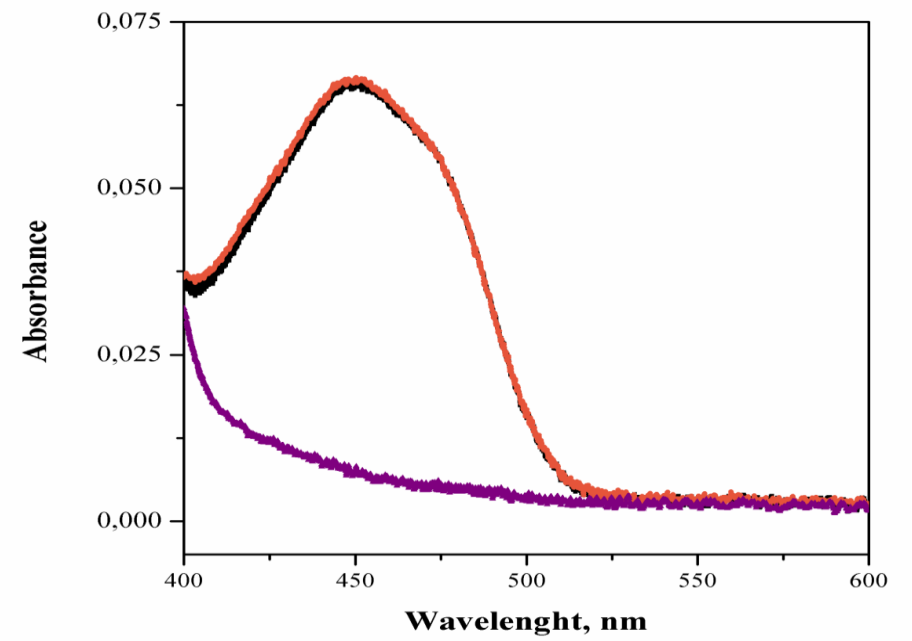

Fig. 43 Absorption spectra of the enzyme in different case. Black curve - absorption spectra of enzyme in buffer; red curve - of enzyme after addition of crystalline D-alanine to a concentration of 5mM; violet curve - of enzyme with D-alanine after addition of 2mg of crystalline sodium dithionite to 1 ml of solution.

The spectra were obtained on one sample of the enzyme. After addition of serine there are no pronounced changes in the absorption spectrum. After addition of sodium dithionite, the enzyme changes to the fully reduced form (violet curve). (Fig. 44)

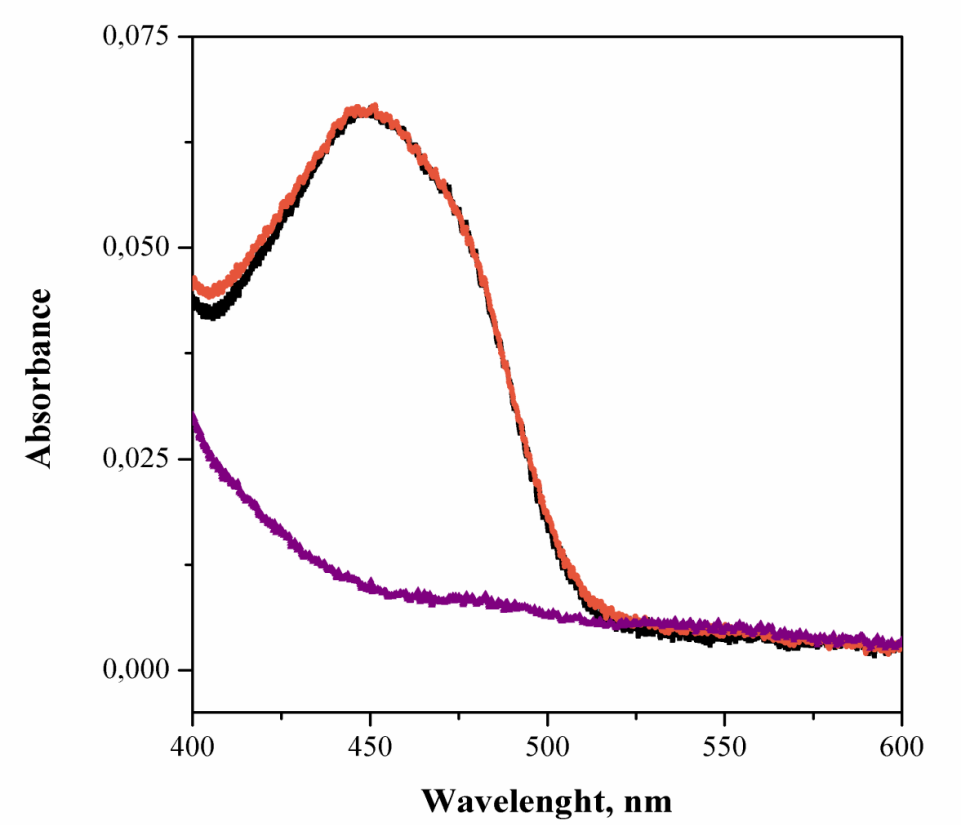

Fig. 44. Absorption spectra of the enzyme in different case. Black curve - absorption spectra of enzyme in buffer; red curve - of enzyme after addition of crystalline D-serine to a concentration of 5mM; violet curve - of enzyme with D-serine after addition of 2mg of crystalline sodium dithionite to 1 ml of solution.

3.3.2 Raman analysis of DAAO with D-alanine and D-serine.

[The joint authors of this paper: Bochkova J V., Liu W]

In this series of experiments, we used the results of the previous chapter to investigate the conformation of proteins during enzyme activation. The oxidized form of the FAD-group SERS spectrum of DAAO is shown in Fig.43. Finally, it should be noted that recording RS spectra without the use of silver nanostructures at the same measurement settings and enzyme concentration did not allow us to determine the position of the individual peaks within a cluster (data not presented). After analyzing the SERS spectra, it was determined that the most prominent peaks within the bands are located at positions 1630, 1584, 1546, 1355, 1252, and 1160cm^{-1}. These peaks correspond to the bond vibrations found in one of the three aromatic rings of the coenzyme FAD, as revealed in the analysis of the spectra (

Table. 9).

The reduced form of flavin is known to have fewer characteristic peaks in the RS spectra in comparison to the oxidized form, which is due to changes in the delocalization of the π-electron orbitals in the N (5) and N (10) atoms [189]. When the substrate D-alanine was added to DATA, changes in the bands of the SERS spectrum were detected already within 10 s, which stabilized after 60 seconds.

Fig. 45. shows a series of SERS spectra obtained one second after the addition of D-alanine to the DAAO solution. It was found that after 1 second a peak at

1612cm^{-1} appears (marked with a red asterisk on the blue spectrum, Fig. 46), which disappears at the 3rd and subsequent seconds and is due to either the semiquinone form of FAD [190] or the fully reduced form of flavin [191]. Also, on the SERS spectrum obtained one second after the addition of D-alanine, the 1252cm^{-1} peak disappears but a peak around 1300cm^{-1} appears, which also disappears by the second and third seconds. A comparable change in the bands of the flavin SERS spectrum was observed when the hydrogen at the N (3)-H position is substituted with deuterium, as well as when the N (3)-H·····R hydrogen bond is formed [192]. Therefore, the 1252cm^{-1} band can be used as an indicator to assess the N (3)-H···· protein interaction.

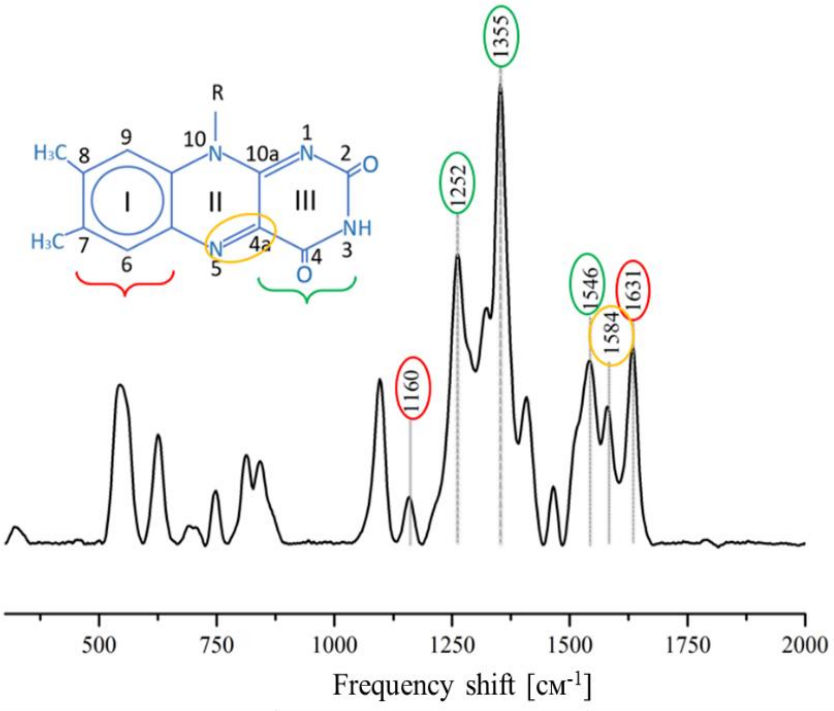

Fig. 45. SERS spectrum of the enzyme DAAO (enzyme solution at a concentration of 1 mg/mL) in the oxidized state. The spectrum corresponds to the spectrum of the oxidized cofactor-FAD. The excitation wavelength was 532nm, laser power was no more than 1 mW per registration area with a diameter of 800nm, and the spectrum

accumulation time was 60s. The positions of the maxima of characteristic peaks in the spectrum and their corresponding groups of atoms in the structural formula of FAD are circled in different colors.

Table. 9. Correlation of peaks SERS spectra of DAAO with FAD-group bond vibrations. [189,192–194]

SERS spectrum bands of oxidized FAD from pkDAAO, cm^{-1}	Putative fluctuations of FAD coenzyme bonds	Reference
1160	Links of ring I	[193]
1252	[C (2)-N (3)H-C (4)] of ring III	[193], [192,194]
1355	[C(4a)-C(10a)-N(1)-C(2)] of ring III	[193][189,192]
1546	[C(4a)-C(4)], [C(4a)-(10a)] ring III bonds	[189,194]
1584	[C(4a)-N(5)] of ring II	[189,192–194]
1631	Links of ring I	[192,194]

During the enzymatic reaction of DAAO with an amino acid, its dehydrogenation and hydrogen transfer to N(5) flavin occurs. In this case, stabilization of the substrate relative to the enzyme is provided by several

hydrogen bonds, and after dehydrogenation this process is also carried out due to electrostatic interactions of atoms in the molecule [195].

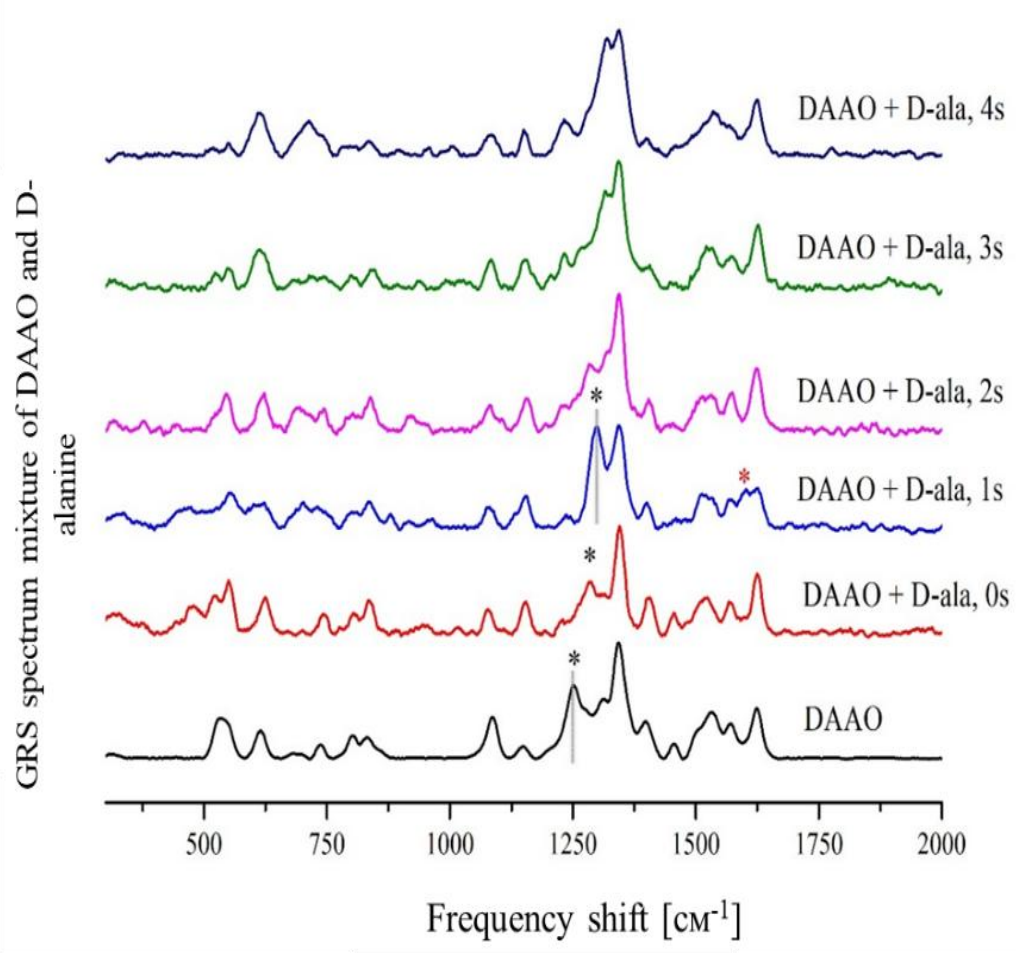

Fig. 46. SERS spectrum of DAAO when excess substrate D-alanine was added (DAAO concentration - 1 mg/mL, final concentration of D-alanine in solution with enzyme - 50mm). The duration of spectra recording was 1 s. On the spectrum recorded 1s after D-alanine addition (blue spectrum labeled "1s"), the peak at 1612cm^{-1} corresponding to the reduced FAD molecule is marked with a red star. The black star on the 0s and 1s spectra shows a shift of the 1252cm^{-1} peak to a position around 1300cm^{-1}, which is probably due to a change in the contribution of hydrogen bonding vibrations in ring III position of the FAD group molecule during

stabilization of the complex with D-alanine.

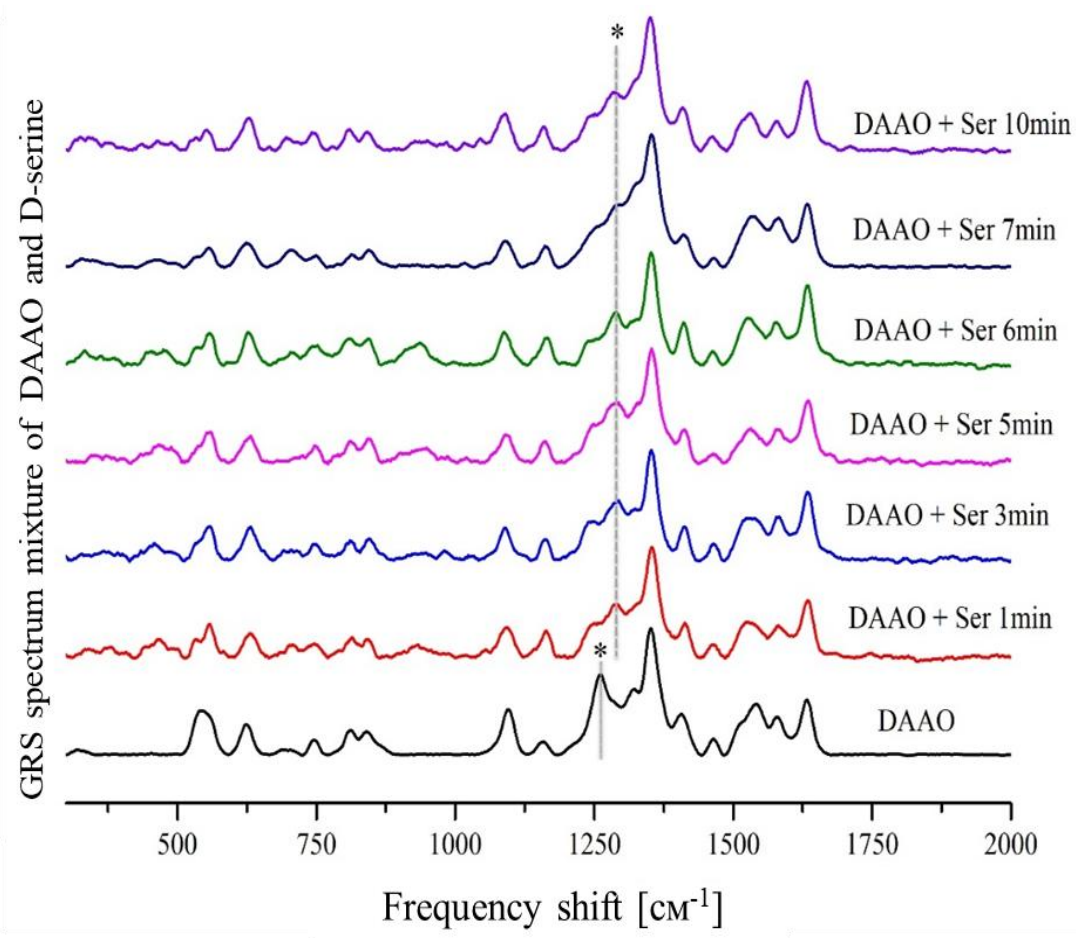

Fig. 47. SERS spectra of DAAO in the presence of D-serine (enzyme concentration - 1 mg/ml, final concentration of D-serine - 50mM). Asterisks denote a change in peak position 1252cm^{-1}.

It is likely that the N (3)-H group of flavin does not directly participate during the enzyme reaction, but the stabilization of the cofactor molecule with respect to the ligand can influence the change in the N (3)-H···R hydrogen bond, which we observe upon introduction of D-alanine to DAAO. The reduced enzyme-amino acid complex is then re-oxidized, and in the second we observe the disappearance

of the peak at 1612cm^{-1}, whereas the peak in the 1600cm^{-1} region again shifts to the low frequency region of the SERS spectrum.

Fig. 47, illustrates the spectroscopic analysis of DAAO (1mg/ml) that investigates the dynamics of FAD conformational alteration in the presence of D-serine (100mM). Previous research has indicated that the Michaelis constant (MC) for the enzymatic reaction between human DAAO and D-serine is fourfold higher compared to the K_M value for the reaction between DAAO and D-alanine[196]. Moreover, it has been established that the relative activity of DAAO isolated from pig kidney against D-alanine surpasses that against D-serine by more than double [197]. These findings are corroborated by the observed phenomenon, as changes in the FAD-group spectrum of DAAO occur over an extended period upon addition of D-serine. In contrast, when D-alanine is added, alterations are detected within the initial seconds of the enzymatic reaction. Upon activation of DAAO by D-serine, the position of the spectral peak at 1252cm^{-1} shifts within a span of 60 seconds, accompanied by the emergence of a new peak in the 1300cm^{-1} region. However, the region of 1200-1355cm^{-1} in the SERS spectrum of FAD ceases to exhibit any further changes within 7-10minutes.

So, by using silver nanoparticles, SERS spectra were obtained and the investigation focused on the alterations in the conformation of the FAD-cofactor during the activation of DAAO through substrates possessing distinct specificities. This study unveiled the existence of distinctive spectral bands positioned at maxima of 1630, 1584, 1546, 1355, 1252, 1160cm^{-1}, which can be attributed to the vibrational movements of the atom groups within the individual FAD-group rings

in their oxidized state. This indicates that during the redox reaction with the substrate there is a shift in the peak 1252cm^{-1} towards the long wavelength region, which presumably is associated with the coordination processes of the active center of DAAO with respect to the amino acid. Furthermore, in the case of enzyme interaction with D-alanine, this allowed us to record the appearance of a peak at 1612cm^{-1} associated with the reduction of the flavin moiety of FAD. In addition, we observed a difference in the time taken to record the SERS spectrum changes of the FAD-group of the DAAO enzyme in the presence of D-alanine and D-serine. For example, in the interaction of DAAO with D-alanine, changes in the SERS spectra took place in a matter of seconds, although when D-serine was added, similar results took minutes to obtain, confirming data from the literature on the differing activity of the DAAO enzyme in interactions with these amino acids.

The proposed approach based on SERS spectroscopy with silver plasmonic nanostructures can be used in further studies of the reaction mechanisms of DAAO with D-amino acids and determination of the efficiency of H_2O_2 generation by different forms of DAAO.

3.3.3 IR investigation of protein conformation changes during DAAO activation.

In this experiments IR spectroscopy investigation of the structure of the protein part during DAAO activation was studied. The bands corresponding to the group vibrations of the protein part of the molecule are well expressed. The band around 1650cm^{-1} corresponds to group vibrations of the peptide bond in the protein

molecule (Amide I), the largest contribution to this type of vibrations is made by vibrations of the carbonyl group C=O of the peptide bond. Around 1550cm^{-1} band corresponds to group vibrations of Amide II peptide bonds including N-H deformation vibrations and valence C-N vibrations.

3.4.3.1 Comparation IR spectrum of pkDAAO before and after addition of D-amino acid.

Experimental studies revealed changes in protein structure during the oxidation of alanine and serine by pkDAAO (Fig. 48, Fig. 49). For pkDAAO the amplitude of band at 1644cm^{-1} corresponds to group vibrations of the peptide bond in the protein molecule (Amide I), the largest contribution to this type of vibrations is made by vibrations of the carbonyl group C=O. The 1544cm^{-1} band corresponds to group vibrations of Amide II peptide bonds including N-H deformation vibrations and valence C-N vibrations. A notable increase in amplitude is observed in the IR spectra following the addition of alanine and serine.

As shown in Fig.49, the addition of alanine increases the peak amplitude by a factor of eleven to sixteen, whereas the addition of serine increases the peak amplitude by a factor of twenty-five to thirty-two. At the same moment, the addition of alanine and serine shifted the peaks towards the short-wave region by 31 and 27nm, respectively. The data obtained indicate that the composition of the components of Amid I changes during the interaction of D-amino acids with the enzyme, with a significant decrease in the weight of the beta page (Fig.49).

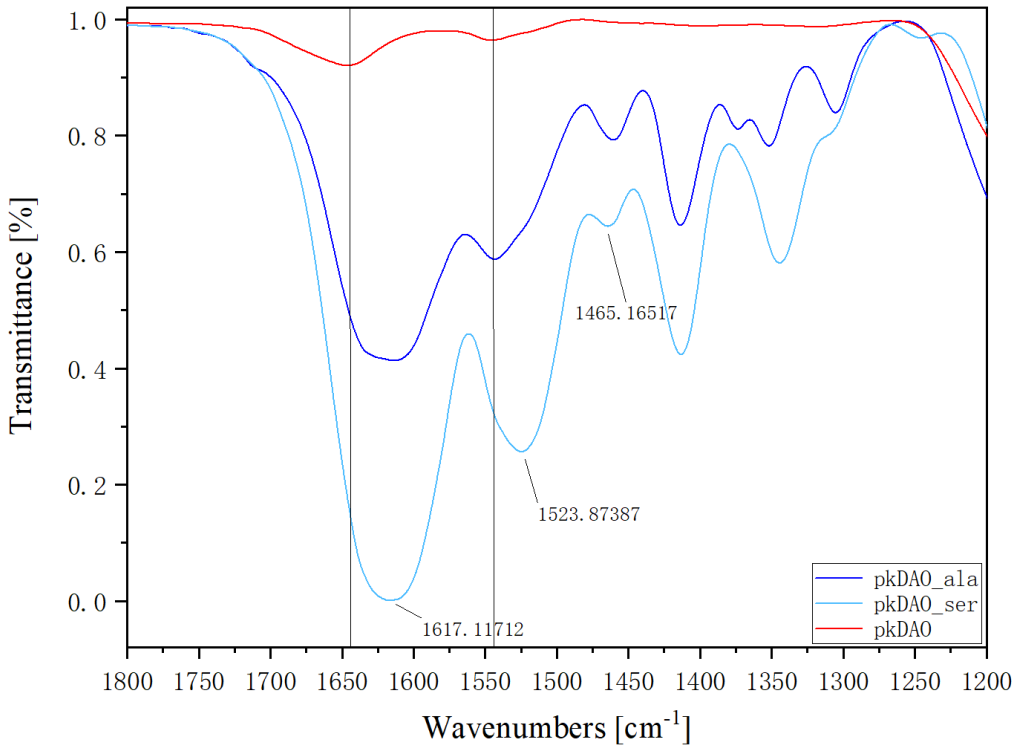

Fig. 48 . IR spectrum of pkDAAO before and after addition of alanine and serine.

3.3.3.2 Comparation IR spectrum of DAAO from *Hansenula polymorpha* before and after addition of D-amino acid

To minimize the interference of excessive concentrations of amino acids with the infrared signal, we diluted alanine and serine 1000-fold to a concentration of 0.001mg/ml. We then investigated HpDAAO and observed that the amplitude of band at 1644cm^{-1} corresponds to group vibrations of the peptide bond in the protein molecule (Amide I), the largest contribution to this type of vibrations is made by vibrations of the carbonyl group C=O. The 1541cm^{-1} band corresponds to group vibrations of Amide II peptide bonds including N-H deformation vibrations and valence C-N vibrations (Fig. 50, **Ошибка! Источник ссылки не найден.**).

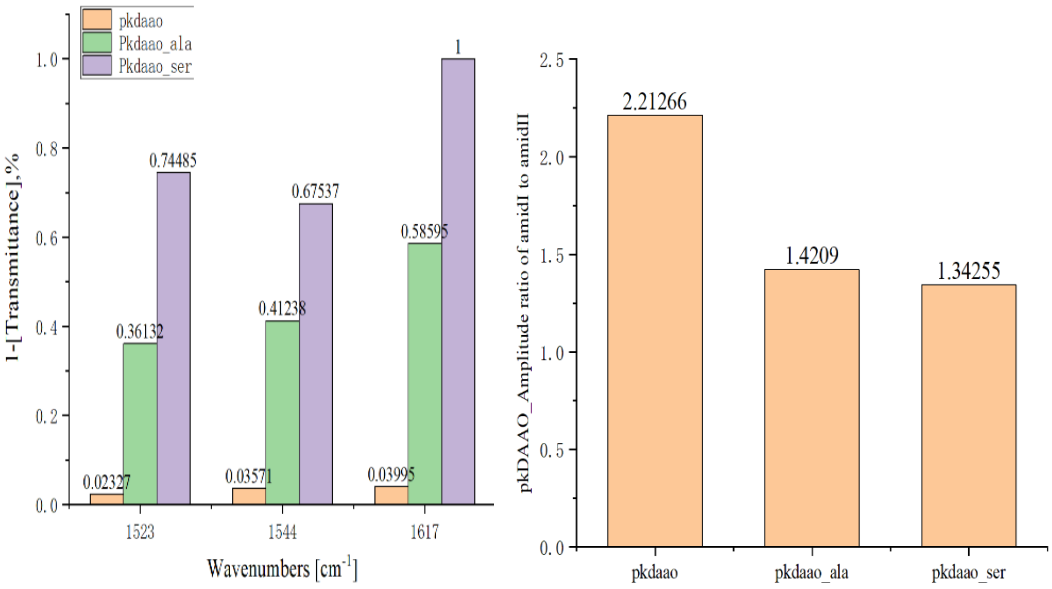

Fig. 49. Change in amid I peak amplitude (left) and amplitude ratio of amid I to amid II for pkDAAO (right)

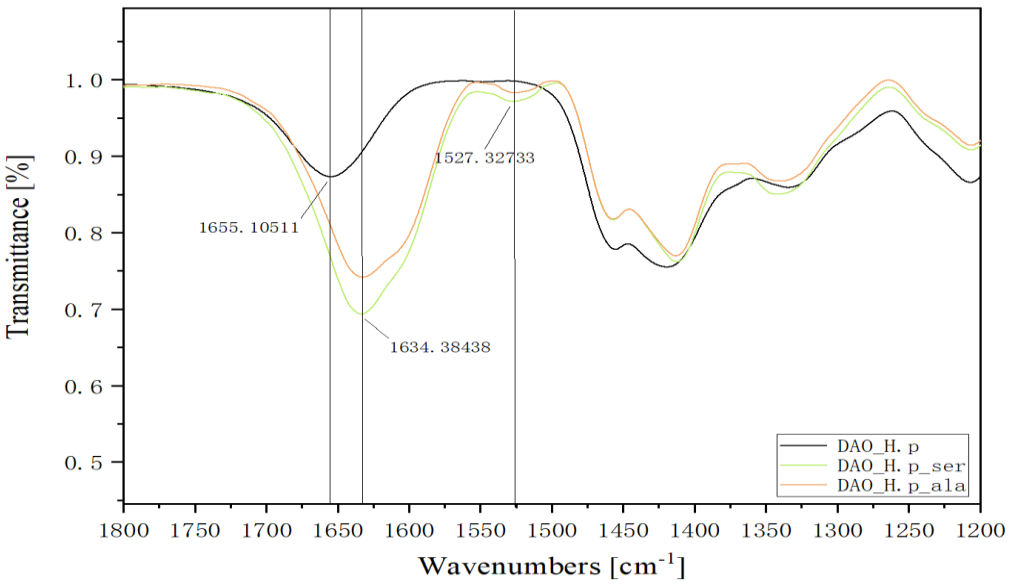

Fig. 50. Comparation IR spectrum of HpDAAO before and after addition of alanine and serine. C_{HpDAAO}=0.25 mg/ml.

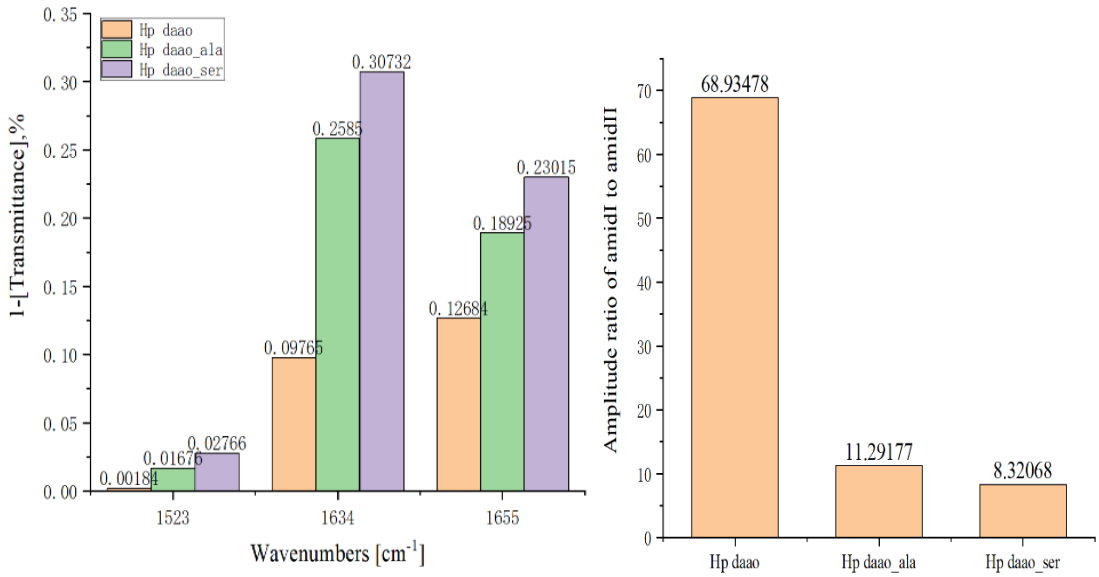

Fig. 51. Change in amid I peak amplitude (left) and amplitude ratio of amid I to amid II for pkDAAO (right)

So, using IR spectroscopy, we revealed changes in the contribution of the amide 1 and amide 2 bands upon activation of both types of DAAO, which indicates conformational transitions in the protein molecule.

Next, we will present for the analysis of Amide I band of HpDAAO changes in the secondary structure of the DAAO protein. The results of fitting the Amide I band are shown in the histogram (Fig. 52) and in the

In our study, we observed that the addition of serine or alanine are not led to a significant increase in the proportion of change in the proportion of α-helix, β-sheet, and β-turn. The presence of additional amino acids did not have a significant impact on the secondary structure of the protein, result as in the research of flavin structure by SERS method. In my opinion, the possible reason for this result is changes during enzyme work are very small or rapidly passing, so we do not see

them with our methods.

Table 10. An example of fitting the second derivative of the spectrum in the region of the Amide I band is shown in Fig.52.

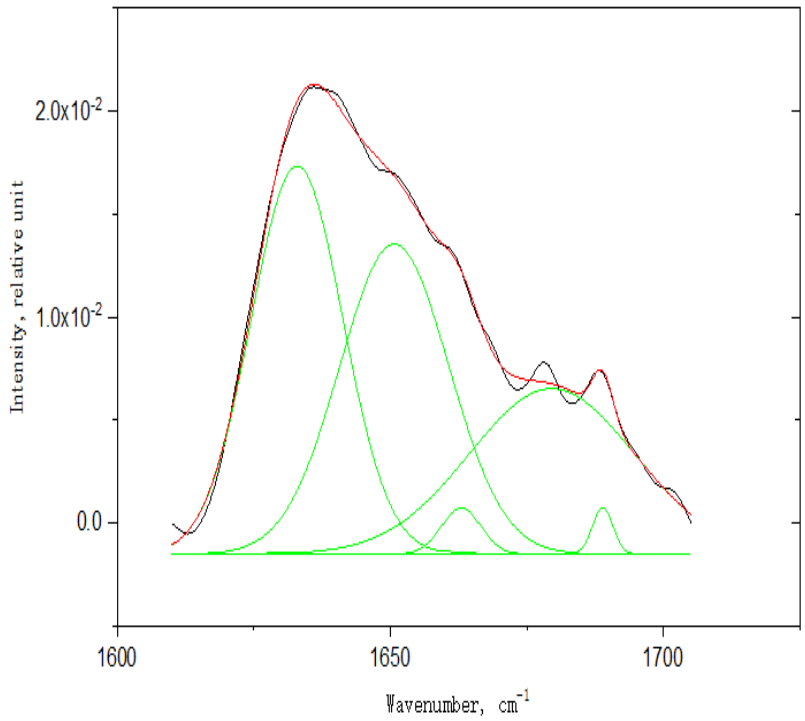

Fig. 51. Example of a deconvolution of HpDAAO IC spectrum. C_{HpDAAO}=1.34 mg/ml.

To characterize the secondary structure of the protein, deconvolution of the second derivative of the Amide I band (region 1600-1700cm^{-1}) was performed with Gaussian curves. The algorithm given in [155] was used for this purpose. OriginPro 2022 software, Peak Analyzer module was used to deconvolve the spectra. The secondary structure was estimated based on the maxima of the 2nd derivative in the range 1600-1700cm^{-1} as reported in [198]. For DAAO, α-helices: 1656 ± 2.0, 1663 ± 3.0cm^{-1}; single-chain protein structures: 1624 ± 1.0, 1627 ± 2.0, 1633 ± 2.0, 1638 ± 2.0, 1642 ± 1.0 ,1691 ± 2.0, 1696 ± 2.0cm^{-1}; β-helices: 1667 ± 1.0, 1675 ± 1.0,

1680 ± 2.0, 1685 ± 2.0cm^{-1}; undetermined structure: 1.648 ± 2.0cm^{-1}.

It was found that secondary structure of HpDAAO observed in our experiment by ATR-FTIR method is very close to pkDAAO [pdb:1VE9] structure, calculated form [199].

In this study, a longitudinal comparison is made between the secondary structural composition of HpDAAO and pkDAAO. It is observed that the proportion of alpha helix and beta structures is relatively large, regardless of the source of the enzyme used. Following the addition of alanine, the content of alpha helices in the secondary structure of the DAAO is increased to 49%, but the content of beta sheets and beta turn decreased (from 22 to 28%) (Fig. 52).

To assess the changes in secondary structure of HpDAAO we also calculate the relation of intensities of Amid I to Amid II peaks (Fig. 53). Significant changes of this parameter were not observed.

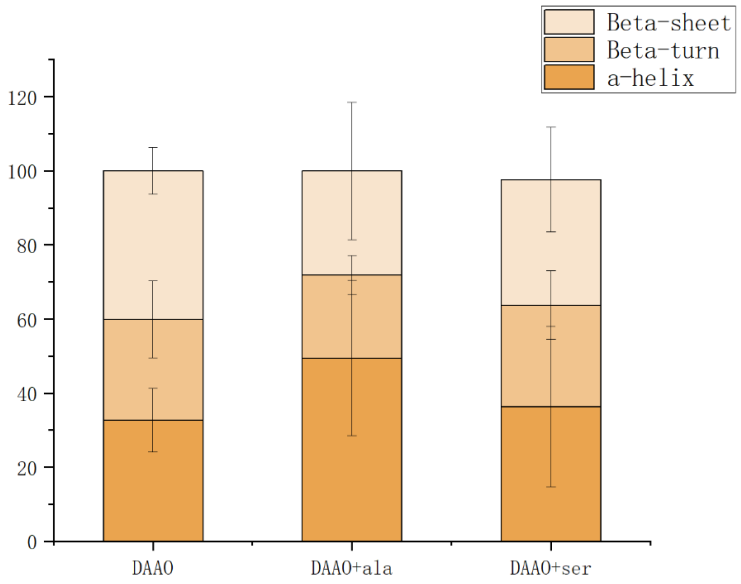

Fig. 52. Structural ratios of different types of secondary proteins before and after HpDAAO interaction with amino acids.

In our study, we observed that the addition of serine or alanine are not led to a significant increase in the proportion of change in the proportion of α-helix, β-sheet, and β-turn. The presence of additional amino acids did not have a significant impact on the secondary structure of the protein, result as in the research of flavin structure by SERS method. In my opinion, the possible reason for this result is changes during enzyme work are very small or rapidly passing, so we do not see them with our methods.

Table 10. The proportion of secondary protein structure after adding different types of amino acids to DAAO.

	α-helix, %	β- turn, %	β-sheet, %
DAAO	32.76±8.6	27.08±10.40	40.14±6.33
DAAO +ala	49.48±20.95	22.43±5.17	28.09±18.55
DAAO +ser	36.34±21.67	27.45±9.23	33.85±14.13

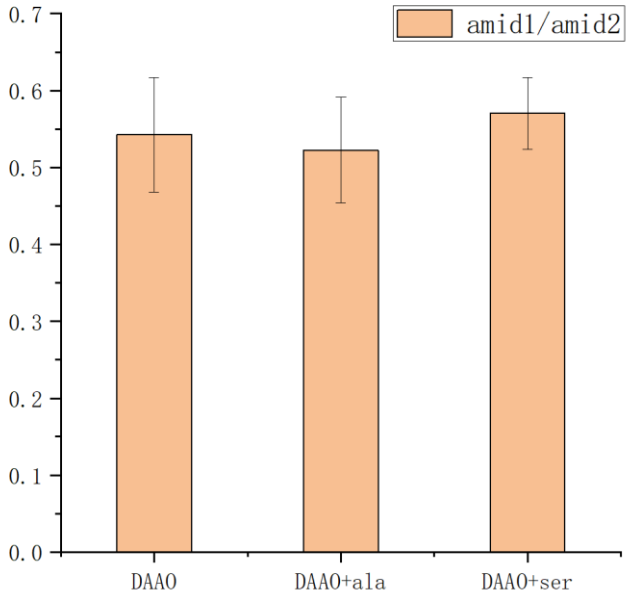

Fig. 53. Change in amid I peak amplitude for HpDAAO

According to the application of the Fourier-IR technique, the secondary structure examination of the protein unveiled that upon the integration of amino

acids, there was an absence of any meaningful alteration observed in the proportion of α-helix, β-turn, and beta-sheet. This outcome aligns with the findings obtained from the flavin structure analysis conducted using the SERS method.

3.3.4 Tryptophan picosecond fluorescence spectroscopy investigation the interaction of the enzyme DAAO with alanine

We analyzed the tryptophan picosecond fluorescence to investigate its role in interactions between active center of DAAO and D - alanine. Tryptophan is a good reference zoned in this study, who has stronger fluorescence compared to other protein amino acids. If the enzyme is excited with an excitation light that can excite the fluorescence of tryptophan, and the change of fluorescence spectra before and after the addition of amino acids to the enzyme protein is observed, it will be very helpful to analyze the conformational change of the enzyme during the interaction of DAAO with amino acids.

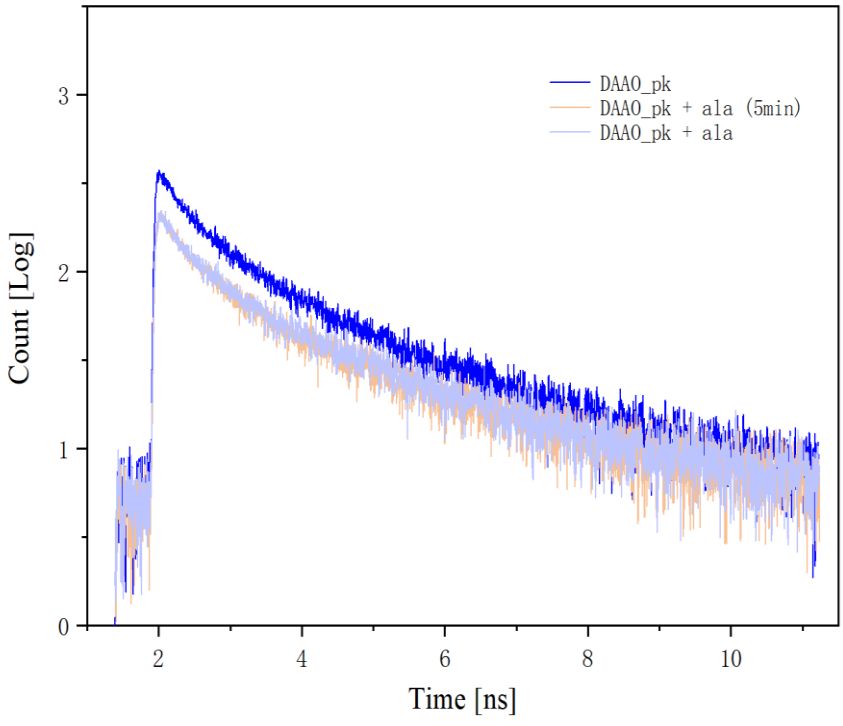

Fig. 54 Spectrum of interaction pkDAAO with D-alanine by tryptophane picosecond fluorescence. C_{pkDAAO}=0.03mg/ml, C_{HpDAAO}=0.02mg/ml; For pkDAAO spectrum measured with 262 nm excitation and emitted light 340 nm, process run 120s.

The Fig. 55 shows, for tryptophan picosecond fluorescence pkDAAO and HpDAAO characteristic kinetics were revealed, which is characterized by approximately two constants. The florescence amplitude value decreased during DAAO alanine activation, with no change in the trend of decreasing quantal output before and after D-alanine addition. After waiting for 5 minutes for the amino acid to fully react with the enzyme, the graphical trend remained unchanged. This excludes the possibility of loss of enzyme activity (since a significant change was observed in the IR spectra before and after the addition of alanine in IR measurements, see Section 3.3.3), which means that the addition of alanine can hardly change the conformation of the enzyme in the region of localization of tryptophan in enzymes isolated from various objects.

The obtained results indicate that the activation of both types of DAAO leads to a slight decrease in the amplitude of tryptophan fluorescence. This decrease suggests an increase in the efficiency of energy migration from tryptophan, possibly due to a reduction in the distance between the donor and acceptor caused by the compression of the enzyme molecule. It is important to note that this process occurs more rapidly in pk DAAO, with no significant differences observed after 5 minutes of incubation, compared to HpDAAO.

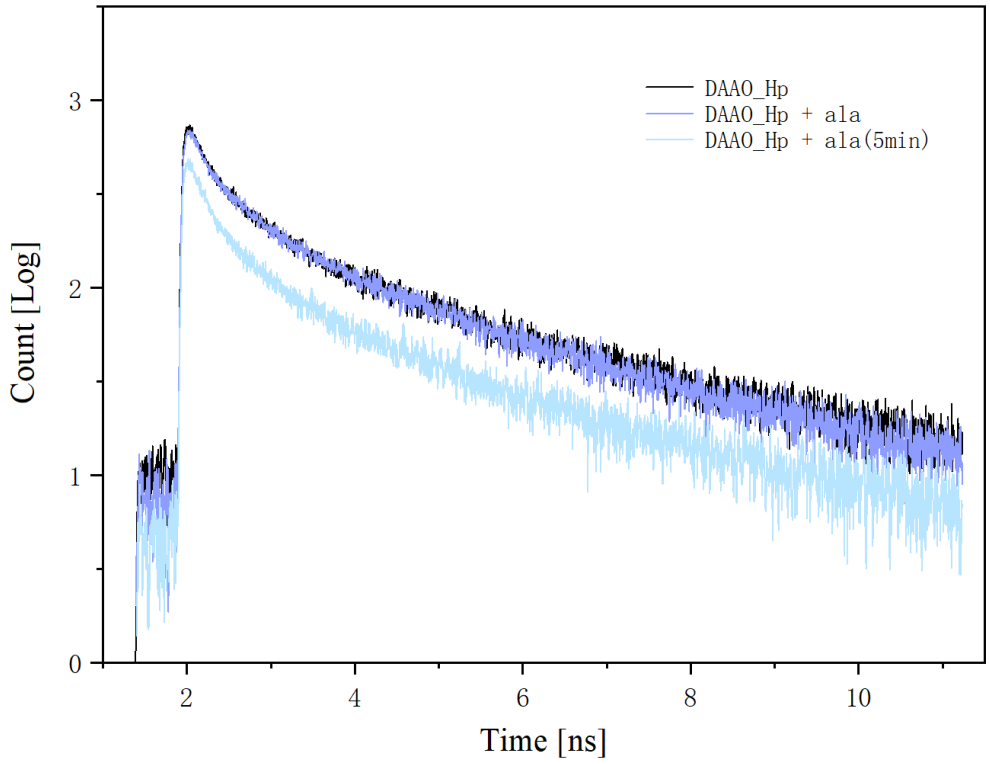

Fig. 55. Spectrum of interaction HpDAAO with D-alanine by tryptophan picosecond fluorescence. C_{HpDAAO}=0.02mg/ml; For pkDAAO spectrum measured with 262nm excitation and emitted light 340nm, process run 120s.

4. DISCUSSION

1. Molecular genetic study of the DAAO enzyme.

Our experiments were successful in establishing a construct for the genetic knockout of the d-amino acid oxidase gene in the polymorphic yeast *Hansenula polymorpha*. We were able to obtain a collection of multiple DAO/DOA knockouts and characterize them genetically and physiologically. Using the knockout strains, we confirmed the substrate specificity of the *H. Polymorpha* oxidase investigated

in an in vitro system. And the combination of D-alanine with 1% glycerol and 1% methanol has been shown to be an inducer of the three major DAO activities of *H. Polymorpha*, while glucose and L-alanine are, in contrast, inhibitors of oxidase activity. It has been shown that the combination of D-alanine with 1% glycerol and 1% methanol induces the expression of the genes HP2165 and HP2914.

2. Physic-chemical study activation of the DAAO enzyme.

We performed a comprehensive investigation of active site conformation and protein structure upon DAAO enzyme activation. Therefore, using silver nanoparticles, SERS spectra were recorded and the changes in the conformation of the FAD-cofactor upon activation of DAAO by substrates with different specificities were studied. Revealed the presence of Characteristic spectral bands with the positions of the maxima: 1630, 1584, 1546, 1355, 1252, 1160cm^{-1}, associated with the vibrations of the atom groups of the individual FAD-group rings in the oxidized state. This indicates that during the redox reaction with the substrate there is a shift in the peak 1252cm^{-1} towards the long wavelength region, which presumably is associated with the coordination processes of the active center of DAAO with respect to the amino acid. Furthermore, in the case of enzyme interaction with D-alanine, this allowed us to record the appearance of a peak at 1612cm^{-1} associated with the reduction of the flavin moiety of FAD. In addition, we observed a difference in the time taken to record the SERS spectrum changes of the FAD-group of the DAAO enzyme in the presence of D-alanine and D-serine. For example, in the interaction of DAAO with D-alanine, changes in the SERS

spectra took place in a matter of seconds, although when D-serine was added, similar results took minutes to obtain, confirming data from the literature on the differing activity of the DAAO enzyme in interactions with these amino acids.

During the enzymatic reaction of DAAO with an amino acid, its dehydrogenation and hydrogen transfer to the flavin N(5) takes place. The stabilization of the substrate with respect to the enzyme is then provided by several hydrogen bonds, and following dehydrogenation this process is also performed due to the electrostatic interactions of the atoms in the molecule. It is likely that the N (3)-H group of the flavin is not directly involved in the progress of the enzyme, but the stabilization of the cofactor molecule with respect to the ligand can influence the change in the N (3)-H···R hydrogen bond that we observe upon introduction of D-alanine to DAAO. The reduced enzyme-amino acid complex is then re-oxidized, and in the second we observe the disappearance of the peak at 1612cm^{-1}, whereas the peak in the 1600cm-1 region again shifts to the low frequency region of the SERS spectrum.

The reaction kinetics between human DAAO enzyme and D-serine is well-documented to have a four-fold higher K_M value compared to the reaction between DAAO and D-alanine. Furthermore, previous studies have shown that the relative activity of DAAO enzyme derived from pig kidney exhibits more than double the potency against D-alanine as compared to D-serine. These findings align with the experimental evidence indicating that alterations in the FAD-group spectrum of DAAO take a longer time to manifest when D-serine is introduced, whereas changes are promptly observed within the initial seconds when D-alanine is

introduced to the enzymatic reaction. Spectroscopic analysis has revealed that upon D-serine activation, the peak at 1252cm^{-1} undergoes relocation within 60 seconds, accompanied by the emergence of a new peak at the 1300cm^{-1} region. However, it is important to note that after 7-10 minutes, the 1200-1355cm^{-1} range in the FAD SERS spectrum of DAAO ceases to exhibit any further alterations.

Therefore, shifts in the SERS spectra were observed within a brief time frame during the interaction between DAAO and D-alanine. Conversely, upon the addition of D-serine, similar results required minutes, which confirms the literature data on the different activity of the DAAO enzyme in interactions with these amino acids.

In the following section, we investigated the configuration of the active site and protein structure when the DAAO enzyme is activated. Through the utilization of Infrared (IR) analysis, we observed alterations in the secondary protein structure while activating DAAO with diverse substrates. In these experiments the second protein structure changes during the alanine HpDAAO activation were found. The amplitude of band at 1652cm^{-1} corresponds to group vibrations of the peptide bond in the protein molecule (Amide I), the largest contribution to this type of vibrations is made by vibrations of the carbonyl group C=O was increased. The band maximum is characteristic of the α-helix structure. The 1548cm^{-1} band corresponds to group vibrations of Amide II peptide bonds including N-H deformation vibrations and valence C-N vibrations, was increased. Therefore, the Fourier-IR technique utilized to analyze the protein's secondary structure revealed that there were insignificant changes in the proportions of α-helix, β-turn, and beta-sheet

during the activation of pkDAAO and HpDAAO, which parallels the findings in the exploration of flavin structure using the Surface-Enhanced Raman Spectroscopy (SERS) method.

In the previous part of experiments, using SERS, it was found that changes in the active site of the enzyme occur in a short time, and using IR spectroscopy under similar conditions for enzyme activation, changes in the secondary structure of DAAO were revealed. To study fast (ns) changes in protein structure, we monitored changes in tryptophan fluorescence of the DAAO protein. The results obtained indicate that upon activation of both types of DAAO, there is a slight decrease in the tryptophan fluorescence amplitude, which probably indicates an increase in the efficiency of energy migration from this amino acid due to a decrease in the distance between the donor and acceptor because of the "compression" of the enzyme molecule. Note that this process is faster in pkDAAO (no differences after 5 minutes of incubation) than in HpDAAO.

5. CONCLUSIONS.

1.A collection of DAAO gene knockouts was obtained, including one single knockout, three double knockouts, and one triple knockout.

2. The substrate specificity of H. polymorpha DL-1 oxidases was confirmed in an in vitro system using knockout strains.

3. It was found that D-alanine in combination with 1% glycerol and 1% methanol was able to induce the activity of all three major DAAOs of H.polymorpha. On the

contrary, glucose, and L-alanine suppress oxidase activity.

4. D-alanine in combination with 1% glycerol and 1% methanol was shown to induce the expression of HP2165 and HP2914 genes.

5. The use of a silver substrate has been shown to increase the sensitivity of RS by 10^5-10^6 (signal registration at 10^{-9} mol/L, which was used to study the conformation of the DAAO flavin.

6. It was found that during the redox reaction of flavin interaction with the substrate, there is a change in its conformation: a shift of the maximum of the RS spectrum at 1252 cm^{-1} to the long-wavelength region, which is probably associated with the processes of coordination of the active center of DAAO with the amino acid molecule.

7. When DAAO interacted with D-alanine, shifts in the SERS spectra were observed over a shorter time interval than when D-serine was added, indicating different substrate specificity of DAAO.

8. IR spectroscopy revealed a change in the contribution of amide 1 and amide 2 bands upon activation of both types of DAAO, which indicates conformational transitions both in flavin and in the protein molecule.

9. The single-photon counting method detected changes in tryptophan fluorescence amplitude upon DAAO activation, which proceed faster in $_{pk}$DAAO than in $_{Hp}$DAAO and are probably related to rapid changes in the conformation of the protein molecule. DAAO and are probably associated with rapid changes in the conformation of the protein molecule.

6. REFERENCE LIST.

1. Оксидаза D-аминокислот: структура, механизм действия и практическое применение – выпуск 1, том 70, 2005 – Биохимия. Accessed August 18, 2023. https://biochemistrymoscow.com/ru/archive/2005/70-01-0051/
2. Khoronenkova S V., Tishkov VI. D-amino acid oxidase: physiological role and applications. *Biochemistry (Mosc)*. 2008;73(13):1511-1518. doi:10.1134/S0006297908130105
3. [Compared D-amino acid oxidase expression in different Pichia pastoris host strains] - PubMed. Accessed August 21, 2023. https://pubmed.ncbi.nlm.nih.gov/15968991/
4. Ravin N V., Eldarov MA, Kadnikov V V., et al. Genome sequence and analysis of methylotrophic yeast Hansenula polymorpha DL1. *BMC Genomics*. 2013;14(1). doi:10.1186/1471-2164-14-837
5. Umhau S, Pollegioni L, Molla G, et al. The x-ray structure of D-amino acid oxidase at very high resolution identifies the chemical mechanism of flavin-dependent substrate dehydrogenation. *Proc Natl Acad Sci U S A*. 2000;97(23):12463-12468. doi:10.1073/PNAS.97.23.12463
6. Pollegioni L, Piubelli L, Sacchi S, Pilone MS, Molla G. Physiological functions of D-amino acid oxidases: from yeast to humans. *Cell Mol Life Sci*. 2007;64(11):1373-1394. doi:10.1007/S00018-007-6558-4
7. V. Ferraris D, Tsukamoto T. Recent advances in the discovery of D-amino acid oxidase inhibitors and their therapeutic utility in schizophrenia. *Curr*

Pharm Des. 2011;17(2):103-111. doi:10.2174/138161211795049633

8. Sacchi S, Rosini E, Pollegioni L, Molla G. D-amino acid oxidase inhibitors as a novel class of drugs for schizophrenia therapy. *Curr Pharm Des*. 2013;19(14):2499-2511. doi:10.2174/1381612811319140002
9. Xin YF, Zhou XJ, Cheng X, Wang YX. Renal D-amino acid oxidase mediates chiral inversion of N(G)-nitro-D-arginine. *J Pharmacol Exp Ther*. 2005;312(3):1090-1096. doi:10.1124/JPET.104.077123
10. Pollegioni L, Molla G, Sacchi S, Rosini E, Verga R, Pilone MS. Properties and applications of microbial D-amino acid oxidases: current state and perspectives. *Appl Microbiol Biotechnol*. 2008;78(1):1-16. doi:10.1007/S00253-007-1282-4
11. Pilone MS, Pollegioni L. D-amino acid oxidase as an industrial biocatalyst. *Biocatal Biotransformation*. 2002;20(3):145-159. doi:10.1080/10242420290020679
12. Pollegioni L, Sacchi S, Caldinelli L, et al. Engineering the properties of D-amino acid oxidases by a rational and a directed evolution approach. *Curr Protein Pept Sci*. 2007;8(6):600-618. doi:10.2174/138920307783018677
13. CASALIN P, POLLEGIONI L, CURTI B, SIMONETTA MP. A study on apoenzyme from Rhodotorula gracilis D-amino acid oxidase. *Eur J Biochem*. 1991;197(2):513-517. doi:10.1111/J.1432-1033.1991.TB15939.X
14. Pollegioni L, Caldinelli L, Molla G, Sacchi S, Pilone MS. Catalytic properties of D-amino acid oxidase in cephalosporin C bioconversion: a comparison between proteins from different sources. *Biotechnol Prog*.

2004;20(2):467-473. doi:10.1021/BP034206Q

15. Yurimoto H, Hasegawa T, Sakai Y, Kato N. Characterization and high-level production of D-amino acid oxidase in Candida boidinii. *Biosci Biotechnol Biochem*. 2001;65(3):627-633. doi:10.1271/BBB.65.627

16. Caligiuri A, D'Arrigo P, Rosini E, et al. Enzymatic conversion of unnatural amino acids by yeast D-amino acid oxidase. *Adv Synth Catal*. 2006;348(15):2183-2190. doi:10.1002/ADSC.200606188

17. RCSB PDB - 3ZNQ: IN VITRO AND IN VIVO INHIBITION OF HUMAN D-AMINO ACID OXIDASE: REGULATION OF D-SERINE CONCENTRATION IN THE BRAIN. Accessed August 23, 2023. https://www.rcsb.org/structure/3ZNQ

18. Hopkins SC, Heffernan MLR, Saraswat LD, et al. Structural, kinetic, and pharmacodynamic mechanisms of d-amino acid oxidase inhibition by small molecules. *J Med Chem*. 2013;56(9):3710-3724. doi:10.1021/JM4002583

19. RCSB PDB - 1KIF: D-AMINO ACID OXIDASE FROM PIG KIDNEY. Accessed August 23, 2023. https://www.rcsb.org/structure/1KIF

20. Mattevi A, Vanoni MA, Todone F, et al. Crystal structure of D-amino acid oxidase: A case of active site mirror-image convergent evolution with flavocytochrome b2. *Proc Natl Acad Sci U S A*. 1996;93(15):7496-7501. doi:10.1073/PNAS.93.15.7496

21. RCSB PDB - 1VE9: Porcine kidney D-amino acid oxidase. Accessed August 23, 2023. https://www.rcsb.org/structure/1VE9

22. Mizutani H, Miyahara I, Hirotsu K, et al. Three-dimensional structure of

porcine kidney D-amino acid oxidase at 3.0 Å resolution. *J Biochem*. 1996;120(1):14-17. doi:10.1093/OXFORDJOURNALS.JBCHEM.A021376

23. Pollegioni L, Diederichs K, Molla G, et al. Yeast D-amino acid oxidase: Structural basis of its catalytic properties. *J Mol Biol*. 2002;324(3):535-546. doi:10.1016/S0022-2836(02)01062-8

24. Molla G, Sacchi S, Bernasconi M, Pilone MS, Fukui K, Pollegioni L. Characterization of human d-amino acid oxidase. *FEBS Lett*. 2006;580(9):2358-2364. doi:10.1016/J.FEBSLET.2006.03.045

25. Müller F. d- and l-Amino Acid Oxidases. Published online July 22, 2019:69-94. doi:10.1201/9781351070560-3

26. Mattevi A, Vanoni MA, Todone F, et al. Crystal structure of D-amino acid oxidase: a case of active site mirror-image convergent evolution with flavocytochrome b2. *Proc Natl Acad Sci U S A*. 1996;93(15):7496-7501. doi:10.1073/PNAS.93.15.7496

27. Mizutani H, Miyahara I, Hirotsu K, et al. Three-dimensional structure of porcine kidney D-amino acid oxidase at 3.0 A resolution. *J Biochem*. 1996;120(1):14-17. doi:10.1093/OXFORDJOURNALS.JBCHEM.A021376

28. Polcari D, Kwan A, Van Horn MR, et al. Disk-shaped amperometric enzymatic biosensor for in vivo detection of D-serine. *Anal Chem*. 2014;86(7):3501-3507. doi:10.1021/AC404111U

29. Kourist R. Biocatalysis in Organic Synthesis. Science of Synthesis, Vol. 1–3. Edited by Kurt Faber, Wolf-Dieter Fessner and Nicholas J. Turner. *Angewandte Chemie International Edition*. 2015;54(43):12547-12547.

doi:10.1002/ANIE.201508130

30. Pollegioni L, Sacchi S, Caldinelli L, et al. Engineering the properties of D-amino acid oxidases by a rational and a directed evolution approach. *Curr Protein Pept Sci*. 2007;8(6):600-618. doi:10.2174/138920307783018677

31. Sacchi S, Caldinelli L, Cappelletti P, Pollegioni L, Molla G. Structure-function relationships in human D-amino acid oxidase. *Amino Acids*. 2012;43(5):1833-1850. doi:10.1007/S00726-012-1345-4/METRICS

32. Tishkov VI, Khoronenkova S V. D-amino acid oxidase: Structure, catalytic mechanism, and practical application. *Biokhimiya*. 2005;70(1):51-67. doi:10.1007/S10541-005-0050-2/METRICS

33. Kawazoe T, Tsuge H, Pilone MS, Fukui K. Crystal structure of human D-amino acid oxidase: context-dependent variability of the backbone conformation of the VAAGL hydrophobic stretch located at the si-face of the flavin ring. *Protein Sci*. 2006;15(12):2708-2717. doi:10.1110/PS.062421606

34. Yasukawa K, Nakano S, Asano Y. Tailoring D-Amino Acid Oxidase from the Pig Kidney to R-Stereoselective Amine Oxidase and its Use in the Deracemization of α-Methylbenzylamine. *Angewandte Chemie International Edition*. 2014;53(17):4428-4431. doi:10.1002/ANIE.201308812

35. Umhau S, Pollegioni L, Molla G, et al. The x-ray structure of D-amino acid oxidase at very high resolution identifies the chemical mechanism of flavin-dependent substrate dehydrogenation. *Proc Natl Acad Sci U S A*. 2000;97(23):12463-12468. doi:10.1073/PNAS.97.23.12463

36. Miura R, Setoyama C, Nishina Y, et al. Structural and mechanistic studies on

D-amino acid oxidase x substrate complex: implications of the crystal structure of enzyme x substrate analog complex. *J Biochem*. 1997;122(4):825-833. doi:10.1093/OXFORDJOURNALS.JBCHEM.A021829

37. Pollegioni L, Diederichs K, Molla G, et al. Yeast D-amino acid oxidase: Structural basis of its catalytic properties. *J Mol Biol*. 2002;324(3):535-546. doi:10.1016/S0022-2836(02)01062-8
38. Rosini E, Molla G, Ghisla S, Pollegioni L. On the reaction of D-amino acid oxidase with dioxygen: O2 diffusion pathways and enhancement of reactivity. *FEBS J*. 2011;278(3):482-492. doi:10.1111/J.1742-4658.2010.07969.X
39. Saam J, Rosini E, Molla G, Schulten K, Pollegioni L, Ghisla S. O2 reactivity of flavoproteins: dynamic access of dioxygen to the active site and role of a H+ relay system in D-amino acid oxidase. *J Biol Chem*. 2010;285(32):24439-24446. doi:10.1074/JBC.M110.131193
40. Subramanian K, Góra A, Spruijt R, et al. Modulating D-amino acid oxidase (DAAO) substrate specificity through facilitated solvent access. *PLoS One*. 2018;13(6):e0198990. doi:10.1371/JOURNAL.PONE.0198990
41. Todone F, Vanoni MA, Mozzarelli A, et al. Active site plasticity in D-amino acid oxidase: a crystallographic analysis. *Biochemistry*. 1997;36(19):5853-5860. doi:10.1021/BI9630570
42. Umhau S, Pollegioni L, Molla G, et al. The x-ray structure of D-amino acid oxidase at very high resolution identifies the chemical mechanism of flavin-dependent substrate dehydrogenation. *Proc Natl Acad Sci U S A*.

2000;97(23):12463-12468. doi:10.1073/PNAS.97.23.12463

43. Ronald L Birke JX, Lombardi JR. Surface-Enhanced Raman Spectroscopy from Flavins Adsorbed on a Silver Electrode: Observation of the Unstable Semiquinone Intermediate. *J Am Chem Soc*. 1987;109(19):5645-5649. doi:10.1021/JA00253A014

44. Expression of D-amino acid oxidase in Rhodotorula gracilis under induction conditions: a biochemical and cytochemical study - PubMed. Accessed August 15, 2023. https://pubmed.ncbi.nlm.nih.gov/1680680/

45. Regulation of peroxisomal proteins and organelle proliferation by multiple carbon sources in the methylotrophic yeast, Candida boidinii - PubMed. Accessed August 15, 2023. https://pubmed.ncbi.nlm.nih.gov/9791889/

46. Physiological role of the D-amino acid oxidase gene, DAO1, in carbon and nitrogen metabolism in the methylotrophic yeast Candida boidinii - PubMed. Accessed August 15, 2023. https://pubmed.ncbi.nlm.nih.gov/10992285/

47. Molla G, Motteran L, Piubelli L, Pilone MS, Pollegioni L. Regulation of D-amino acid oxidase expression in the yeast Rhodotorula gracilis. *Yeast*. 2003;20(12):1061-1069. doi:10.1002/YEA.1023

48. Simonetta MP, Verga R, Fretta A, Hanozet GM. Induction of d-Amino-acid Oxidase by d-Alanine in Rhodotorula gracilis Grown in Defined Medium. *Microbiology (N Y)*. 1989;135(3):593-600. doi:10.1099/00221287-135-3-593

49. Sikora L, Marzluf GA. Regulation of L-amino acid oxidase and of D-amino acid oxidase in Neurospora crassa. *Mol Gen Genet*. 1982;186(1):33-39. doi:10.1007/BF00422908

50. Wei C -J, Huang J -C, Tsai Y -P. Study on the synthesis of D-amino acid oxidase in Trigonopsis variabilis in continuous culture. *Biotechnol Bioeng*. 1989;34(4):570-574. doi:10.1002/BIT.260340418

51. Hörner R, Wagner F, Fischer L. Induction of the d-Amino Acid Oxidase from Trigonopsis variabilis. *Appl Environ Microbiol*. 1996;62(6):2106-2110. doi:10.1128/AEM.62.6.2106-2110.1996

52. Liu Y, Koh CMJ, Ngoh S Te, Ji L. Engineering an efficient and tight D-amino acid-inducible gene expression system in Rhodosporidium/Rhodotorula species. *Microb Cell Fact*. 2015;14(1). doi:10.1186/S12934-015-0357-7

53. Setoyama C, Miura R, Nishina Y, et al. Crystallization of expressed porcine kidney D-amino acid oxidase and preliminary X-ray crystallographic characterization. *J Biochem*. 1996;119(6):1114-1117. doi:10.1093/OXFORDJOURNALS.JBCHEM.A021356

54. Molla G, Vegezzi C, Pilone MS, Pollegioni L. Overexpression in Escherichia coli of a recombinant chimeric Rhodotorula gracilis d-amino acid oxidase. *Protein Expr Purif*. 1998;14(2):289-294. doi:10.1006/PREP.1998.0956

55. Isogai T, Ono H, Ishitani Y, Kojo H, Ueda Y, Kohsaka M. Structure and expression of cDNA for D-amino acid oxidase active against cephalosporin C from Fusarium solani. *J Biochem*. 1990;108(6):1063-1069. doi:10.1093/OXFORDJOURNALS.JBCHEM.A123306

56. Deng S, Su E, Ma X, Yang S, Wei D. High-level soluble and functional expression of Trigonopsis variabilis D-amino acid oxidase in Escherichia coli. *Bioprocess Biosyst Eng*. 2014;37(8):1517-1526. doi:10.1007/S00449-013-

1123-Z

57. Dib I, Stanzer D, Nidetzky B. Trigonopsis variabilis D-amino acid oxidase: control of protein quality and opportunities for biocatalysis through production in Escherichia coli. *Appl Environ Microbiol*. 2007;73(1):331-333. doi:10.1128/AEM.01569-06

58. Rosini E, Boreggio M, Verga M, Caldinelli L, Pollegioni L, Fasoli E. The D-amino acid oxidase-carbon nanotubes: evaluation of cytotoxicity and biocompatibility of a potential anticancer nanosystem. *3 Biotech*. 2023;13(7):1-11. doi:10.1007/S13205-023-03568-1/FIGURES/3

59. Kim SJ, Kim NJ, Shin CH, Kim CW. Optimization of culture condition for the production of D-amino acid oxidase in a recombinant Escherichia coli. *Biotechnology and Bioprocess Engineering*. 2008;13(2):144-149. doi:10.1007/S12257-008-0005-8

60. Abad S, Nahalka J, Bergler G, et al. Stepwise engineering of a Pichia pastoris D-amino acid oxidase whole cell catalyst. *Microb Cell Fact*. 2010;9. doi:10.1186/1475-2859-9-24

61. Abad S, Nahalka J, Winkler M, et al. High-level expression of Rhodotorula gracilis D-amino acid oxidase in Pichia pastoris. *Biotechnol Lett*. 2011;33(3):557-563. doi:10.1007/S10529-010-0456-9

62. Zheng H, Wang X, Chen J, et al. Expression, purification, and immobilization of His-tagged D-amino acid oxidase of Trigonopsis variabilis in Pichia pastoris. *Appl Microbiol Biotechnol*. 2006;70(6):683-689. doi:10.1007/S00253-005-0158-8

63. [Expression of modified oxidase of D-aminoacids of Trigonopsis variabilis in methylotrophic yeasts Pichia pastoris] - PubMed. Accessed August 15, 2023. https://pubmed.ncbi.nlm.nih.gov/21442919/

64. Friedman M. Chemistry, nutrition, and microbiology of D-amino acids. *J Agric Food Chem*. 1999;47(9):3457-3479. doi:10.1021/JF990080U

65. Nieh CH, Kitazumi Y, Shirai O, Kano K. Sensitive D-amino acid biosensor based on oxidase/peroxidase system mediated by pentacyanoferrate-bound polymer. *Biosens Bioelectron*. 2013;47:350-355. doi:10.1016/J.BIOS.2013.03.042

66. Lata S, Batra B, Kumar P, Pundir CS. Construction of an amperometric D-amino acid biosensor based on D-amino acid oxidase/carboxylated mutliwalled carbon nanotube/copper nanoparticles/polyalinine modified gold electrode. *Anal Biochem*. 2013;437(1):1-9. doi:10.1016/J.AB.2013.01.030

67. Molla G, Piubelli L, Volontè F, Pilone MS. Enzymatic detection of D-amino acids. *Methods Mol Biol*. 2012;794:273-289. doi:10.1007/978-1-61779-331-8_18

68. Seo YM, Mathew S, Bea HS, et al. Deracemization of unnatural amino acid: homoalanine using D-amino acid oxidase and ω-transaminase. *Org Biomol Chem*. 2012;10(12):2482-2485. doi:10.1039/C2OB07161D

69. Pollegioni L, Molla G. New biotech applications from evolved D-amino acid oxidases. *Trends Biotechnol*. 2011;29(6):276-283. doi:10.1016/J.TIBTECH.2011.01.010

70. Domínguez R, Serra B, Reviejo AJ, Pingarrón JM. Chiral analysis of amino

acids using electrochemical composite bienzyme biosensors. *Anal Biochem*. 2001;298(2):275-282. doi:10.1006/ABIO.2001.5371

71. García-García M, Martínez-Martínez I, Sánchez-Ferrer Á, García-Carmona F. Production of the apoptotic cellular mediator 4-Methylthio-2-oxobutyric acid by using an enzymatic stirred tank reactor with in situ product removal. *Biotechnol Prog*. 2008;24(1):187-191. doi:10.1021/BP0702424
72. Elander RP. Industrial production of beta-lactam antibiotics. *Appl Microbiol Biotechnol*. 2003;61(5-6):385-392. doi:10.1007/S00253-003-1274-Y
73. Barber MS, Giesecke U, Reichert A, Minas W. Industrial enzymatic production of cephalosporin-based beta-lactams. *Adv Biochem Eng Biotechnol*. 2004;88:179-215. doi:10.1007/B99261
74. Betancor L, Hidalgo A, Fernández-Lorente G, et al. Use of physicochemical tools to determine the choice of optimal enzyme: stabilization of D-amino acid oxidase. *Biotechnol Prog*. 2003;19(3):784-788. doi:10.1021/BP025761F
75. Khang YH, Kim IW, Hah YR, Hwangbo JH, Kang KK. Fusion protein of Vitreoscilla hemoglobin with D-amino acid oxidase enhances activity and stability of biocatalyst in the bioconversion process of cephalosporin C. *Biotechnol Bioeng*. 2003;82(4):480-488. doi:10.1002/BIT.10592
76. Yurimoto H, Oku M, Sakai Y. Yeast methylotrophy: metabolism, gene regulation and peroxisome homeostasis. *Int J Microbiol*. 2011;2011. doi:10.1155/2011/101298
77. Nakagawa T, Yoshida K, Takeuchi A, et al. The peroxisomal catalase gene in the methylotrophic yeast Pichia methanolica. *Biosci Biotechnol Biochem*.

2010;74(8):1733-1735. doi:10.1271/BBB.100329

78. Gellissen G. Heterologous protein production in methylotrophic yeasts. *Appl Microbiol Biotechnol*. 2000;54(6):741-750. doi:10.1007/S002530000464

79. Gellissen Gerd. Hansenula polymorpha : biology and applications: Technical enzyme production and whole-cell biocatalysis:application of Hansenula polymorpha. Published online 2002:347. Accessed August 16, 2023. https://archive.org/details/hansenulapolymor0000unse

80. Levine DW, Cooney CL. Isolation and characterization of a thermotolerant methanol-utilizing yeast. *Appl Microbiol*. 1973;26(6):982-990. doi:10.1128/AM.26.6.982-990.1973

81. Kunze G, Kang HA, Gellissen G. Hansenula polymorpha (Pichia angusta): Biology and applications. *Yeast Biotechnology: Diversity and Applications*. Published online 2009:47-64. doi:10.1007/978-1-4020-8292-4_3

82. Suh SO, Zhou JJ. Methylotrophic yeasts near Ogataea (Hansenula) polymorpha: a proposal of Ogataea angusta comb. nov. and Candida parapolymorpha sp. nov. *FEMS Yeast Res*. 2010;10(5):631-638. doi:10.1111/J.1567-1364.2010.00634.X

83. Siverio JM. Assimilation of nitrate by yeasts. *FEMS Microbiol Rev*. 2002;26(3):277-284. doi:10.1111/J.1574-6976.2002.TB00615.X

84. Martín Y, González Y V., Cabrera E, Rodríguez C, Siverio JM. Npr1 Ser/Thr protein kinase links nitrogen source quality and carbon availability with the yeast nitrate transporter (Ynt1) levels. *J Biol Chem*. 2011;286(31):27225-

27235. doi:10.1074/JBC.M111.265116

85. Ishchuk OP, Voronovsky AY, Abbas CA, Sibirny AA. Construction of Hansenula polymorpha strains with improved thermotolerance. *Biotechnol Bioeng*. 2009;104(5):911-919. doi:10.1002/BIT.22457

86. Kurylenko OO, Ruchala J, Hryniv OB, Abbas CA, Dmytruk K V., Sibirny AA. Metabolic engineering and classical selection of the methylotrophic thermotolerant yeast Hansenula polymorpha for improvement of high-temperature xylose alcoholic fermentation. *Microb Cell Fact*. 2014;13(1). doi:10.1186/S12934-014-0122-3

87. Yurimoto H, Kato N, Sakai Y. Assimilation, dissimilation, and detoxification of formaldehyde, a central metabolic intermediate of methylotrophic metabolism. *Chem Rec*. 2005;5(6):367-375. doi:10.1002/TCR.20056

88. Ozimek P, Veenhuis M, Van Der Klei IJ. Alcohol oxidase: a complex peroxisomal, oligomeric flavoprotein. *FEMS Yeast Res*. 2005;5(11):975-983. doi:10.1016/J.FEMSYR.2005.06.005

89. Ito T, Fujimura S, Uchino M, et al. Distribution, diversity and regulation of alcohol oxidase isozymes, and phylogenetic relationships of methylotrophic yeasts. *Yeast*. 2007;24(6):523-532. doi:10.1002/YEA.1490

90. Szamecz B, Urbán G, Rubiera R, Kucsera J, Dorgai L. Identification of four alcohol oxidases from methylotrophic yeasts. *Yeast*. 2005;22(8):669-676. doi:10.1002/YEA.1236

91. Cereghino GPL, Cregg JM. Applications of yeast in biotechnology: protein production and genetic analysis. *Curr Opin Biotechnol*. 1999;10(5):422-427.

doi:10.1016/S0958-1669(99)00004-X

92. van der Klei IJ, Yurimoto H, Sakai Y, Veenhuis M. The significance of peroxisomes in methanol metabolism in methylotrophic yeast. *Biochim Biophys Acta*. 2006;1763(12):1453-1462. doi:10.1016/J.BBAMCR.2006.07.016

93. Yurimoto H, Lee B, Yasuda F, Sakai Y, Kato N. Alcohol dehydrogenases that catalyse methyl formate synthesis participate in formaldehyde detoxification in the methylotrophic yeast Candida boidinii. *Yeast*. 2004;21(4):341-350. doi:10.1002/YEA.1101

94. Sakai Y, Murdanoto AP, Konishi T, Iwamatsu A, Kato N. Regulation of the formate dehydrogenase gene, FDH1, in the methylotrophic yeast Candida boidinii and growth characteristics of an FDH1-disrupted strain on methanol, methylamine, and choline. *J Bacteriol*. 1997;179(14):4480-4485. doi:10.1128/JB.179.14.4480-4485.1997

95. Gellissen G, Kunze G, Gaillardin C, et al. New yeast expression platforms based on methylotrophic Hansenula polymorpha and Pichia pastoris and on dimorphic Arxula adeninivorans and Yarrowia lipolytica - a comparison. *FEMS Yeast Res*. 2005;5(11):1079-1096. doi:10.1016/J.FEMSYR.2005.06.004

96. Yurimoto H, Sakai Y. Methanol-inducible gene expression and heterologous protein production in the methylotrophic yeast Candida boidinii. *Biotechnol Appl Biochem*. 2009;53(Pt 2):85. doi:10.1042/BA20090030

97. Ahmad M, Hirz M, Pichler H, Schwab H. Protein expression in Pichia

pastoris: recent achievements and perspectives for heterologous protein production. *Appl Microbiol Biotechnol*. 2014;98(12):5301-5317. doi:10.1007/S00253-014-5732-5

98. van der Klei IJ, Veenhuis M. Hansenula polymorpha : A Versatile Model Organism in Peroxisome Research . *Hansenula polymorpha*. Published online January 28, 2005:76-94. doi:10.1002/3527602356.CH6
99. Love KR, Shah KA, Whittaker CA, et al. Comparative genomics and transcriptomics of Pichia pastoris. *BMC Genomics*. 2016;17(1). doi:10.1186/S12864-016-2876-Y
100. Jacobs PP, Geysens S, Vervecken W, Contreras R, Callewaert N. Engineering complex-type N-glycosylation in Pichia pastoris using GlycoSwitch technology. *Nat Protoc*. 2009;4(1):58-70. doi:10.1038/NPROT.2008.213
101. Mattanovich D, Graf A, Stadlmann J, et al. Genome, secretome and glucose transport highlight unique features of the protein production host Pichia pastoris. *Microb Cell Fact*. 2009;8. doi:10.1186/1475-2859-8-29
102. De Schutter K, Lin YC, Tiels P, et al. Genome sequence of the recombinant protein production host Pichia pastoris. *Nat Biotechnol*. 2009;27(6):561-566. doi:10.1038/NBT.1544
103. Sturmberger L, Chappell T, Geier M, et al. Refined Pichia pastoris reference genome sequence. *J Biotechnol*. 2016;235:121-131. doi:10.1016/J.JBIOTEC.2016.04.023
104. Valli M, Tatto NE, Peymann A, et al. Curation of the genome annotation of Pichia pastoris (Komagataella phaffii) CBS7435 from gene level to protein

function. *FEMS Yeast Res*. 2016;16(6). doi:10.1093/FEMSYR/FOW051

105. Chung BKS, Selvarasu S, Andrea C, et al. Genome-scale metabolic reconstruction and in silico analysis of methylotrophic yeast Pichia pastoris for strain improvement. *Microb Cell Fact*. 2010;9. doi:10.1186/1475-2859-9-50
106. Rußmayer H, Buchetics M, Gruber C, et al. Systems-level organization of yeast methylotrophic lifestyle. *BMC Biol*. 2015;13(1). doi:10.1186/S12915-015-0186-5
107. Zahrl RJ, Peña DA, Mattanovich D, Gasser B. Systems biotechnology for protein production in Pichia pastoris. *FEMS Yeast Res*. 2017;17(7). doi:10.1093/FEMSYR/FOX068
108. Ramezani-Rad M, Hollenberg CP, Lauber J, et al. The Hansenula polymorpha (strain CBS4732) genome sequencing and analysis. *FEMS Yeast Res*. 2003;4(2):207-215. doi:10.1016/S1567-1356(03)00125-9
109. van Zutphen T, Baerends RJS, Susanna KA, et al. Adaptation of Hansenula polymorpha to methanol: a transcriptome analysis. *BMC Genomics*. 2010;11(1). doi:10.1186/1471-2164-11-1
110. Ravin N V., Eldarov MA, Kadnikov V V., et al. Genome sequence and analysis of methylotrophic yeast Hansenula polymorpha DL1. *BMC Genomics*. 2013;14(1). doi:10.1186/1471-2164-14-837
111. Jeffrey V, Joachim M. New pUC-derived cloning vectors with different selectable markers and DNA replication origins. *Gene*. 1991;100(C):189-194. doi:10.1016/0378-1119(91)90365-I

112. Kiel JAKW, Otzen M, Veenhuis M, Van Der Klei IJ. Obstruction of polyubiquitination affects PTS1 peroxisomal matrix protein import. *Biochim Biophys Acta*. 2005;1745(2):176-186. doi:10.1016/J.BBAMCR.2005.01.004

113. Kiel JAKW, Keizer-Gunnink I, Krause T, Komori M, Veenhuis M. Heterologous complementation of peroxisome function in yeast: the saccharomyces cerevisiae PAS3 gene restores peroxisome biogenesis in a Hansenula polymorpha per9 disruption mutant. *FEBS Lett*. 1995;377(3):434-438. doi:10.1016/0014-5793(95)01385-7

114. Faber KN, Kram AM, Ehrmann M, Veenhuis M. A novel method to determine the topology of peroxisomal membrane proteins in vivo using the tobacco etch virus protease. *J Biol Chem*. 2001;276(39):36501-36507. doi:10.1074/JBC.M105828200

115. Deviant Pex3p levels affect normal peroxisome formation in Hansenula polymorpha: high steady-state levels of the protein fully abolish matrix protein import - PubMed. Accessed August 18, 2023. https://pubmed.ncbi.nlm.nih.gov/9434349/

116. Kurbatova E, Otzen M, van der Klei IJ. p24 proteins play a role in peroxisome proliferation in yeast. *FEBS Lett*. 2009;583(19):3175-3180. doi:10.1016/J.FEBSLET.2009.08.040

117. Gietl C, Faber KN, Van Der Klei IJ, Veenhuis M. Mutational analysis of the N-terminal topogenic signal of watermelon glyoxysomal malate dehydrogenase using the heterologous host Hansenula polymorpha. *Proc Natl Acad Sci U S A*. 1994;91(8):3151-3155. doi:10.1073/PNAS.91.8.3151

118. Haan GJ, Faber KN, Baerends RJS, et al. Hansenula polymorpha Pex3p is a peripheral component of the peroxisomal membrane. *J Biol Chem*. 2002;277(29):26609-26617. doi:10.1074/JBC.M108569200

119. Gidijala L, Kiel JAKW, Douma RD, et al. An engineered yeast efficiently secreting penicillin. *PLoS One*. 2009;4(12). doi:10.1371/JOURNAL.PONE.0008317

120. Saraya R, Gidijala L, Veenhuis M, van der Klei IJ. Tools for genetic engineering of the yeast Hansenula polymorpha. *Methods Mol Biol*. 2014;1152:43-62. doi:10.1007/978-1-4939-0563-8_3

121. Saraya R, Krikken AM, Veenhuis M, van der Klei IJ. Peroxisome reintroduction in Hansenula polymorpha requires Pex25 and Rho1. *J Cell Biol*. 2011;193(5):885-900. doi:10.1083/JCB.201012083

122. Agaphonov MO. Improvement of a yeast self-excising integrative vector by prevention of expression leakage of the intronated Cre recombinase gene during plasmid maintenance in Escherichia coli. *FEMS Microbiol Lett*. 2017;364(22). doi:10.1093/FEMSLE/FNX222

123. Okonechnikov K, Golosova O, Fursov M, et al. Unipro UGENE: a unified bioinformatics toolkit. *Bioinformatics*. 2012;28(8):1166-1167. doi:10.1093/BIOINFORMATICS/BTS091

124. Glazer AN. Light guides. *Journal of Biological Chemistry*. 1989;264(1):1-4. doi:10.1016/S0021-9258(17)31212-7

125. Zheng J, Inoguchi T, Sasaki S, et al. Phycocyanin and phycocyanobilin from Spirulina platensis protect against diabetic nephropathy by inhibiting

oxidative stress. *Am J Physiol Regul Integr Comp Physiol*. 2013;304(2). doi:10.1152/AJPREGU.00648.2011

126. Ismaiel MMS, El-Ayouty YM, Piercey-Normore M. Role of pH on antioxidants production by Spirulina (Arthrospira) platensis. *Braz J Microbiol*. 2016;47(2):298-304. doi:10.1016/J.BJM.2016.01.003
127. Nabiev IR, Efremov RG, Chumanov GD. Surface-enhanced Raman scattering and its application to the study of biological molecules. *Uspekhi Fizicheskih Nauk*. 1988;154(3):459. doi:10.3367/UFNR.0154.198803D.0459
128. Fleischmann M, Hendra PJ, McQuillan AJ, Fleischmann M, Hendra PJ, McQuillan AJ. Raman spectra of pyridine adsorbed at a silver electrode. *CPL*. 1974;26(2):163-166. doi:10.1016/0009-2614(74)85388-1
129. Jeanmaire DL, Van Duyne RP. Surface raman spectroelectrochemistry. Part I. Heterocyclic, aromatic, and aliphatic amines adsorbed on the anodized silver electrode. *Journal of Electroanalytical Chemistry*. 1977;84(1):1-20. doi:10.1016/S0022-0728(77)80224-6
130. Albrecht MG, Creighton JA. Anomalously Intense Raman Spectra of Pyridine at a Silver Electrode. *J Am Chem Soc*. 1977;99(15):5215-5217. doi:10.1021/JA00457A071
131. PLASMON-ENHANCED VIBRATIONAL; SPECTROSCOPY OF SEMICONDUCTOR NANOCRYSTALS. *Автометрия*. 2020;(5). doi:10.15372/AUT20200508
132. Metasurfaces: Ultrabroadband Metasurface for Efficient Light Trapping and Localization: A Universal Surface-Enhanced Raman Spectroscopy Substrate

for “All” Excitation Wavelengths (Adv. Mater. Interfaces 10/2015) | Request PDF. Accessed August 18, 2023. https://www.researchgate.net/publication/275523076_Metasurfaces_Ultrabroadband_Metasurface_for_Efficient_Light_Trapping_and_Localization_A_Universal_Surface-Enhanced_Raman_Spectroscopy_Substrate_for_All_Excitation_Wavelengths_Adv_Mater_Interfaces_1020

133. Wang Y, Irudayaraj J. Surface-enhanced Raman spectroscopy at single-molecule scale and its implications in biology. *Philos Trans R Soc Lond B Biol Sci*. 2012;368(1611). doi:10.1098/RSTB.2012.0026
134. inVia^{TM} 共焦显微拉曼光谱仪. Accessed August 18, 2023. https://www.renishaw.com.cn/zh/invia-confocal-raman-microscope--6260
135. Pézolet M, Georgescauld D. Raman spectroscopy of nerve fibers. A study of membrane lipids under steady state conditions. *Biophys J*. 1985;47(3):367-372. doi:10.1016/S0006-3495(85)83927-8
136. Xue L, Zhen Z, Guang-hui H, et al. Usage and Maintenance of InVia-Reflex Micro-Confocal Raman Spectrometer. *Analysis and Testing Technology and Instruments, 2021, Vol 27, Issue 4, Pages: 233-239*. 2021;27(4):233-239. doi:10.16495/J.1006-3757.2021.04.001
137. Beck MT, Nagypál I (1944). Issledovanie kompleksoobrazovaniâ novejšimi metodami. Published online 1989.
138. Прикладная ИК-спектроскопия. Основы техника, аналитическое применение - Смит А. - 1982. Accessed August 18, 2023.

https://djvu.online/file/SUGUmYfSodtPS?ysclid=llgwtu0uq623169672

139. Б.Н. Тарасевич - ИК спектры основных классов органических соединений (справочные материалы): ИК спектроскопия - PDF (54167) - СтудИзба. Accessed August 18, 2023. https://studizba.com/files/show/pdf/54167-1-b-n-tarasevich--ik-spektry-osnovnyh.html
140. Скачать Колесник И.В., Саполетова Н.А. Инфракрасная спектроскопия. Методическая разработка [PDF] - Eruditor. Accessed August 19, 2023. https://g.eruditor.one/file/2289052/?ysclid=llh33vo3qi704242558
141. Lakowicz JR. Principles of fluorescence spectroscopy. *Principles of Fluorescence Spectroscopy*. Published online 2006:1-954. doi:10.1007/978-0-387-46312-4/COVER
142. Van Oort B, Amunts A, Borst JW, et al. Picosecond fluorescence of intact and dissolved PSI-LHCI crystals. *Biophys J*. 2008;95(12):5851-5861. doi:10.1529/BIOPHYSJ.108.140467
143. Maksimov EG, Sluchanko NN, Slonimskiy YB, et al. The photocycle of orange carotenoid protein conceals distinct intermediates and asynchronous changes in the carotenoid and protein components. *Sci Rep*. 2017;7(1). doi:10.1038/S41598-017-15520-4
144. Zhang G, Que Q, Pan J, Guo J. Study of the interaction between icariin and human serum albumin by fluorescence spectroscopy. *J Mol Struct*. 2008;881(1-3):132-138. doi:10.1016/J.MOLSTRUC.2007.09.002
145. Фотобиология - Конев С.Н., Волотовский И.Д. - 1979. Accessed August

18, 2023. https://djvu.online/file/frNSqnPldVq8F?ysclid=llgxbx4enx582053417

146. Intrinsic Fluorescence of Proteins and Peptides. Accessed August 18, 2023. https://web.archive.org/web/20100516054153/http://dwb.unl.edu/Teacher/NSF/C08/C08Links/pps99.cryst.bbk.ac.uk/projects/gmocz/fluor.htm

147. Bogdanova AI, Agaphonov MO, Ter-Avanesyan MD. Plasmid reorganization during integrative transformation in Hansenula polymorpha. *Yeast*. 1995;11(4):343-353. doi:10.1002/YEA.320110407

148. Shilova S a A, Rakitin T V., Popov VO, Bezsudnova EYu. PROSPECTS OF APPLICATION OF D-AMINO ACID TRANSAMINASE FROM AMINOBACTERIUM COLOMBIENSE FOR (R)-SELECTIVE AMINATION OF α-KETOACIDS. *Lomonosov chemistry journal*. 2023;64(№2, 2023):85-98. doi:10.55959/MSU0579-9384-2-2023-64-2-85-98

149. Parshina EY, Liu W, Yusipovich AI, et al. Spectral and conformational characteristics of phycocyanin associated with changes of medium pH. *Photosynth Res*. Published online 2024. doi:10.1007/s11120-023-01068-0

150. Wang X, Li W, Xie M, et al. The energy transfer dynamics in C-phycocyanin hexamer from <italic>Spirulina platensis</italic>. *Chinese Science Bulletin*. 2018;63(7):641-648. doi:10.1360/N972017-01026

151. Bochkova J V., Liu W, Brazhe NA, Zhgun AA, Maksimov G V. A Raman Spectroscopic Study of the Conformation of Flavin Adenine Dinucleotide, a CoEnzyme of D-Amino Acid Oxidase. *Biophysics (Russian Federation)*. 2023;68(5):719-724. doi:10.1134/S0006350923050068

152. Semenova AA, Goodilin EA, Brazhe NA, et al. Planar SERS nanostructures with stochastic silver ring morphology for biosensor chips. *J Mater Chem*. 2012;22(47):24530-24544. doi:10.1039/C2JM34686A

153. Liu W, Shutova V V., Maksimov G V., Hao J, He Y. USE OF NANOSTRUCTURED SILVER SUBSTRATES (COATINGS) TO STUDY THE CONTENT AND CONFORMATION OF p-CAROTENE. *Herald of the Bauman Moscow State Technical University, Series Natural Sciences*. 2022;(2):112-124. doi:10.18698/1812-3368-2022-2-112-124

154. He S, Xie W, Zhang P, et al. Preliminary identification of unicellular algal genus by using combined confocal resonance Raman spectroscopy with PCA and DPLS analysis. *Spectrochim Acta A Mol Biomol Spectrosc*. 2018;190:417-422. doi:10.1016/J.SAA.2017.09.036

155. Yang H, Yang S, Kong J, Dong A, Yu S. Obtaining information about protein secondary structures in aqueous solution using Fourier transform IR spectroscopy. *Nat Protoc*. 2015;10(3):382-396. doi:10.1038/NPROT.2015.024

156. Tsoraev G V., Protasova EA, Klimanova EA, et al. Anti-Stokes fluorescence excitation reveals conformational mobility of the C-phycocyanin chromophores. *Struct Dyn*. 2022;9(5). doi:10.1063/4.0000164

157. Agaphonov M, Alexandrov A. Self-excising integrative yeast plasmid vectors containing an intronated recombinase gene. *FEMS Yeast Res*. 2014;14(7):1048-1054. doi:10.1111/1567-1364.12197

158. Müller F. d- and l-Amino Acid Oxidases. Published online July 22, 2019:69-

94. doi:10.1201/9781351070560-3

159. Asiala SM, Schultz ZD. Surface enhanced Raman correlation spectroscopy of particles in solution. *Anal Chem*. 2014;86(5):2625-2632. doi:10.1021/AC403882H

160. Huang YY, Beal CM, Cai WW, Ruoff RS, Terentjev EM. Micro-Raman spectroscopy of algae: composition analysis and fluorescence background behavior. *Biotechnol Bioeng*. 2010;105(5):889-898. doi:10.1002/BIT.22617

161. Deng YL, Juang YJ. Black silicon SERS substrate: effect of surface morphology on SERS detection and application of single algal cell analysis. *Biosens Bioelectron*. 2014;53:37-42. doi:10.1016/J.BIOS.2013.09.032

162. Legesse FB, Rüger J, Meyer T, Krafft C, Schmitt M, Popp J. Investigation of Microalgal Carotenoid Content Using Coherent Anti-Stokes Raman Scattering (CARS) Microscopy and Spontaneous Raman Spectroscopy. *Chemphyschem*. 2018;19(9):1048-1055. doi:10.1002/CPHC.201701298

163. Nikelshparg EI, Grivennikova VG, Baizhumanov AA, et al. Probing lipids in biological membranes using SERS. *Mendeleev Communications*. 2019;29(6):635-637. doi:10.1016/J.MENCOM.2019.11.009

164. Brazhe NA, Evlyukhin AB, Goodilin EA, et al. Probing cytochrome c in living mitochondria with surface-enhanced Raman spectroscopy. *Sci Rep*. 2015;5. doi:10.1038/SREP13793

165. Subramanian B, Thibault MH, Djaoued Y, Pelletier C, Touaibia M, Tchoukanova N. Chromatographic, NMR and vibrational spectroscopic investigations of astaxanthin esters: application to “Astaxanthin-rich shrimp

oil" obtained from processing of Nordic shrimps. *Analyst*. 2015;140(21):7423-7433. doi:10.1039/C5AN01261A

166. Cavonius L, Fink H, Kiskis J, Albers E, Undeland I, Enejder A. Imaging of lipids in microalgae with coherent anti-stokes Raman scattering microscopy. *Plant Physiol*. 2015;167(3):603-616. doi:10.1104/PP.114.252197
167. Zhang C, Liu P. The New Face of the Lipid Droplet: Lipid Droplet Proteins. *Proteomics*. 2019;19(10). doi:10.1002/PMIC.201700223
168. Neufeld GJ, Riggs AF. Aggregation properties of C-Phycocyanin from Anacystis nidulans. *Biochim Biophys Acta*. 1969;181(1):234-243. doi:10.1016/0005-2795(69)90246-3
169. Glazer AN, Fang S, Brown DM. Spectroscopic properties of C phycocyanin and of its α and β subunits. *Journal of Biological Chemistry*. 1973;248(16):5679-5685. doi:10.1016/s0021-9258(19)43559-x
170. Lakowicz JR. On Spectral Relaxation in Proteins†¶‖. *Photochem Photobiol*. 2000;72(4):421-437. doi:10.1562/0031-8655(2000)0720421OSRIP2.0.CO2
171. Leopold HJ, Leighton R, Schwarz J, Boersma AJ, Sheets ED, Heikal AA. Crowding Effects on Energy-Transfer Efficiencies of Hetero-FRET Probes As Measured Using Time-Resolved Fluorescence Anisotropy. *J Phys Chem B*. 2019;123(2):379-393. doi:10.1021/acs.jpcb.8b09829
172. Szalontai B, Gombos Z, Csizmadia V. Resonance Raman spectra of phycocyanin, allophycocyanin and phycobilisomes from blue-green alga Anacystis nidulans. *Biochem Biophys Res Commun*. 1985;130(1):358-363. doi:10.1016/0006-291X(85)90425-5

173. Wynn-Williams DD, Edwards HGM, Newton EM, Holder JM. Pigmentation as a survival strategy for ancient and modern photosynthetic microbes under high ultraviolet stress on planetary surfaces. *Int J Astrobiol*. 2002;1(1):39-49. doi:10.1017/S1473550402001039

174. Pezzotti G, Adachi T, Imamura H, et al. In Situ Raman Study of Neurodegenerated Human Neuroblastoma Cells Exposed to Outer-Membrane Vesicles Isolated from Porphyromonas gingivalis. *Int J Mol Sci*. 2023;24(17). doi:10.3390/IJMS241713351

175. Dong A, Huang P, Caughey WS. Protein secondary structures in water from second-derivative amide I infrared spectra. *Biochemistry*. 1990;29(13):3303-3308. doi:10.1021/BI00465A022

176. Lorenz-Fonfria VA. Infrared Difference Spectroscopy of Proteins: From Bands to Bonds. *Chem Rev*. 2020;120(7):3466-3576. doi:10.1021/ACS.CHEMREV.9B00449

177. Venyaminov SY, Kalnin NN. Quantitative IR spectrophotometry of peptide compounds in water (H2O) solutions. II. Amide absorption bands of polypeptides and fibrous proteins in alpha-, beta-, and random coil conformations. *Biopolymers*. 1990;30(13-14):1259-1271. doi:10.1002/BIP.360301310

178. Chi Z, Hong B, Tan S, et al. Impact Assessment of heavy metal cations to the characteristics of photosynthetic phycocyanin. *J Hazard Mater*. 2020;391:122225. doi:10.1016/j.jhazmat.2020.122225

179. Yang R, Ma T, Shi L, et al. The formation of phycocyanin-EGCG complex

for improving the color protection stability exposing to light. *Food Chem*. 2022;370:130985. doi:10.1016/j.foodchem.2021.130985

180. Byler DM, Susi H. Examination of the secondary structure of proteins by deconvolved FTIR spectra. *Biopolymers*. 1986;25(3):469-487. doi:10.1002/BIP.360250307
181. *Extraction and Purification of C-Phycocyanin and Genome Analysis of an Indigenous Hypersaline Cyanobacterium*. Durban University of Technology; 2020. doi:10.51415/10321/3602
182. Brejc K, Ficner R, Huber R, Steinbacher S. Isolation, crystallization, crystal structure analysis and refinement of allophycocyanin from the cyanobacterium Spirulina platensis at 2.3 A resolution. *J Mol Biol*. 1995;249(2):424-440. doi:10.1006/JMBI.1995.0307
183. Wang XQ, Li LN, Chang WR, et al. Structure of C-phycocyanin from Spirulina platensis at 2.2 A resolution: a novel monoclinic crystal form for phycobiliproteins in phycobilisomes. *Acta Crystallogr D Biol Crystallogr*. 2001;57(Pt 6):784-792. doi:10.1107/s0907444901004528
184. Padyana AK, Bhat VB, Madyastha KM, Rajashankar KR, Ramakumar S. Crystal Structure of a Light-Harvesting Protein C-Phycocyanin from Spirulina platensis. *Biochem Biophys Res Commun*. 2001;282(4):893-898. doi:10.1006/bbrc.2001.4663
185. Bai Y, Li X, Xie Y, Wang Y, Dong X, Qi H. Ultrasound treatment enhanced the functional properties of phycocyanin with phlorotannin from Ascophyllum nodosum. *Front Nutr*. 2023;10. doi:10.3389/fnut.2023.1181262

186. Eisele LE, Bakhru SH, Liu X, MacColl R, Edwards MR. Studies on C-phycocyanin from Cyanidium caldarium, a eukaryote at the extremes of habitat. *Biochimica et Biophysica Acta (BBA) - Bioenergetics*. 2000;1456(2-3):99-107. doi:10.1016/S0005-2728(99)00110-3

187. Edwards MR, Hauer C, Stack RF, Eisele LE, MacColl R. Thermophilic C-phycocyanin: effect of temperature, monomer stability, and structure. *Biochimica et Biophysica Acta (BBA) - Bioenergetics*. 1997;1321(2):157-164. doi:10.1016/S0005-2728(97)00056-X

188. Usoltsev, Sitnikova, Kajava, Uspenskaya. Systematic FTIR Spectroscopy Study of the Secondary Structure Changes in Human Serum Albumin under Various Denaturation Conditions. *Biomolecules*. 2019;9(8):359. doi:10.3390/biom9080359

189. Nishina Y, Miura R, Tojo H, Miyake Y, Watari H, Shiga K. A resonance Raman study on the structures of complexes of flavoprotein D-amino acid oxidase. *J Biochem*. 1986;99(2):329-337. doi:10.1093/OXFORDJOURNALS.JBCHEM.A135487

190. Nishina Y, Shlga K, Horiike K, et al. Resonance Raman spectra of semiquinone forms of flavins bound to riboflavin binding protein. *J Biochem*. 1980;88(2):411-416. doi:10.1093/OXFORDJOURNALS.JBCHEM.A132987

191. Nishina Y, Shiga K, Miura R, et al. On the structures of flavoprotein D-amino acid oxidase purple intermediates. A resonance Raman study. *J Biochem*. 1983;94(6):1979-1990. doi:10.1093/OXFORDJOURNALS.JBCHEM.A134552

192. Kitagawa T, Kyogoku Y, Nishina Y, et al. Resonance Raman spectra of carbon-13- and nitrogen-15-labeled riboflavin bound to egg-white flavoprotein. *Biochemistry*. 1979;18(9):1804-1808. doi:10.1021/BI00576A026

193. Nishina Y, Kitagawa T, Shiga K, et al. Resonance Raman spectra of riboflavin and its derivatives in the bound state with egg riboflavin binding proteins. *J Biochem*. 1978;84(4):925-932. doi:10.1093/OXFORDJOURNALS.JBCHEM.A132205

194. Nishina Y, Tojo H, Shiga K. Resonance Raman spectra of anionic semiquinoid form of a flavoenzyme, D-amino acid oxidase. *J Biochem*. 1988;104(2):227-231. doi:10.1093/OXFORDJOURNALS.JBCHEM.A122447

195. Frontiers in Molecular Biosciences. Accessed August 19, 2023. https://www.researchgate.net/journal/Frontiers-in-Molecular-Biosciences-2296-889X

196. DAO - D-amino-acid oxidase - Homo sapiens (Human) | UniProtKB | UniProt. Accessed August 19, 2023. https://www.uniprot.org/uniprotkb/P14920/entry

197. Gabler M, Hensel M, Fischer L. Detection and substrate selectivity of new microbial D-amino acid oxidases. *Enzyme Microb Technol*. 2000;27(8):605-611. doi:10.1016/S0141-0229(00)00262-3

198. Byler DM, Susi H. Examination of the secondary structure of proteins by deconvolved FTIR spectra. *Biopolymers*. 1986;25(3):469-487.

doi:10.1002/BIP.360250307

199. Caldinelli L, Iametti S, Barbiroli A, et al. Unfolding intermediate in the peroxisomal flavoprotein D-amino acid oxidase. *J Biol Chem*. 2004;279(27):28426-28434. doi:10.1074/JBC.M403489200